JOURNAL OF MECHANICAL ENGINEERING

STROJNIŠKI VESTNIK

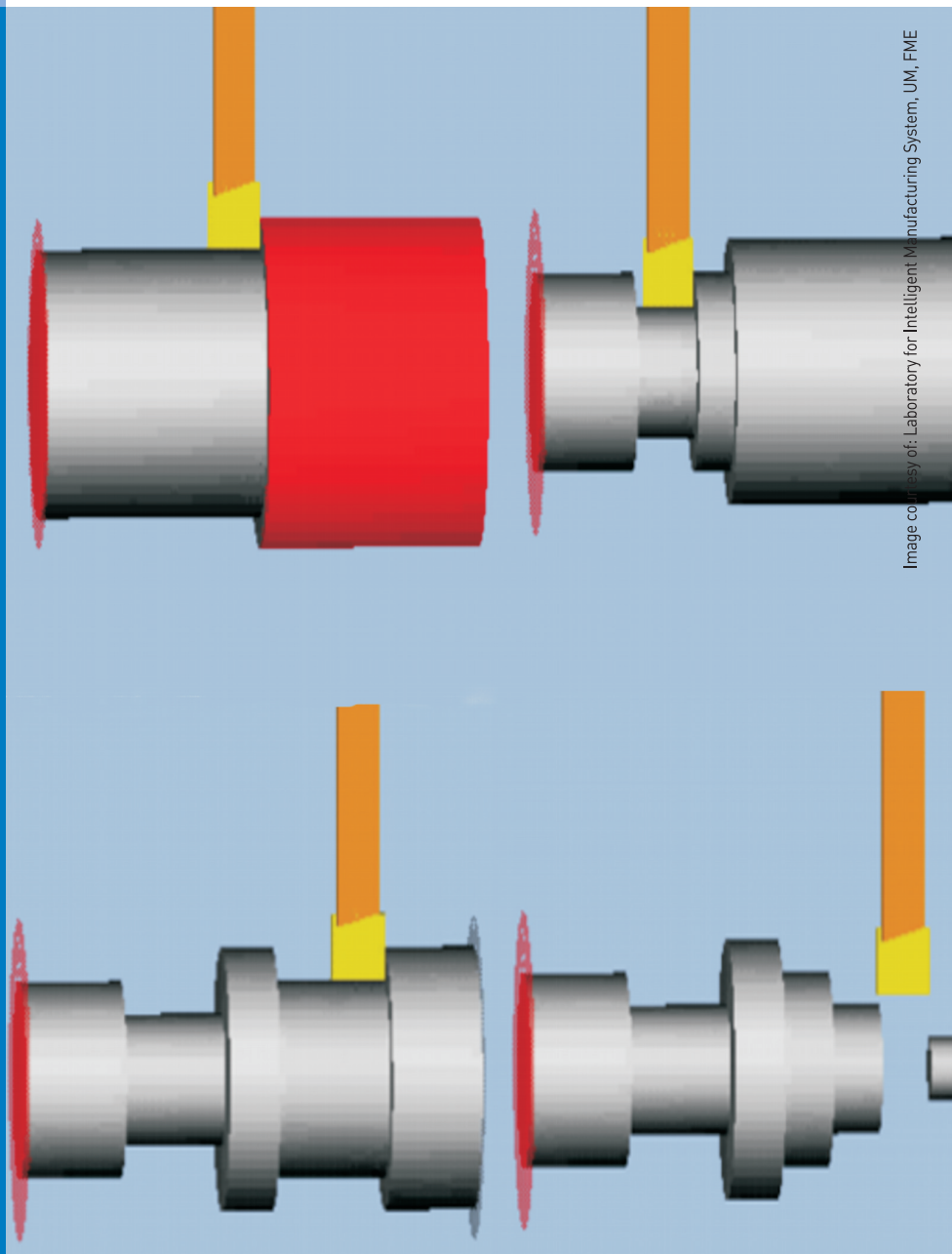

Image courtesy of: Laboratory for Intelligent Manufacturing System, UM, FME

no. 5
year 2008
volume 54

Contents

Strojniški vestnik - Journal of Mechanical Engineering
volume 54, (2008), number 5
Ljubljana, May 2008
ISSN 0039-2480

Published monthly

Papers

Strojniški vestnik - Journal of Mechanical Engineering 54(2008)5, 301-307
UDC 621.914
Paper received: 7.4.2008
Paper accepted: 15.5.2008

Feature Extraction from CAD Model for Milling Strategy Prediction

Jože Balič* - Simon Klančnik - Simon Brezovnik
University of Maribor, Faculty of Mechanical Engineering, Slovenia

In this paper we present a procedure of feature determination from a CAD model. From the model we extract information, which has the greatest influence on the technological parameters of treatment and then transform this information into appropriate input data for different intelligent processing strategy prediction systems (for example artificial neural network). With formally complex CAD models, different processing strategies are required on a single workpiece. For this reason we use segmentation as described in this paper, to partition the surface of the CAD model into regions, so that we treat each region as an independent model and determine its features.

Keywords: CAD-CAM systems, milling strategies, feature extraction, CAD models, segmentation

0 INTRODUCTION

The rising complexity of the industrial production, the need for higher efficiency, better adaptability, higher quality and lower costs, has changed the production processes substantially in the last few years. Modern production science is interdisciplinary and often employs results of research from other fields of science such as: computer sciences, management, marketing and system theory [1] to [4]. The use of artificial intelligence in production systems [5] to [10] has increased greatly in the last two decades because of the adequate efficiency and availability of computers for a broader circle of researchers and industrial users.

In the commercially available CAD/CAM systems, a problem of converting a complex free surface of the product into a formal building block and later into a technological building block still appears. Most of the systems for recognition and connection of building blocks are based on basic geometrical solids, which do not allow satisfying cataloguing of complex free surfaces and their subsequent transformation into building blocks. CAD databases, from which building blocks are captured and identified, also do not contain elements, which would enable satisfying recognition of the free surface as a conglomerate of building blocks. With artificial neural network we can efficiently predict milling strategy from CAD model [11] to [15].

1 STATE OF THE ART

The procedures of automatic milling strategy prediction from surface CAD model can generally be divided in two areas; feature extraction from a 3D model, and feature recognition and classification [16] to [20]. In this paper we will limit to describe feature extraction from CAD model.

We have to take into account that 3D objects can be stored in different formats, such as triangle meshes, volumetric data, parametric or implicit equations, etc. There are different approaches to acquiring features from a 3D model.

2D methods are based on the fact that the 3D model is described with a series of 2D images acquired from different viewpoints. We retrieve useful data from these images with the help of methods used in digital image processing [21]. Different authors use different approaches, namely: Löffler [22] describes a method, which is based on comparison of shapes from images. Min [23] introduces a 2D procedure for detection of 3D objects on the image.

The second group of methods for determining features of a 3D model is comprised of methods based on mathematical description of 3D objects, the so-called histogram methods. Boyer and Srikantiah [24] present a procedure, which segments object in a network of cells and then calculates the so-called key value for each cell. Different values are used, such as: Gaussian

*Corr. Author's Address: University of Maribor, Faculty of Mechanical Engineering, Smetanova 17, 2000 Maribor, Slovenia, joze.balic@uni-mb.si

curvature and variation of normals. Papers like [24] to [26] represent the use of differential equations for describing 3D objects, specifically - an estimation of Gaussian and mean curvature for describing 3D models. Then there are Kazhdan and others, who describe an object with the help of reflexive symmetry [27] and [28] or spherical harmonic representation [29].

In the next group of methods for extracting features from a 3D model, are methods based on description of topology of an object. Generally, the result describing an object is presented in form of a graph. Exact comparison of two graphs can be computationally very demanding. Hilaga [30] suggested a method, which uses the so-called Reeb graph. Topology of object is written in the graph, according to the geodetic distance calculated for all points on the surface of the body.

Novotni and Klein [31] present a method, which belongs to a group of methods based on measuring the errors between objects.

In general it is difficult to say which of the mentioned methods for determining features of a 3D object is better than others. Feature determination is a very important and interesting problem. We can conclude that each of the mentioned methods has its weaknesses and that an ideal method has still not been suggested yet.

2 FEATURE EXTRACTION

In classification procedure it is extremely important to describe the object with its essential characteristics, important for the given assignment.

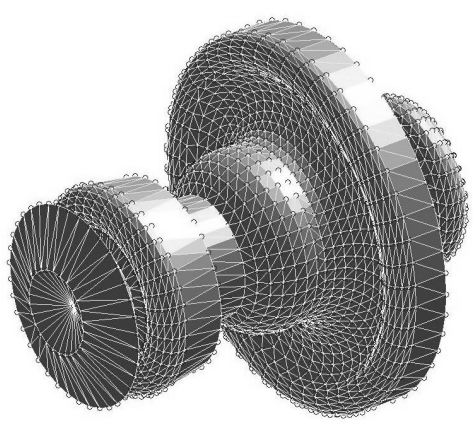

Fig. 1. *CAD model example composed from STL triangles*

In the recognition process, we arrange patterns in M classes, which means that from the perspective of pattern classification, the important characteristics of objects are only those, which emphasize the particularities of the individual pattern classes. We call such pattern characteristic feature. In our application triangle corners represent the pattern. In Figure 1, we can see a CAD model composed of triangles read from an STL file. STL file was stored in one of the commercial CAD packages (CATIA, SolidWorks etc.) Triangles describing face of the model are of different sizes (depending on the shape of the face).

Each triangle corner is a point, located on the surface of the model. Now we know the coordinates of the corners, and we also know that a between these points there lies a straight face (triangle) - we have described the whole surface of the body. To obtain useful and characteristic information of the pattern, this data has to be appropriately processed. We also need to adequately rearrange these data in order to enter it into the neural network.

Figure 2 presents the phases of data processing:

- In phase one, we have to use the appropriate algorithm to remove faces, which are not visible. First we define the plane from which we will project the network of points to the body. The normal to this plane represents the direction of our view.
- In the phase of segmentation, we partition the whole face representing the body into smaller sub-faces (surface patches) and then treat each of this sub-faces as an independent model.
- In the plane according to which we defined the direction of our view, we create a mesh of symmetrically arranged points and project it to the model at the right angle.
- In the last phase, we standardize the values obtained when projecting the network to the model, and write it in the form of a vector appropriate for input into our classifier.

2.1 Removing the Hidden Surfaces of a Body

The concealment of some parts of a body depends on the chosen viewpoint. If the body is shown with full faces, we use the hidden-surface removal algorithms. Although many hidden-surface removal algorithms exist today [32], we can't

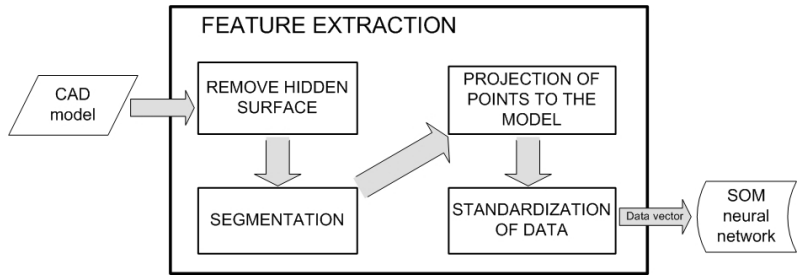

Fig. 2. *Block scheme of data processing*

determine which one is the best, since their results depend on the complexity of the scene.

In application we »shoot« symmetrically arranged points at the body. For the description of the model, we are interested only in the front surface therefore we use the appropriate algorithm to remove faces hidden to our view – faces hidden by the body itself, the so-called back-faces. For this we need normal vectors of all faces of the body, and they all have to be directed outward form the body or into the interior of the body. Each of the faces is a plane polygon, in our case a triangle. On the face we choose three adjacent corners (in our case these are corners of the triangle): $\boldsymbol{p}_{i-1}$, $\boldsymbol{p}_i$ in $\boldsymbol{p}_{i+1}$. We calculate normal face vector for each triangle with the following vector product:

$$n = (p_{i-1} - p_i) \times (p_{i+1} - p_i) = \begin{bmatrix} a & b & c \end{bmatrix}^T \quad (1).$$

The equation of the plane in which the surface lies is defined with:

$$ax + by + cz + d = 0 \quad (2).$$

Coefficients *a, b* and *c* correspond to the components of normal vector *n*, coefficient *d* is calculated with the help of the following expression:

$$d = -(ax_i + by_i + cz_i) \quad (3),$$

where x_i, y_i and z_i are the coordinates of the corner $\boldsymbol{p}_i$ (otherwise we can select any point on the face). In this way we calculate equations of planes for all *m* faces of the object. Plane defined by the equation (2), divides the space into two half-spaces. Normal vector points to the half-space in which lies the point $p=[x\ \ y\ \ z]^T$, under the following conditions:

$$[a\ \ b\ \ c\ \ d]\ [x\ \ y\ \ z\ \ 1]^T > 0 \quad (4).$$

In the Equation (4), the positive elements in the product signify that the normal vectors of the corresponding planes are directed to the interior of the body, while negative elements signify that vectors are directed outwards from the body. Coefficients of planes, whose vectors are pointing outwards from the body, have to be multiplied by -1. In this way we achieve that all the normal face vectors are directed into the interior of the body.

Hidden-surface removal algorithm uses the fact that the angle between the normal of the visible face and the direction of view is smaller than 90°, while the angle between the normal of the hidden face and the direction of view is larger or equal to 90°. In Figure 3, we indicate the direction of view by vector *g*. If the scalar product of the view direction vector and the normal of the face is positive, the face is visible, while in the opposite case it is not. In Figure 4 (left) we can see an

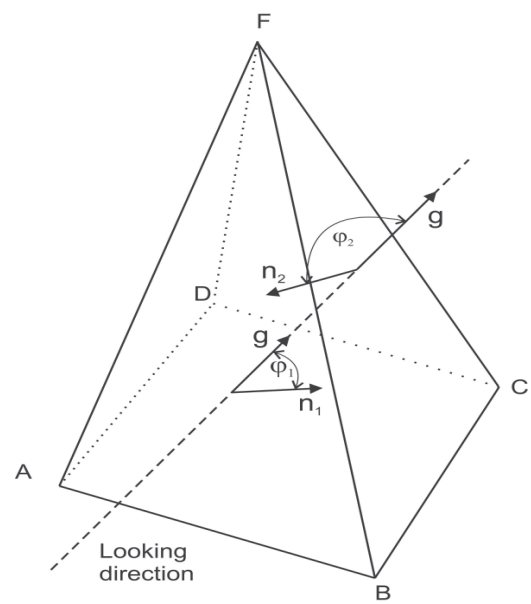

Fig. 3. *Surface "ABF is visible, because* $\varphi_1 < 90°$ *and surface "CDF is invisible, because* $\varphi_2 > 90°$

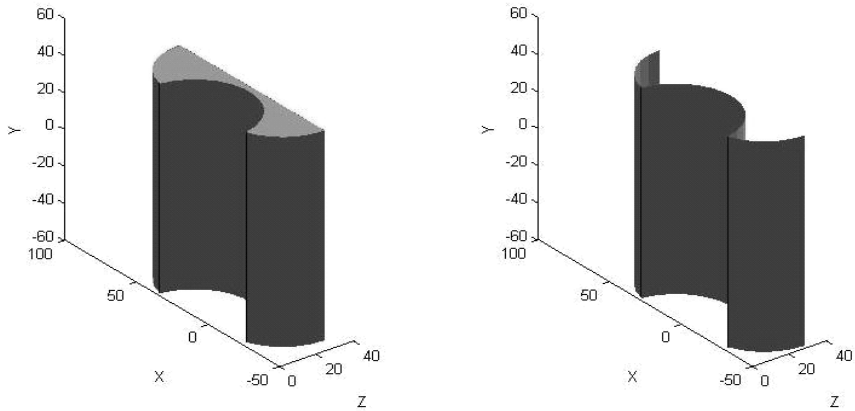

Fig. 4. *Representation of hidden surface algorithm's functioning*

example of CAD Model drawn with the help of our application. In the Figure 4 (right) we can see the same model after it as been processed with the hidden-surface removal algorithm.

2.2 Segmentation of CAD Model

In this phase we have to partition the entire surface of the CAD model into smaller sub-faces [33]. In other words, we have to segment the triangles describing the surface of the workpiece into regions, which are suitable for independent planning of milling strategy.

We have implemented segmentation of the model according to the size of the angle between the normal of triangles representing the surface of the body. The normal of triangle defined by the three corners $\boldsymbol{p}_{i-1}$, $\boldsymbol{p}_i$ and $\boldsymbol{p}_{i+1}$ is calculated by Equation (1). For each triangle (the triangle for which we are trying to find its neighbours, will from this point on be called basic triangle) we search for adjacent triangles, which share two common corners with the chosen triangle. In this way each triangle can have one, two or a maximum of three neighbours (Fig. 5). Then we calculate the angle between the normal of the basic triangle and the normal of its neighbours. If the calculated angle is smaller than the threshold value, we add this triangle into the region established by the basic triangle. If the angle is larger or equal to the threshold value, the triangle is not added to the region and is treated later when we determine the members of the next region. Each new triangle added to the region has to be treated later as basic triangle and examined whether its neighbours satisfy the conditions for classification into this region. The algorithm is executed until each triangle belongs to a certain region. In Figure 7 (left) we can see an example of workpiece drawn with the help of our application. In the right section of the Figure 7, we can see a segmented CAD model in which the segmentation algorithm has divided the model into three regions. In the following procedure we treat each of these regions, obtained

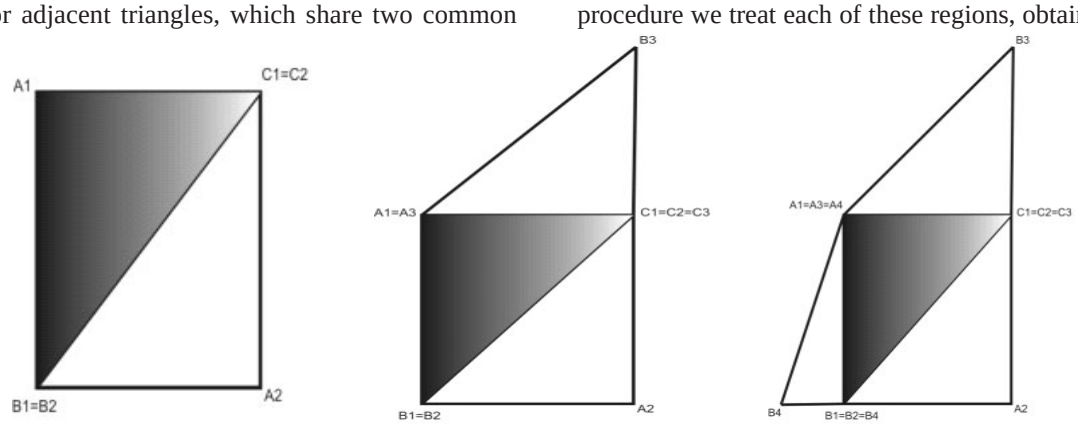

Fig. 5. *Basic triangle and its neighbourhood*

by the process of segmentation, as an independent CAD model and determine appropriate treatment strategy for each one separately.

2.3 "Scattering" Points Over the Model

Each region of the model is "scattered" with points in a certain mesh. In the x-y plane, we create a window the size of the largest possible drawn-in rectangle. In the window we determine points, which are symmetrically arranged. By increasing the number of points, we improve the reliability of our system but this also increases the number of data representing CAD model and causes more complex and slower processing. The number of points in directions x and y is a parameter which can be modified. In our testing we chose 200 points in direction x and 200 points in direction y.

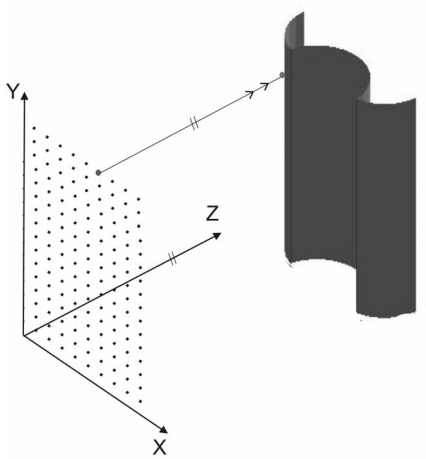

Fig. 6. *Schematic representation of points in the plane x-y, which are projected to the body parallel to the z-axis*

Figure 6 shows a schematic representation of points in the plane x-y, which are projected to the body parallel to the z-axis. From mathematical standpoint, this means that for each point *P(x,y)*, defined by the raster of points in the plane x-y, we calculate the value of coordinate z, occupied in that position by the surface of the model. Since the triangles describing the face are of different sizes, while we are interested in values of component *Z* for fixed coordinates *X* and *Y*, we have to perform interpolation between these points. We have used triangle-based interpolation presented in detail in [34].

Numbers of points and raster have to be identical for all the models in the learning base. Configuration of model in the direction *Z* has the greatest influence on the technological parameters; therefore we use only these data for input in the neural network. Values Z, which are calculated for each point *P(x,y)*, are written in the form of vector $S_N=\{x_1^*, x_2^*,\ldots,x_N^*\}$. In the test example we have chosen mesh of 200 points in direction x and 200 points in direction y, thus receiving a vector the size of 40,000 elements.

Certain extents of similarity between patterns are highly dependant on the criteria in which we present the features. If we wish for all the features in the pattern to have the same contribution to the calculation of the extent of similarity, we have to standardize pattern features appropriately. The vector obtained in this way, whose elements are standardized values, represents the input into a system for intelligent prediction of processing strategy (SOM neural network, feed-forward neural networks etc.).

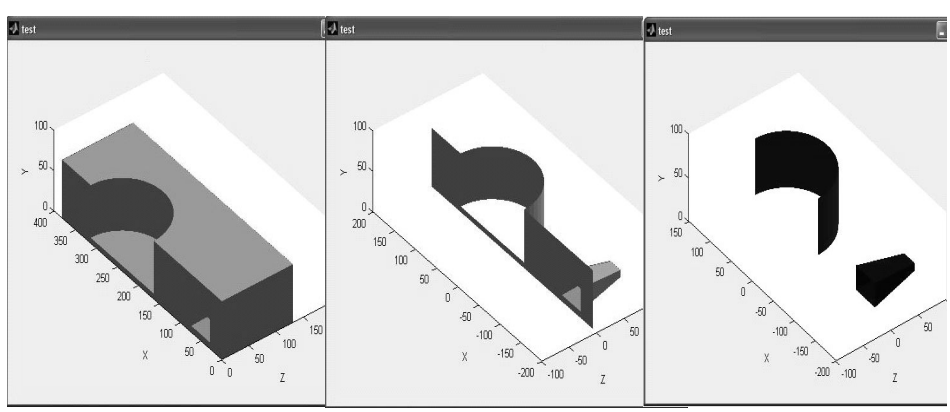

Fig. 7. *Representation of processing results for the test model*

3 RESULTS

Feature extraction system has been tested on different CAD models, which have been modelled in SolidWorks package. Figure 7 presents processing results of one of the test models. In the first phase we can see that the faces not visible from the x-y plane were removed from the model (middle figure). The right figure shows the model after the segmentation. We can see that we have obtained two independent regions, each of which has to be treated as an independent CAD model and analyzed according to its features for the appropriate processing strategy.

As seen from the Figure 7 and results of other tests performed with models of different shapes, the suggested procedure of feature extraction are very efficient and appropriate for use in prediction of milling strategy. Model segmentation was performed in a manner whose efficiency largely depends on the appropriate selection of threshold value, which varies form model to model. Therefore it has to be stressed that we can obtain good results only with the appropriate threshold value selection.

4 CONCLUSION

System testing has shown that with the help of the procedure presented in this paper, we can efficiently extract valuable information from a CAD model. Those informations are needed in determining strategy according to the shape of the workpiece. Such system would offer users a good supplement tool and help when working with modern CAM systems. Feature extraction program was implemented in the MATLAB integrated development environment. System has been implemented in such a way that its use is universal and allows processing of CAD models made in different commercial packages and stored in STL formats. The topics presented in this paper offers excellent foundation for additional research. In the future we intend to expand the system with intelligent system, which will be capable to predict appropriate processing strategy based on extracted features.

5 REFERENCES

[1] Shishir Bhat, B. N. Profits and reduce cycle time with manufacturing cells. *Advances in Production Engineering & Management*, vol. 3, no. 1, p. 17-26, 2008.

[2] Tyagi, V., Jain, A. Assessing the effectiveness of flexible process plans for loading and part type selection in FMS. *Advances in Production Engineering & Management*, vol. 3, no. 1, p. 27-44, 2008.

[3] Buchmeister, B., Pavlinjek, J., Palcic, I. Polajnar, A.: Bullwhip effect problem in supply chains. *Advances in Production Engineering & Management*, vol. 3, no. 1, p. 45-55, 2008.

[4] Rahimić, S., Višekruna,V. Optimization of generative CAPP system with minimum cost per piece. *Advances in Production Engineering & Management*, vol. 2, no. 4, p. 177-185, 2007.

[5] Carpenter, I. D., Maropoulos, P. G. Automtic tool selection for milling operations Part 1: cutting data generation. *Journal of Engineering Manufacture*, 214(4), p. 271-282, 2000.

[6] Balic, J. Intelligent CAD/CAM system for CNC programming-an overview. *Advances in Production Engineering & Management*, vol. 1, p. 13-21, 2007.

[7] Renner, G.; Ekárt, A. Genetic algorithms in computer Aided design. *Computer-Aided Design*, vol. 35, p. 709-726, 2003.

[8] Colak, O., Kurbanoglu, C., Kayacan, M. C. Milling surface roughness prediction using evolutionary programming methods. *Materials and Design*, vol. 28, p. 657-666, 2005.

[9] Kovacic, M., Brezocnik, M., Pahole, I. , Balic, J. , Kecelj, B. Evolutionary programming of CNC machines. *Journal of Materials Processing Technology*, vol. 164-165, p. 1379-1387, 2005.

[10] Valenti, M. Machine tools get smarter. *Mech. Engrg.*, vol. 117, 1995.

[11] Balic, J.; Korosec, M. Intelligent tool path generation for milling of free surfaces using neural networks. *International Journal of Machine Tools & Manufacture*. vol. 42, p. 1171–1179, 2002.

[12] Balič, J. *Intelligent manufactory systems*. University of Maribor, Faculty of mechanical engineering, Maribor, 2004.

[13] Benardos P. G., Vosniakos G. C. Prediction of surface roughness in CNC face milling

using neural networks and Taguchi's design of experiments. *Robotics and Computer Integrated Manufacturing*, vol. 18, p. 343-354, 2002.

[14] Azouzi, R., Guillot, M. On-line prediction of surface finish and dimensional deviation in turning using neural network based sensor fusion. *Int J MachTools Manuf*, vol. 37, p. 1201–1217, 1997.

[15] Yu-Hsuan, T., Chen J.C., Shi-Jer, L. An in process surface recognition system based on neural networks in end milling cutting operations. *Int J MachTools Manuf*, Vol. 39, p. 583–605.

[16] Potočnik, B. *Pattern recognition with neural networks*. University of Maribor, Faculty of Electrical Engineering and Computer Science, Maribor, 2007.

[17] Berikov, V., Litvinenko, A. *Methods for statistical data analysis with decision trees*. 2003.

[18] Domingos, P., Pazzani,M. On the optimality of the simple Bayesian classifier under zero-one loss. *Machine Learning*, vol. 29, p. 103–137, 1997.

[19] Cristianini, N., Shawe-Taylor, J. *An introduction to support vector machines and other kernel-based learning methods*. Cambridge University Press, 2000.

[20] Fradkin, D., Muchnik, I. Support vector machines for classification. *DIMACS Series in Discrete Mathematics and Theoretical Computer Science*, vol. 70, p. 13-20, 2006.

[21] Klančnik, S., Balič, J., Planinšič, P. Obstacle detection with active laser triangulation. *Advances in Production Engineering & Management*, vol. 2, p. 79-90, 2007.

[22] Lőffler, J. Content-based Retrieval of 3D models in Distributed Web Database by Visual Shape Information. *Int. Conf. On Information Visualisation*, 2000.

[23] Min, P., Chen, J., Funkhouser, T. *A 2D sketch interface for a 3D model search egine*. 2002.

[24] Boyer, K. L., Srikantiah, R., Flynn, P.J. Salience sequential surface organization for free-form object recognition. *Computer vision and image understanding*, vol. 88, 2002.

[25] Mokhtarian, F., Khalili, N., Yuen, P. Multi-scale free-form 3D object recognition using 3D models. *Image and vision computing*, vol. 19, p. 271-281, 2001.

[26] Quek, K. H., Yarger, R.W. I., Kirbas, C.: Surface parameterization in volumetric images for curvature-based feature classification. *IEEE transactions on system, Man and Cybernetics*, 2001.

[27] Kazhdan, M., Chazelle, B., Dobkin, D., Finkelstein, A., Funkhouser, T. A reflective symmetry description. E*uropean conf. on computer vision*, 2002.

[28] Kazhdan, M., Chazelle, B., Dobkin, D., Finkelstein, A., Funkhouser, T. *A reflective symmetry description for 3D model*. Algorithmica, 2003.

[29] Funkhouser, T., Min, P., Kazhdan, M., Chen, J., Halderman, A., Dobkin, D. Asearch engine for 3D models. *ACM transactions on graphics*, vol. 22, p. 83-105, 2003.

[30] Hilaga, M., Shinagawa, Y., Kohmura, T., Kunii, T. L. *Topology matching for fully automatic similarity estimation of 3D shapes*. SIGGRAPH, p. 203-212, 2001.

[31] Novotni, M., Klein, R. A geometric approach to 3D object comparison. *Int. Conf. on shape modeling and applications*, p. 154-166, 2001.

[32] Guid, N. *Computer graphics*. University of Maribor, Faculty of electrical engineering and computer science, Maribor, 2001.

[33] Lefebvre, P., Lauwers, B. *STL Model Segmentation for Multi-Axis Machining Operations Planning*

[34] Watson, D.F., Philip, G. M. *Triangle based interpolation. Mathematical Geology*. p. 779-795, 1984.

Strojniški vestnik - Journal of Mechanical Engineering 54(2008)5, 308-321
UDC 658.5
Paper received: 13.9.2007
Paper accepted: 19.12.2007

Predicting Order Lead Times

Tomaž Berlec* - Edvard Govekar - Janez Grum - Primož Potočnik - Marko Starbek
University of Ljubljana, Faculty of Mechanical Engineering, Slovenia

Entering on market, companies confront with different problems. But the largest problems of today's time are too long lead times of orders. A client that wants a particular product to be made will select the best bidder considering on delivery time.

To make a bid just on the basis of experience of employees is very risky nowadays. Therefore we propose a procedure by which - on the basis of actual lead times of orders processed in the company's workplaces in the past - expected lead times of planned (and indirectly - production) orders can be predicted. The result of the proposed procedure is an empirical distribution of possible lead times for the new order, and on the basis of this distribution it is possible to predict the most probable lead time of a new order. Using the proposed procedure, the sales department can make a prediction for the customer about delivery time of the planned order.

As an illustration of the procedure for predicting lead times of orders, a case study is presented: lead time of order for the "tool for manufacturing the filter housing" was predicted; the tool is manufactured in the Slovenian company ETI Ltd.

Keywords: lead times, prediction, operation order, empirical distribution

0 INTRODUCTION

Companies on the global market offer similar or the same products at comparable price and quality. The main difference between these companies is in the predicted order development time and in observance of the deadlines for delivery time.

Before making a bid, the sales department has to provide data on operations that will have to be carried out for a particular order, data on the time required for performing these operations, and data on requested delivery time. Currently, the data at times of realization of operations are obtained from experienced company employees, while the customer specifies delivery time. However, estimates based on personal experience can be rather misleading. Consequently, the bids may be based on wrong delivery time which can couse that the company does not receive the order.

Development of ICT – which are important resources for improving and maintaining the competitive advantages of the company on the market [1] – made radical changes as ICT simplifies many business-related tasks. Every company that wants to be competitive on the global market needs a suitable enterprise resource planning system – ERP system. There are several ERP systems available on the market [2] and it is the task of each company to select the optimum system [3].

The paper will present how the data stored in the ERP system can be used for calculation of lead times of orders (and indirectly: lead times of manufacturing orders) on the basis of theory developed at the IFA Hannover [4] and [5]. Furthermore, the calculation of percentage of manufacturing order lead times will be shown, which allows the calculation of the confidence interval. The purpose of this paper is therefore to propose a procedure for predicting lead times of manufacturing orders on the basis of past gathered data on actual lead times.

In our research we have not found an approach for predicting lead times as described in this paper, so we assume that it is a new approach which uses already known and developed theory of IFA Hannover, and adds a new method for predicting order lead times.

1 METHOD FOR PREDICTING MANUFACTURING ORDER LEAD TIMES

When talking about “an order”, it is necessary to distinguish between operational, manufacturing, assembly and production order [4], as presented in Figure 1.

*Corr. Author’s Address: University of Ljubljana, Faculty of Mechanical Engineering, Aškerčeva 6, SI-1000 Ljubljana, Slovenia, tomaz.berlec@fs.uni-lj.si

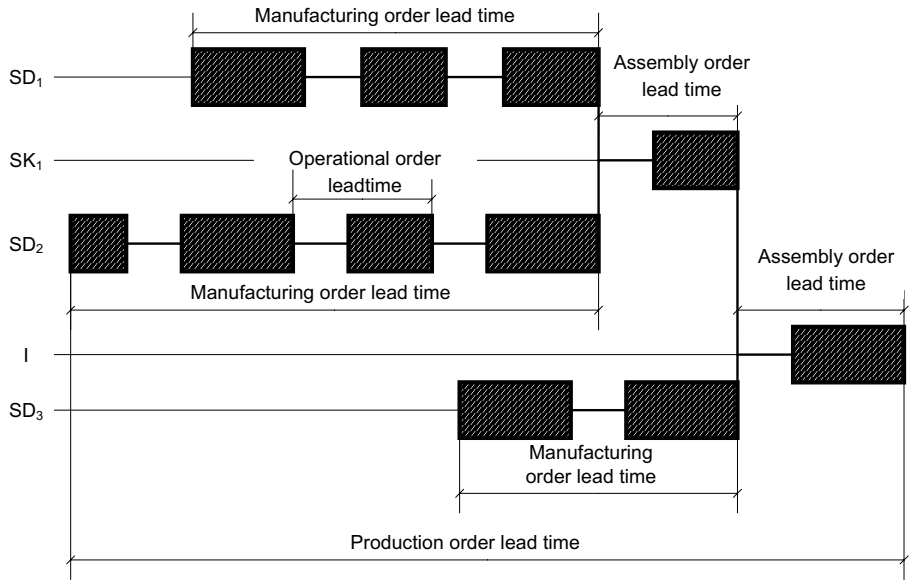

Fig. 1. *Order lead times [4]*

When designing a procedure for predicting manufacturing order lead times, it will be assumed that the company uses an ERP system, whose database contains data about past operational and assembly orders in company workplaces. Any ERP system should therefore provide data on:

- production-order code,
- assembly-order code,
- manufacturing-order code,
- operational-order code,
- type and sequence of operations on manufacturing and assembly orders,
- IDs of workplaces where operational orders have been carried out,
- actual execution times of operational orders,
- date of completing a particular operational or assembly order in the previous workplace,
- date of finishing a particular operational or assembly order in the observed workplace.

ERP system output data should be available in Microsoft Excel format (xls).

Based on previous research on problems of determination of lead times let us to the conclusion, that the proposed procedure for predicting order lead times consists of the following steps:

Step 1: Determining actual lead times of already processed operational orders in the company's workplaces

H. P. Wiendahl [4] says that the lead time of the *i*-th operational order N_i *(1 ≤ i ≤ n)* which has been executed in the *j*-th workplace DM_j *(1 ≤ j ≤ m)* is defined as an interval, calculated from the time when the *i*-th operational order has been completed in the previous, i.e. *(j-1)*-th workplace, till the time when the *i*-th operational order has been completed in the observed, i.e. *j*-th workplace (Fig. 2).
Lead time of an operational order is therefore:

$$TO_{i,j} = tK_{i,j} - tK_{i,(j-1)} \qquad (1),$$

$TO_{i,j}$ – lead time of the *i*-th operational order in the *j*-th workplace
$tK_{i,j}$ – completion time of the *i*-th operational order in the *j*-th workplace
$tK_{i,(j-1)}$ – completion time of the *i*-th operational order in the previous *(j-1)*-th workplace

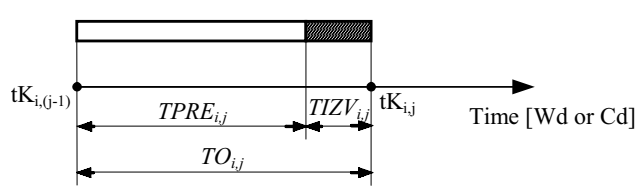

Fig. 2. *Lead time of operational order [4]*

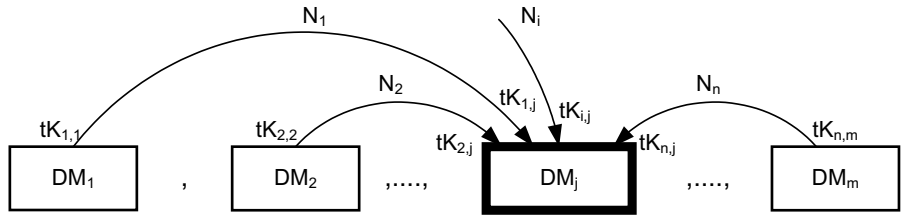

Fig. 3. *Flow of operational orders through the DM_j workplace [4]*

i – operational order number
j – workplace number

On the basis of the ERP system output data it is possible to calculate (for any ***j***-th workplace $\boldsymbol{DM_j}$) the actual lead times of previously executed operational orders, i.e. orders that have been processed in the ***j***-th workplace in the observed time interval P (Fig. 3).

The actual lead times of operational orders, executed in the ***j***-th workplace in the observed time interval are therefore:

$$\begin{aligned} TO_{1,j} &= tK_{1,j} - tK_{1,(j-1)} \\ TO_{2,j} &= tK_{2,j} - tK_{2,(j-1)} \\ &\ldots \\ TO_{i,j} &= tK_{i,j} - tK_{i,(j-1)} \\ &\ldots \\ TO_{n,j} &= tK_{n,j} - tK_{n,(j-1)} \end{aligned} \qquad (2)$$

n – number of processed operational orders in the past on i-th workplace
m – number of workplaces

Vectors of actual lead times of operational orders, executed in the past in all company workplaces (table 1), will present the basis for predicting expected lead times of the planned new production orders.

Step 2: Forming assembly structure of the planned production order and technology routings for parts and components of planed order

The assembly structure and technology routings of realization of component parts and assemblies of manufacturing orders are made on the basis of available documentation of the planned production order. Figure 4 presents the principle of building the assembly structure.

Table 1. *Vectors of lead times of operational orders*

	Workplace					
	DM 1	DM 2		DM j		DM m
Vectors of lead times	$\begin{bmatrix} TO_{1,1} \\ TO_{2,1} \\ \vdots \\ TO_{n,1} \end{bmatrix}$	$\begin{bmatrix} TO_{1,2} \\ TO_{2,2} \\ \vdots \\ TO_{n,2} \end{bmatrix}$	…	$\begin{bmatrix} TO_{1,j} \\ TO_{2,j} \\ \vdots \\ TO_{n,j} \end{bmatrix}$	…	$\begin{bmatrix} TO_{1,m} \\ TO_{2,m} \\ \vdots \\ TO_{n,m} \end{bmatrix}$

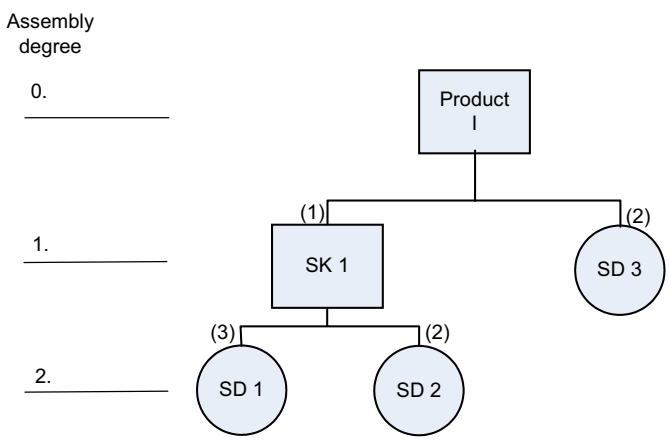

Fig. 4. *Principle of construction of assembly structure of production order I*

Legend:
I – product
SK – mark of asembly
SD – mark of component part
(x) – number of built ins of component parts and assemblies in assembly of higher degree

Figure 5, presents technology and assembly routings for manufacturing parts and components of the production order I.

Step 3: Random sampling and summing of vector element values of actual lead times of operational orders of individual manufacturing or assembly order

Figure 6 presents the principle of random sampling and summing of vector element values of operational order actual lead times in the past of planned manufacturing and assembly orders.

$TO_{SD1,1}$ – lead time of component part SD_1, got after first iteration

$TO_{SK1,1}$ – lead time of assembly SK_1, got after first iteration

$TO_{I,1}$ – lead time of product I, got after first iteration

Figure 6 shows a schematic presentation of random sampling and addition of lead times values achieved in the past from workplace vectors, defined by technology and assembly routings for manufacturing parts and assembly of

Part / component	Prescribed sequence of operations
SD 1	Turning DM1 → Milling DM3 → Grinding DM4
SD 2	Turning DM1 → Milling DM3 → Planing DM2 → Grinding DM4
SD 3	Planing DM2 → Grinding DM4
SK 1	Assembling DM5
I	Assembling DM5 → Control DM6

Fig. 5. *Technology and assembly routings of parts and components of production order I*

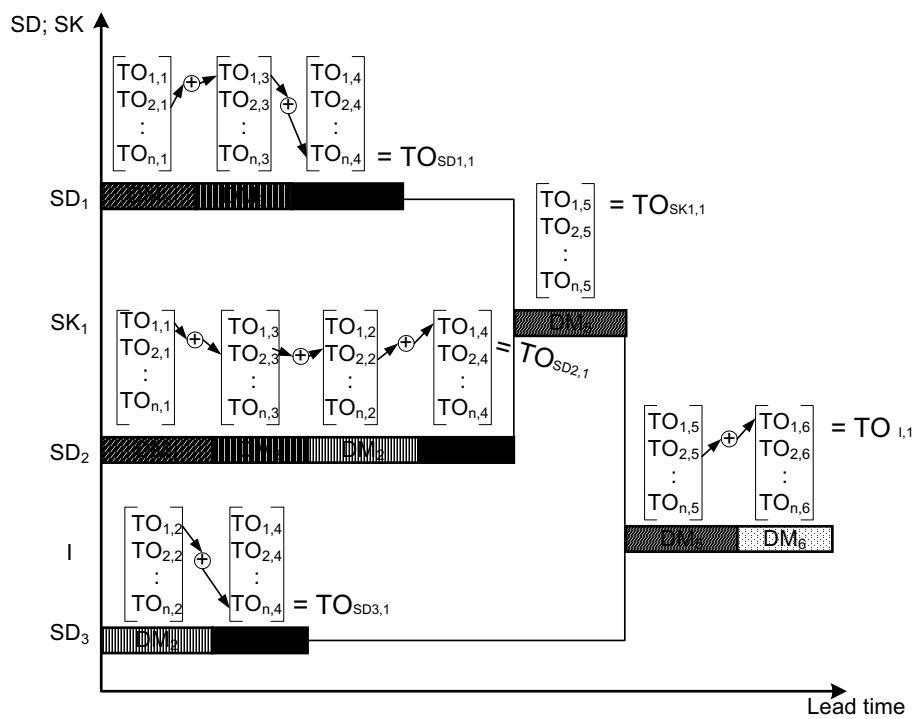

Fig. 6. *Random sampling and summing of vector element values of actual operational order lead times achieved in the past*

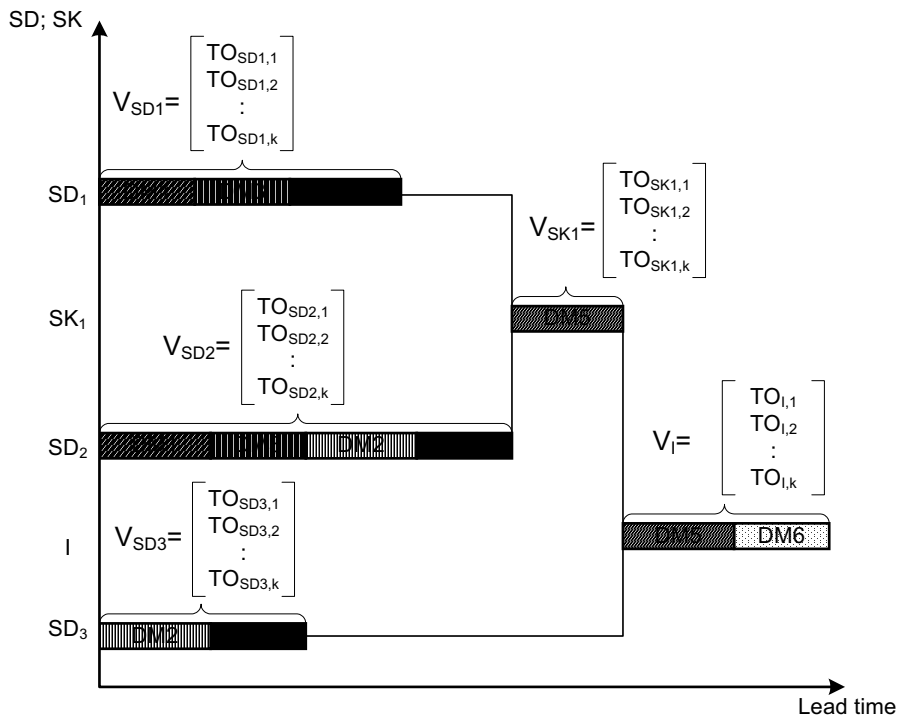

Fig. 7. *Setting up vectors of expected lead times of planned manufacturing and assembly orders*

components.

It is necessary to select the number of iterations for random sampling of lead times of manufacturing and assembly orders of planned production order (computer supported). The number of iterations is affected by the order type – by increasing its complexity, the number of iterations should be increased, too.

Step 4: Setting up vectors of expected lead times of manufacturing and assembly orders of planned order

Results of step 3 allow setup of vectors of the expected lead times of the manufacturing and assembly orders of planned production order, as presented in Figure 7.

$TO_{SD1,k}$ – lead time of component part SD_1, got after k - th iteration

V_{SD1} – lead time vector of assembly SD_1

k – number of iteration

The number of elements in individual vector depends on the number of performed iterations k. The number of required iterations can be established on the basis of tests, as it is necessary to assure a stable process, which cannot be achieved by a small number of iterations. A criterion for an adequate number of iterations is that multiple use of the procedure must yield comparable results, by which the stability (convergence) of the procedure is achieved.

Step 5: Definition of vector of expected lead times of the planned order

In order to define the vector of expected lead times of the planned production order V_I, it is necessary to transform the Gantt chart of production order (Fig. 7) into an activity network diagram of order and enter into it the vectors of expected lead times of manufacturing and assembly orders of planned order (Fig. 8).

Initial data of activity network diagram of planned order are:

- date of starting the execution of the virtual order $\boldsymbol{SD_0}$:

$$TZ_{SD_0} = 0 \qquad (4),$$

- vector of the virtual manufacturing and assembly order $\boldsymbol{V_{SD0}}$ is:

$$V_{SD_0} = \begin{bmatrix} 0 \\ 0 \\ \vdots \\ 0 \end{bmatrix} \qquad (5),$$

- vectors of expected lead times of manufacturing and assembly orders of the planned order are:

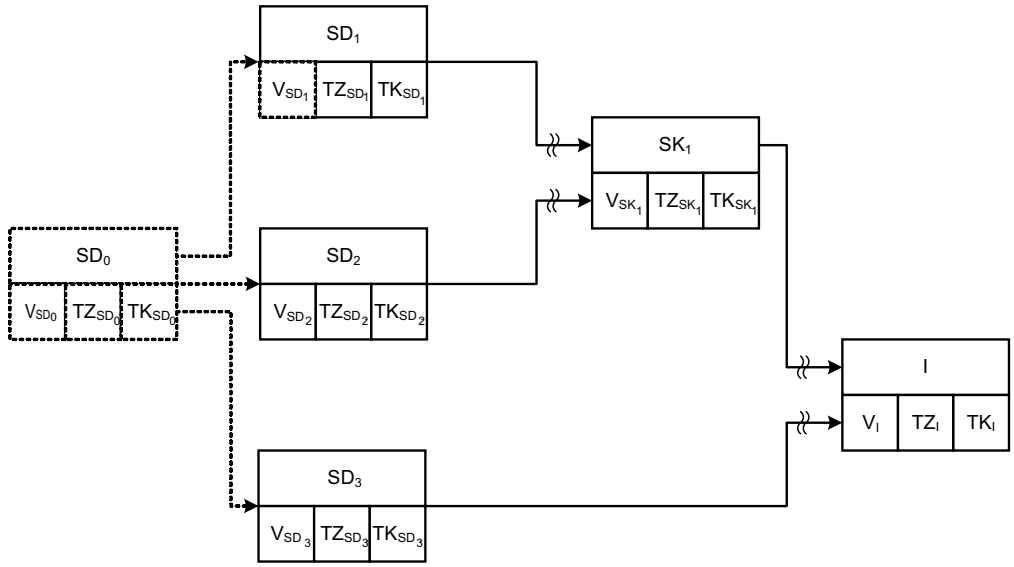

Fig. 8. *Activity network diagram of the planned (new) order*

$$V_{SD_1}, V_{SD_2}, ..., V_{SK_1}, V_I \qquad TK_I = TO \qquad (10).$$

For a virtual order $\boldsymbol{SD_0}$, which has no predecessors in activity network diagram, it is assumed that the date of starting the execution of order is (for the first iteration):

$$TZ_{SD_{0,1}} = 0 \qquad (6),$$

and the date of finishing the execution of order is

$$TK_{SD_{0,1}} = TZ_{SD_{0,1}} + TO_{SD_{0,1}} = 0 + 0 = 0 \qquad (7).$$

For other manufacturing or assembly orders, which have one or more predecessors (Fig. 9) is the date of starting the execution of orders then:

$$TZ_{SD_{b,1}} = \max_{k \in P^*} \left\{ TZ_{SD_{a,1}} + TO_{SD_{a,1}} \right\} \qquad (8)$$

P^* – predecessors of the observed order $\boldsymbol{N_j}$
and the date of finishing the execution of orders

$$TK_{SD_{b,1}} = TZ_{SD_{b,1}} + TO_{SD_{b,1}} \qquad (9).$$

Date of completing the last manufacturing or assembly order **I** is equivalent to the expected lead time of the planned order *TO* in the activity network diagram:

Figure 8 shows the calculation for one vector element of expected lead time of the planned order. Such a calculation must be done for a selected number of iterations of randomly sampled values from vectors of individual component partsand assemblies of planned order. The calculation is carried out as follows:

- For sequential operations, individual randomly sampled lead times from vectors of sequentially listed workplaces are summed up. The result of each iteration is stored into a new vector, which represents the sum for one component or part.
- For parallel operations it is necessary to collect randomly sampled lead times from vectors of parallel workplaces, and then find a maximum lead time for each parallel path. Thus obtained results in each iteration should be stored in the common vector of maximum times of parallel paths, as the critical path in the activity network diagram is always the path with the longest required lead time for realization the manufacturing order.

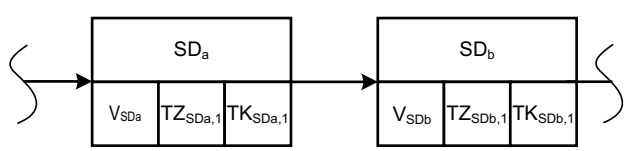

Fig. 9. *Basic element of activity network diagram*

Calculation has to be repeated for the selected number of iterations.

Thus obtained expected lead times of the planned order will represent empirical distribution of lead times of the planned order.

Step 6: Predicting delivery time of the planned order

Step 5 in predicting order lead time has lead to the vector of expected lead times of order, i.e. to a certain distribution of lead times.

In real life, however, an exact value of lead time for delivery of order is required.

The most probable delivery lead time for the planned order can be estimated by using median, which means that there is a 50% probability that the actual delivery time will be shorter, and 50% probability that it will be longer than stated. As the 50% risk is usually unacceptable for the client, so the estimated value should be stated for a wider confidence interval.

For instance, 90% confidence interval is defined as 90% probability that the order will be delivered before the stated time. Therefore, maximum delivery time that can be guaranteed to the customer with 90% reliability, corresponds to the 90th percentage of empirical distribution of prediction of the planned order.

Percentage [6] and [7] provides the value of ***Y***, which is larger than ***P*** % of the values in the ***X*** set. In other words, e.g. 90th percentage gives the value, which is larger than 90% of all values (sorted from smallest to largest) in the ***X*** set (Fig. 10).

In order to obtain the ***P***-th percentage of ***X*** sorted values, it is necessary to calculate the ***R*** rank [8]:

$$R = P(X+1)/100 \quad (11),$$

which is rounded to the first integer and then the value from the ***X*** set is selected, which corresponds to this rank.

R – percentage rank

P – percentage

X – number of sorted set elements

Based on the above explanation and our tests, we propose that the 90th percentage be used as a standard. In this way it is possible to state with 90% confidence that the order will be completed within the expected time.

If the company wants to achieve even higher reliability, it can use an even higher percentile (for example 99th) – and thus minimize the risk.

Naturally, the choice of the percentage may depend on importance of the order and the customer – the more important the customer, or the more important the order, the higher is the interest of the company to get a particular order.

In the proposed procedure for predicting manufacturing order lead times, in addition to MS Excel, the MATLAB software will be used [6], which allows execution of mathematical operations and graphical presentation of results.

2 TESTING THE PROCEDURE FOR PREDICTING ORDER LEAD TIMES

The procedure for predicting order lead times was tested in the tool shop of ETI Ltd. company from Izlake, Slovenia. It produces tools for transforming and cutting, tools for injection moulding of thermoplastic and duroplastic materials, jet and press machines for duroplastic

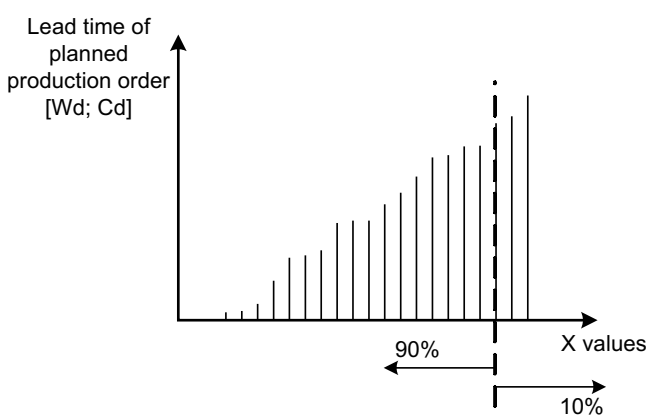

Fig. 10. *An example of the 90th percentile*

materials, press machines for ceramic materials, and automated assembly appliances.

This tool shop speciality is design and manufacturing of high-quality tools for injection moulding of thermoplastic and duroplastic materials. Thanks to its many years of experience in making tools for ETI company, the tool shop started producing tools and appliances for external customers in the following fields: automotive industry, household appliances, medical technology, electrical engineering, electronics and illumination.

Tool shop uses Largo ERP system, developed by Perftech Ltd. company from Bled [9], Slovenia. Because of their way of production (tools are made for known customers and each tool is unique) it is very difficult to precisely predict duration of production – but this is essential data for making bids and winning orders.

Company management decided to test the suitability of the proposed procedure for predicting lead times of orders in a case study of determining lead time of order for the "tool for manufacturing filter housing # 705429" (Fig. 11).

Steps of the procedure for predicting manufacturing order lead time for the "tool for manufacturing filter housing # 705429":

Step 1: Determining actual lead times of operational orders finished in the past in the company's workplaces

For the experiment, the Largo ERP system data were used in the period from December 12, 2002 till August 22, 2005.

First it was necessary to export data from Largo ERP system to MS Excel format. The following data were exported from the database: order number, arrival date, departure date, manufacturing time, and sequence of operational orders.

Largo ERP system uses calendar dates and does not take into account the company's labour-days calendar. Therefore the data which are not adapted to the company's labour days are useful mainly for predicting the duration of production from the sales department's point of view and not that much for manufacturing planning – for this purpose it would be necessary to take into account the company's labour-days.

In agreement with the tool shop management it was decided that for determining actual lead times of operational orders finished in the past, the data from the ERP system would be used from December 12, 2002 till August 22, 2005. During that time, 22,850 manufacturing orders were processed in the production, with 57,951 operational orders in 35 workplaces (Table 2).

It can be seen that during the observed time a rather varying number of operational orders passed across workplaces (minimum of 2 orders over workplace 44321 and maximum of 7307 orders over workplace 44253).

Actual lead times of individual operational orders were calculated on the basis of the data obtained from the ERP system. The calculation was made in MS Excel on the basis of Equation (1). Figure 12 presents a part of the calculation of actual lead times of operational orders in Excel table.

The results have shown that majority of actual lead times shorter then 1 Cd or 1 Cd, exceptions to the rule are some extreme cases, e.g. 464 Cd.

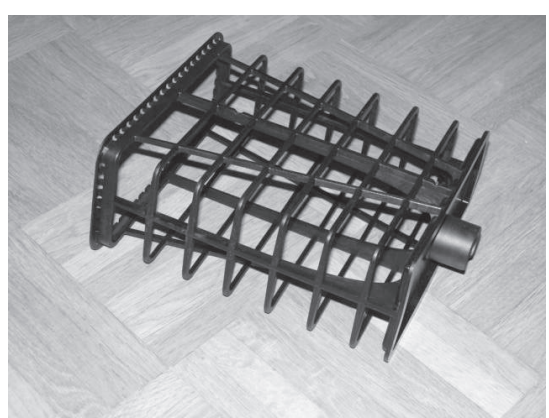

Fig. 11. Filter housing made by tool # 705429

Table 2. *Number of operational orders finished on workplaces in the tool shop*

Code:	Workplace name:	Number of finished orders in three years:
44000	Cooperation – service	21
44141	Design of devices	151
44142	Machine electronics	130
44143	Design of tools	2288
44211	Slitting	1420
44221	Turning	3706
44222	CNC turning	1052
44231	CNC programming	371
44232	CNC Milling Micron	2660
44241	CNC programming	668
44242	CNC Milling Picomax 60	4153
44243	CNC programming	9
44244	CNC Milling Deckel Maho	1400
44251	CNC Milling Picomax 54	2018
44252	Milling	235
44253	Rough milling	7307
44261	Plane grinding	1972
44262	Plane/profile grinding	4225
44263	Round grinding	2894
44264	Tools sharpening	159
44265	CNC coordinate grinding	7
44271	CNC programming of wire erosion	1126
44272	Wire erosion	1927
44273	Wire erosion -Makino	3161
44281	Dip erosion - AGIE	439
44282	Dip erosion - Charmilles	1565
44283	Dip erosion - Sinitron	513
44286	Omega punching	745
44291	Heat treatment	5172
44311	Manual machining	4288
44312	Assembly of tools	812
44313	Assembly of machines and devices	197
44321	Sampling	2
44331	Measurement	885
44332	DEA Omicron measurement	273
	Three years production:	57951

Step 2: Using or forming assembly structure of the planned order and technology routings of parts and components of order – for tool # 705429

In this step known assembly structure is formed (Fig. 13), as well as known type and sequence of operations (Fig. 14) for the tool under discussion - tool # 705429.

It can be seen from Figure 13 that the tool consists of two parts: ejecting and feeding part. The tool consists of bought parts and of parts/components made in the tool shop. There is just one assembly operation at the end, which is followed by testing.

For tool parts and components that are manufactured in the tool shop it was necessary to gather data on type and sequence of required operations, which

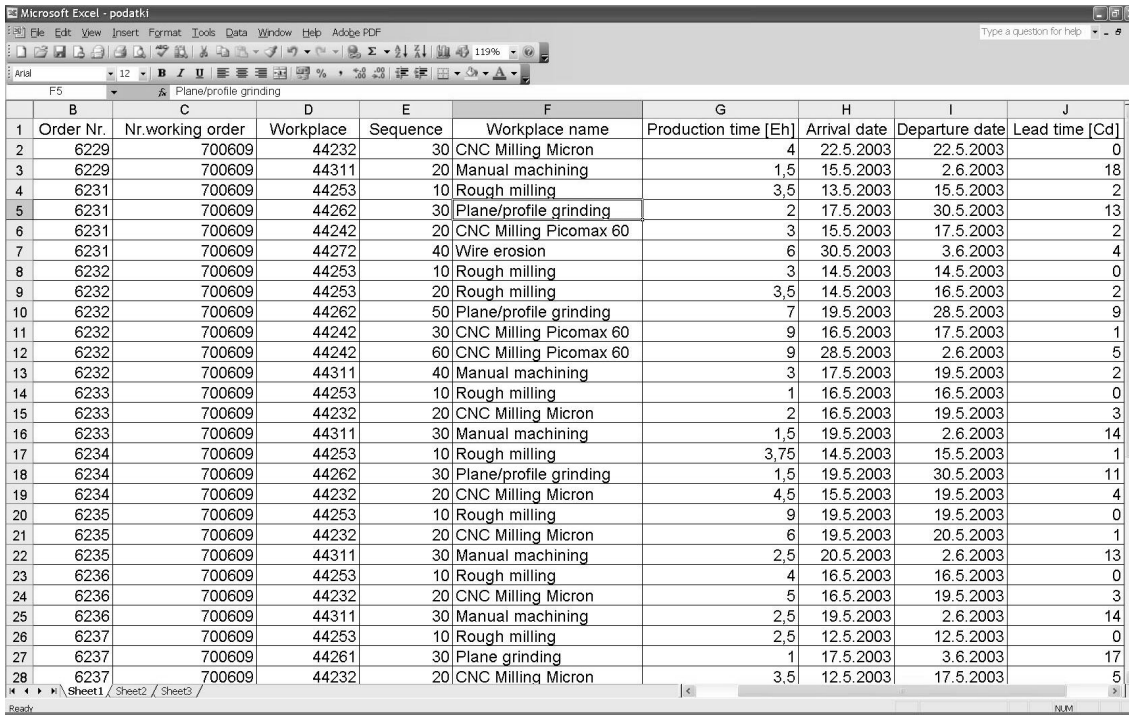

Microsoft Excel - podatki

F5: Plane/profile grinding

	B	C	D	E	F	G	H	I	J
1	Order Nr.	Nr.working order	Workplace	Sequence	Workplace name	Production time [Eh]	Arrival date	Departure date	Lead time [Cd]
2	6229	700609	44232	30	CNC Milling Micron	4	22.5.2003	22.5.2003	0
3	6229	700609	44311	20	Manual machining	1,5	15.5.2003	2.6.2003	18
4	6231	700609	44253	10	Rough milling	3,5	13.5.2003	15.5.2003	2
5	6231	700609	44262	30	Plane/profile grinding	2	17.5.2003	30.5.2003	13
6	6231	700609	44242	20	CNC Milling Picomax 60	3	15.5.2003	17.5.2003	2
7	6231	700609	44272	40	Wire erosion	6	30.5.2003	3.6.2003	4
8	6232	700609	44253	10	Rough milling	3	14.5.2003	14.5.2003	0
9	6232	700609	44253	20	Rough milling	3,5	14.5.2003	16.5.2003	2
10	6232	700609	44262	50	Plane/profile grinding	7	19.5.2003	28.5.2003	9
11	6232	700609	44242	30	CNC Milling Picomax 60	9	16.5.2003	17.5.2003	1
12	6232	700609	44242	60	CNC Milling Picomax 60	9	28.5.2003	2.6.2003	5
13	6232	700609	44311	40	Manual machining	3	17.5.2003	19.5.2003	2
14	6233	700609	44253	10	Rough milling	1	16.5.2003	16.5.2003	0
15	6233	700609	44232	20	CNC Milling Micron	2	16.5.2003	19.5.2003	3
16	6233	700609	44311	30	Manual machining	1,5	19.5.2003	2.6.2003	14
17	6234	700609	44253	10	Rough milling	3,75	14.5.2003	15.5.2003	1
18	6234	700609	44262	30	Plane/profile grinding	1,5	19.5.2003	30.5.2003	11
19	6234	700609	44232	20	CNC Milling Micron	4,5	15.5.2003	19.5.2003	4
20	6235	700609	44253	10	Rough milling	9	19.5.2003	19.5.2003	0
21	6235	700609	44232	20	CNC Milling Micron	6	19.5.2003	20.5.2003	1
22	6235	700609	44311	30	Manual machining	2,5	20.5.2003	2.6.2003	13
23	6236	700609	44253	10	Rough milling	4	16.5.2003	16.5.2003	0
24	6236	700609	44232	20	CNC Milling Micron	5	16.5.2003	19.5.2003	3
25	6236	700609	44311	30	Manual machining	2,5	19.5.2003	2.6.2003	14
26	6237	700609	44253	10	Rough milling	2,5	12.5.2003	12.5.2003	0
27	6237	700609	44261	30	Plane grinding	1	17.5.2003	3.6.2003	17
28	6237	700609	44232	20	CNC Milling Micron	3,5	12.5.2003	17.5.2003	5

Sheet1 / Sheet2 / Sheet3

Ready NUM

Fig. 12. *Calculation of actual lead times of finished operational orders in interval from December 12, 2002 till August 22, 2005*

provide quality parts and components. For the tool # 705429 some of these data are presented in Figure 14.

In tool shop in ETI Ltd. they do an conglomeration of operations named preparing on manufacturing, which for this order contains: machine electronics (44142), design of tools (44143) and slitting (44211). This is actually not a real part of the tool, which can be shown in Figure 14, but it consumes time, so it is necessary to count it in by the sequence of operations.

Steps 3 and 4: Random sampling and summing of vector element values of actual operational order lead times of individual manufacturing or assembly order of the planned order, and setup of vectors of expected lead times of manufacturing and assembly orders of the planned order for the tool # 705429

On the basis of defined sequence of machining on parts and components for the tool # 705429 made by MATLAB software, the vectors of expected lead

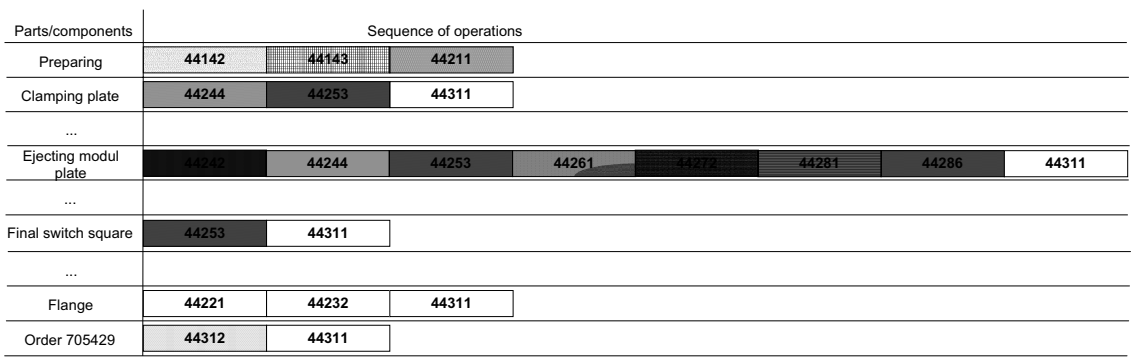

Fig. 14. *Type and sequence of operations required for manufacturing parts and components of the tool # 705429*

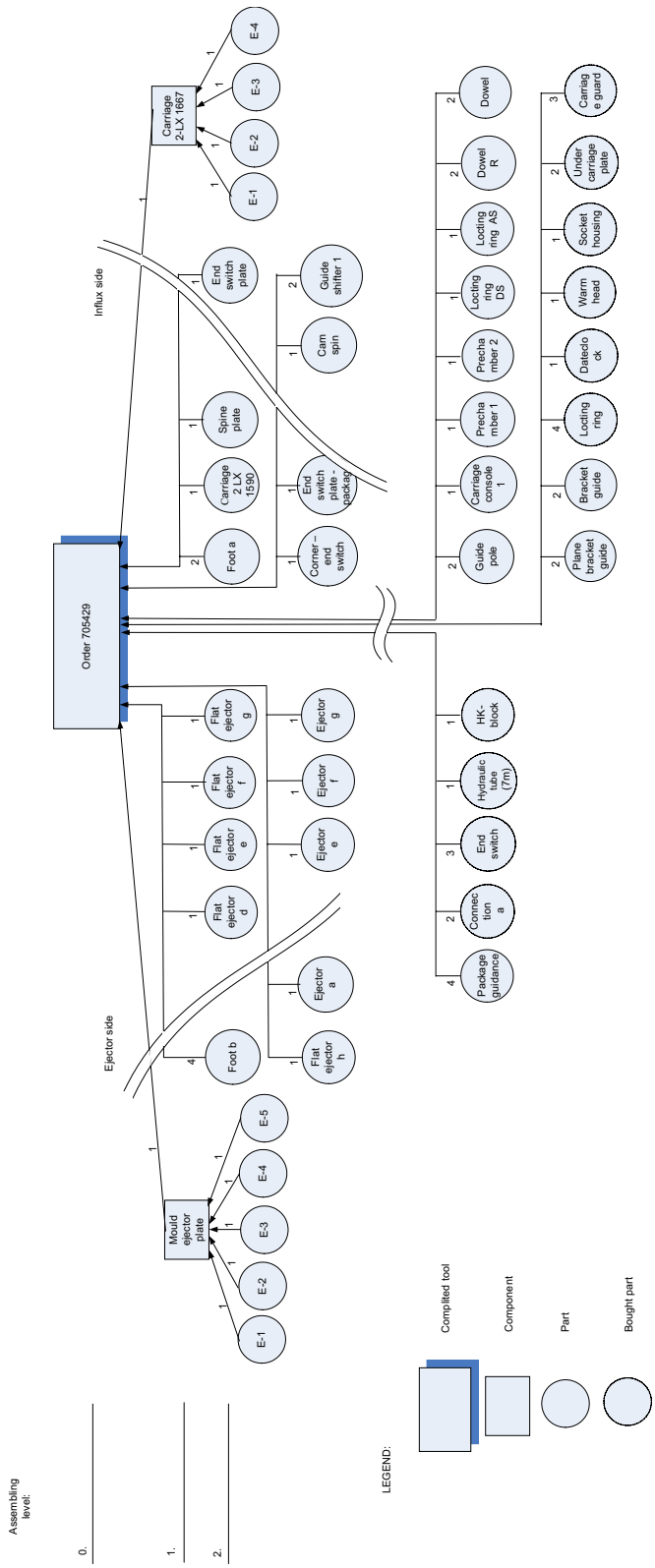

Note: All component parts made in this tool shop, have the first treatment named preparing, which for this order contains: Machine electronics (44142), Design of tools (44143) and Slitting (44211).

Fig. 13. *Part of assembly structure of the tool # 705429*

times of manufacturing and assembly orders have been set up, as described in the theoretical part of this paper.

On the basis of tests with 500, 1000, 5000, 10,000, 20,000 and 50,000 iterations we concluded that the prediction process stabilizes at approximately 10,000 iterations. If much fewer iterations are used, predictions are unstable, as insufficient data are used. If many more than 10,000 iterations are selected, the data used are repeated, so the result is not any better, while the processing time increases. We therefore used 10,000 iterations during a random selection of lead times.

On the basis of these 10,000 iterations of random selection of order operation lead times, the vectors of expected lead times of manufacturing and assembly orders have been obtained - tool # 705429 (Fig. 15).

Step 5: Definition of vector of expected lead times of the planned manufacturing order for the tool # 705429

10,000 iterations were made for the calculation of expected lead time vector of the planned order for the tool # 705429. A sample calculation of lead time for one iteration is presented in Figure 16. Expected lead time of the planned order is calculated as the sum of time of preparing, maximum time of parallel manufacturing orders, and assembly order, which in our case amounts to 16 + 28 + 9 = 53 Cd.

After 10,000 iterations the final vector of expected order lead time for the planned order for the tool # 705429 with distribution presented in Figure 17 was obtained.

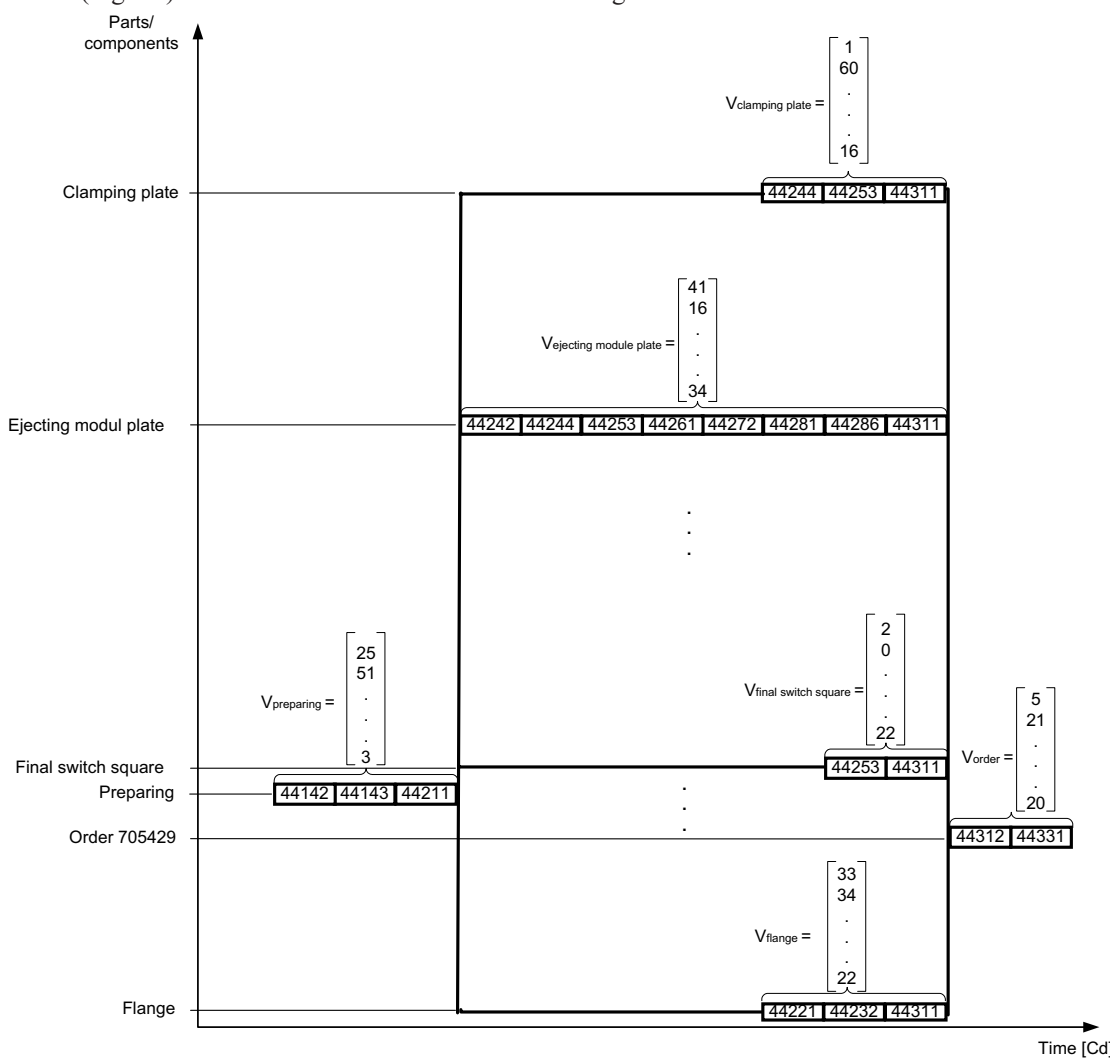

Fig. 15. *Setup of vectors of expected lead times of manufacturing and assembly orders*

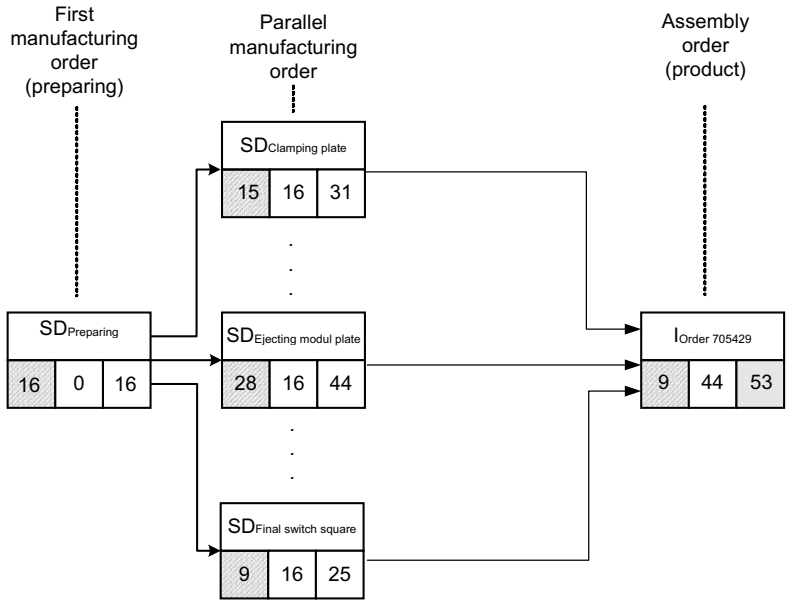

Fig. 16. *Activity network diagram of one iteration of the order # 705429*

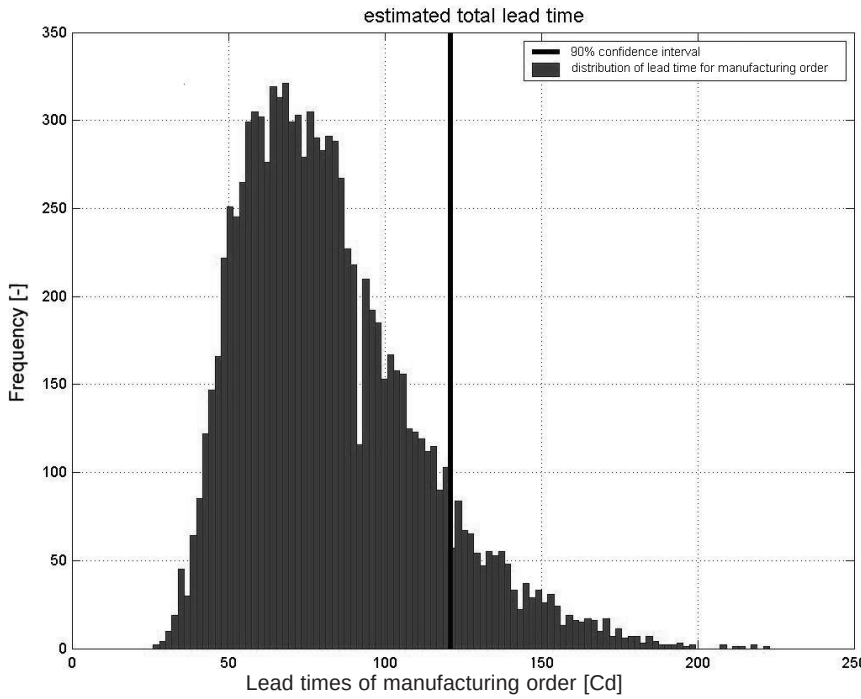

Fig. 17. Distribution of lead times for manufacturing order # 705429

Step 6: Predicting delivery time of the planned tool production order # 705429

In the fifth step the vector of lead time of the planned order (i.e. distribution of lead times of order) was set. However, no customer is interested in a lead-time vector (or distribution of lead times), so as the first approximate delivery time value, the median of this vector is used; for this order it is:

$$TO_{med} = 77 \text{ Cd}$$

TO_{med} – median lead time of the tool production order # 705429

Expected lead time therefore equals to the 50th percentage of the vector of expected lead times.

Confidence intervals are defined according to the selected confidence levels.

If a very high confidence level is required, the 90th percentage is used. So, for the order # 705429 it can be stated with 90% confidence level that this order will be produced within

$$TO_{90\%} = 120 \text{ Cd}$$

$TO_{90\%}$ – lead time at 90^{th} percentage

The company has to decide itself, which risk level it is ready to accept when signing the contract with the customer.

3 CONCLUSION

Due to ever fiercer competition of companies on domestic and foreign markets, and due to transition from the market of sellers to the market of customers, the companies have to continuously reduce delivery times of the order.

The paper proposes a procedure for predicting manufacturing order lead times on the basis of past actual lead times of operational orders. The use of the proposed procedure allows:

- prediction of lead time needed for delivery of any new order,
- variation of delivery-time calculations on the basis of acceptable risk level by selecting the confidence interval.

The basis for calculation of delivery time is median, while 90th percentage may represent the upper (safe) limit, which can be offered to the customer as the latest delivery lead time. On the basis of its experience and its willingness to risk, the company can choose different confidence interval.

The procedure for predicting order lead times has been tested in a case study of predicting lead times for producing a tool for manufacturing a filter casing in the tool shop of the ETI Ltd. Case study was performed on the basis of data, defined in calendar days collected in three years in the data base of ERP system Largo.

By using this procedure of predicting manufacturing order lead times, sales department can make a well-defined bid for the customer in a short time without the sales person needing many years of experience – (s)he only needs well-defined technology routings, while the company management provides the confidence interval.

In the future it is planned that the proposed procedure will be improved by taking into account the sequence of operations required to complete an order, the influence of the number of operations per order, the influence of manufacturing time, etc.

Acknowledgements

We would like to thank to the tool shop of ETI Ltd. company for disposal of the data from their ERP system, for their help. We would also like to thank to the Slovenian Ministry of Higher Education, Science and Technology for their financial aid during development of this method.

4 REFERENCES

[1] Leem, C.S., Suh, J.W. Techniques in integrated development and implementation of enterprise information systems. *Intelligent Knowledge-Based Systems, Business and Technology in the New Millennium*, vol. 2, 2005, p. 3-26.

[2] Scherer, E. *ERP – Projekte auf dem Prüfstand der Praxis*. ERP Management, GITO mbH Verlag, 2005, p. 34-37.

[3] Starbek, M., Grum, J. Selection and implementation of a PPC system. *Production Planning & Control*, 2000, vol. 11, p.765-774.

[4] Wiendahl H.P. *Load-oriented manufacturing control*. Berlin: Springer Verlag, 1995, p. 37-199.

[5] Nyhuis, P., Wiendahl, H.P. Logistische Kennlinien. Berlin: Springer Verlag, 1999, p. 81-94.

[6] *Getting Started with MATLAB*. The MathWorks, Inc., ver. 6, 2002.

[7] Rice, A.J. Mathematical statistics and data analysis, 2nd Ed. California: International Thomson Publishing, 1995.

[8] http://en.wikipedia.org/wiki/Percentile, 25 November 2006.

[9] http://www2.perftech.si/sxp/default.sxp?lang=1&wp=2&id=62&lid=2088, May 29, 2007.

Strojniški vestnik - Journal of Mechanical Engineering 54(2008)5, 322-333
UDC 621.941
Paper received: 16.7.2007
Paper accepted: 28.9.2007

Examination and Modelling of the Influence of Cutting Parameters on the Cutting Force and the Surface Roughness in Longitudinal Turning

Dražen Bajić[1] - Branimir Lela[1] - Goran Cukor[2]
[1]University of Split, Faculty of Electrical Engineering, Mechanical Engineering and Naval Architecture, Croatia
[2]University of Rijeka, Faculty of Engineering, Croatia

This paper examines the influence of three cutting parameters on the surface roughness and the cutting force components in longitudinal turning. The cutting speed, the feed rate and the depth of cut have been taken as influential factors. Two modelling methodologies, namely regression analysis and neural networks, have been applied to experimentally determined data. Also, for both methodologies the ability of interpolation and extrapolation has been tested. Results obtained by neural network models have been compared to those obtained by regression models. Both methodologies give nearly similar results when interpolation is observed. However, regarding extrapolation neural network models give better results. In order to find the optimum values of the cutting parameters an optimization has been carried out.

Keywords: longitudinal turning, cutting forces, surface roughness, neural networks

0 INTRODUCTION

Chip-forming machining is a multi-disciplinary scientific area based on the theory of plasticity, thermodynamics, tribology and material science. Parameters that influence the machining process can be divided into two categories:

- physical phenomena during cutting, related to influence of material structure, chip compression ratio, appearance of friction, heat development, cutting angles, etc.,
- technique of machining along with the belonging cutting parameters (cutting speed, depth of cut and feed rate), cutting force, power, etc.

Complex technological and manufacturing processes nowadays demand implementation of sophisticated mathematical and other methods for the purpose of their efficient control. Therefore a research is needed to obtain the mathematical approximations of machining processes and appearing phenomena as better as possible. Understanding the machining principles and mathematical relations among influential parameters is an important prerequisite for:

- machine tool designing that corresponds to manufacturing optimum,
- achieving product quality besides the ever-growing demands in respect to the accurate production and quality of surface roughness,
- machine tool play an important role in the design of manufacturing processes, not only in fulfilment the demands for higher productivity, but also in the requirements for production economy.

The goal of this paper is to obtain a mathematical model that relates the cutting force components and the surface roughness with the cutting parameters in longitudinal turning. In this search two different approaches have been used in order to get the mathematical models. The first approach is a design of experiment (DOE) together with an analysis of variance (ANOVA) and regression analysis. The second approach is modelling by means of artificial neural networks (ANNs). In the past, the DOE approach has been used to quantify the impact of various machining parameters on various output parameters at turning [1] to [7]. But in the last decade neural networks have experienced real prosperity in their application to various complex problems in different engineering fields. A review of scientific researches dealing with the application of ANNs to turning process can be found in [1]. It has been reported that ANNs have

*Corr. Author's Address: University of Split, Faculty of Electrical Engineering, Mechanical Engineering and Naval Architecture, Ruđera Boškovića bb, HR-21000 Split, Croatia, dbajic@fesb.hr

ability for mapping very complex and nonlinear systems. Turning process is an example of such a system and that justifies the usage of ANNs.

1 THE SCOPE OF THE RESEARCH

It is estimated that of all machining processes about 40% pertain to turning. Turning is the most common way for processing rotational (symmetrical or non-symmetrical, round or non-round) surfaces with single-point cutting tool. Cutting force is the basic indicator of cutting process behaviour. Having knowledge of the cutting force it is possible to:

- calculate the necessary power for carrying out appropriate operation, i.e. choose appropriate drive motor,
- calculate systems of all main and auxiliary transmission mechanisms from motor to tool,
- calculate and design the elements and parts of machine tools,
- define the dimensions of auxiliary devices,
- choose dimensions and types of cutting tool and verify the stability of tool in entirety,
- determine cutting parameters and conditions in the design of economical variants of technological machining process,
- perform the calculation of accuracy and the ability of machining of a workpiece at an appropriate machine tool, cutting parameters and conditions.

On the basis of knowledge of the cutting force function, the rational construction and economical efficiency of production systems, the optimization of machining process and the development of particular concepts for adaptively controlled manufacturing systems are ensured.

Surface of a workpiece can be obtained with various machining processes and various machining parameters and the roughness depends on it. Surface roughness is one of the most important criteria for the quality of machine parts and products. As the competition grows and customers have the increased demands for quality, the surface roughness becomes one of the most important disciplines in market competition. Optimally smooth surface is needed at seat surface where a certain machine parts are permanently or periodically joined with other parts (pistons and cylinders, bearings and trunks, slide guides, couplings, etc.), and at parts where the surface loading is pronounced. For the first it is endeavoured to reduce the friction between parts and for the latter the appearance of notch effect that reduces the strength of dynamically loaded machine parts is avoided. Optimum surface quality is therefore needed due to the improvement of tribological properties, driving strength, resistance to corrosion and aesthetic appearance of products. The excessive surface quality requires considerably higher machining costs. This has to be taken into account when the optimally needful surface quality of machined parts is determined and therefore certain machining processes should be used when there is a valid reason. The accurate estimation of machined surface roughness has been brought into the focus of research for many scientists during a few decades.

2 INFLUENTIAL FACTORS ON CUTTING FORCE AND MACHINED SURFACE ROUGHNESS

2.1 Influential Factors on the Cutting Force

Figure 1 shows cutting force components during the longitudinal turning. The resultant force (cutting force) F_R can be decomposed into:

- tangential component of cutting force, F_c,
- feed component of cutting force, F_f,
- radial component of cutting force, F_p.

Expression for the resultant force is:

$$F_R = \sqrt{\left(F_c^{\,2} + F_f^{\,2} + F_p^{\,2}\right)} \qquad (1).$$

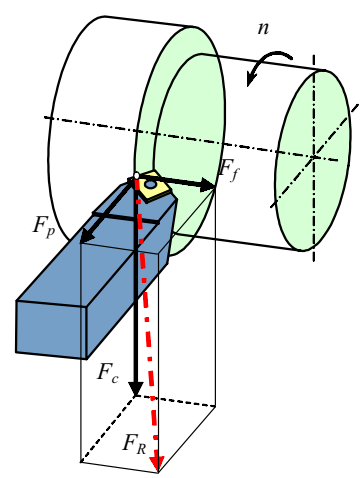

Fig. 1. *Cutting force components in the longitudinal turning process*

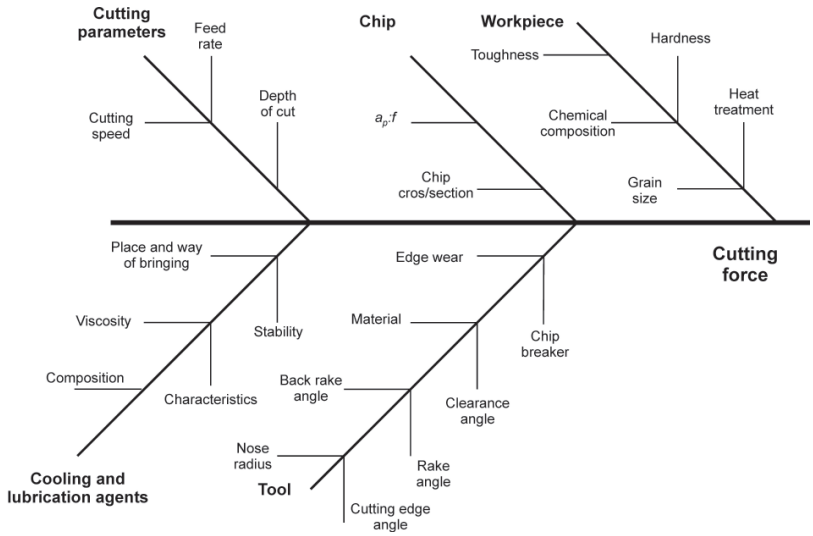

Fig. 2. *Fishbone diagram with the factors that influence the cutting force*

The tangential force component F_c always acts in the direction of cutting speed vector, the feed force component F_f is opposite to the feed rate and the radial force component F_p is perpendicular to these two force components.

The cutting force depends on:

- workpiece: hardness, toughness, heat treatment,
- tool: geometry (clearance angle α, rake angle γ, back rake angle λ, cutting edge angle κ, cutting tool nose radius r_ε), wear and chip breaker,
- size and shape of chip section,
- cutting parameters: speed v_c, dept of cut a_p, feed f,
- cooling and lubrication.

Figure 2 shows fishbone diagram with influential factors on the cutting force.

The values of feed rate and depth of cut define the undeformed chip cross-section. The larger chip cross-section follows the higher cutting force. The research [8] has shown that the cutting force is not increased proportionally with the increase of chip cross-section. The cause for that phenomenon is that lesser compression gives higher chip cross-sectional area.

Apart from the chip cross-section, considerable influence has the depth of cut to the feed rate ratio. The cross-section with the higher ratio gives the larger tangential component of the cutting force.

In the turning of steel it is observed that with the increase of cutting speed up to 0.83 m/s the cutting force rises a little and afterwards decreases. This phenomenon depends not only on the cutting force but also on the rake angle γ. With the further increase of cutting speed up to the value of 3.3 m/s the cutting force experiences decrement. The cutting speed values within interval 3.3 to 8.3 m/s almost have no influence on the cutting force [8]. These results are obtained for f = 0.74 mm/rev and a_p = 2 mm.

2.2 Influential Factors on the Surface Roughness

There are a great number of factors influencing the surface roughness. The most important of them are:

- machining parameters,
- build-up edge,
- tool geometry,
- machining time,
- tool and workpiece material,
- tool wear,
- dynamic behaviour of machining system,
- application of cooling and lubrication agent.

Fig. 3 shows influential factors on the machined surface roughness.

The influence of cutting speed is closely related to emergence of build-up edge (BUE) and that implies its effect on machined surface roughness. At lower cutting speed (within interval 0.16 and 0.6 m/s) the generation of BUE results with grater surface roughness. Increasing the cutting speed the influence of BUE is reduced and that entails the reduction of surface roughness. But exaggeration in the increase of cutting speed does

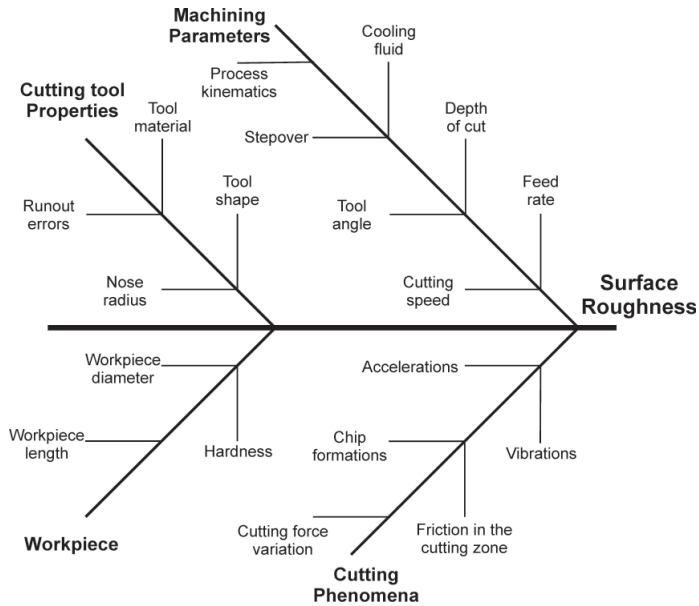

Fig. 3. *Fishbone diagram with the factors that affect the surface roughness* [9]

not influence the further reduction of surface roughness because tool wear is simultaneously increased and it keeps roughness nearly constant. Feed rate influence is directly proportional to surface roughness with the power of two. Larger feed rate causes higher machined surface roughness. The influence of feed rate is closely related to cutting tool nose radius. The reduction of feed even if its value is very small, does not result with the further reduction of surface roughness. At some boundary feed rate, which depends on cutting tool nose radius, roughness remains approximately constant at minimum possible level. Cutting tool nose radius influences surface roughness inversely proportionally, i.e. its increment causes the reduction of surface roughness. This reduction of roughness is also limited with some minimum value because the further increase of cutting tool nose radius causes vibrations that influence negatively on surface roughness. From a geometrical point of view, the depth of cut does not influence surface roughness because it has no influence on size and form of bumps. On the other hand, the depth of cut has the influence indirectly through the BUE generation, deformation of separated chips, cutting temperature, cutting force, vibrations, etc. [10].

3 DESIGN OF EXPERIMENTS

The planning of experiment means, on the basis of present cognition from the literature, experience or expected aim, beforehand prediction of all influential factors and actions that will result with new cognitions utilizing the rational researches. The experiments have been carried out using the factorial design of experiment. The turning is characterized with many factors, which directly or interconnected act on the course and outcome of an experiment. It is necessary to manage experiment with the statistical multifactor method due to statistical character of a machining process. In this search the design of experiment was achieved using the rotatory central composite design (RCCD). In the experimental research, modelling and adaptive control of multifactor processes the RCCD of experiment is very often used because it offers optimization possibility [11]. The aim of this search is to find mathematical models that describe the dependence of machined surface roughness and cutting force components on three cutting parameters:

- the cutting speed, v_c,
- the feed rate, f,
- the depth of cut, a_p.

The basis of the multifactor design of experiment can be visualized in the form of "black box". Figure 4 shows a "black box" for the longitudinal turning.

RCCD models the response using the empirical second-order polynomial:

$$y = b_0 + \sum_{i=0}^{k} b_i \cdot X_i + \sum_{1 \le i \lhd j}^{k} b_{ij} \cdot X_i \cdot X_j + \sum_{i=1}^{k} b_{ii} \cdot X_i^2 \quad (2),$$

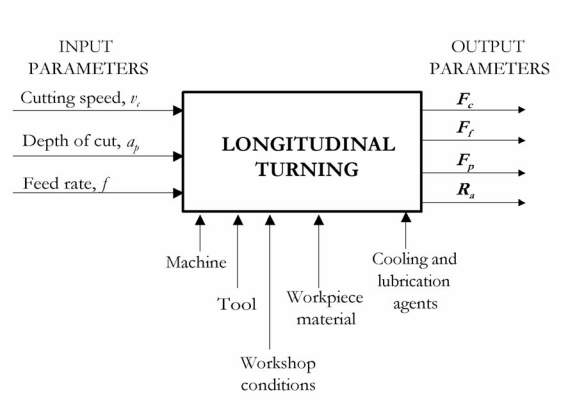

Fig. 4. *Form of "black box" for longitudinal turning*

where:
- b_0, b_i, b_{ij}, b_{ii} are the regression coefficients,
- X_i are the coded values of input parameters.

In order to determine the required number of experimental points for RCCD the following expression is used:

$$N = 2^k + 2k + n_0 = n_k + n_\alpha + n_0 \qquad (3),$$

where:
- k is the number of parameters,
- n_0 is the repeated design number of the average level,
- n_α is the design number on the central axes.

RCCD of experiment demands 8 experiments (3 factors on two levels, 2^3), 6 experiments on the central axes and 6 experiments on the average level, what makes total of 20 experiments.

Adding the points to the central axes where $x_i = \pm \alpha_\alpha$, and $\alpha_\alpha = 1.682$, the 3-factorial RCCD of experiment is obtained. The minimum and maximum values of chosen cutting parameters as well as the coded input factors are presented in Table 1.

4 NEURAL NETWORK MODELING

Artificial neural networks grew out of attempts to mimic the ability of biological nervous system to learn from the environment. Biological nervous systems perform extremely complex tasks using a very large number of simple processing units (called neurons) and their numerous interconnections. Similar structure uses ANN. The units in an ANN are arranged in a layered feed forward topology. Artificial neuron receives numerous inputs (either from original data, or from the output of other neurons in the neural network). Each input comes via a connection that has strength (or *weight*). Each neuron also has a threshold value that is subtracted from the calculated weighted sum of the inputs. In this way the activation signal of the neuron is obtained. The activation signal is passed through an activation function (also called transfer function) in order to produce the output of the neuron. If the number of layers and the number of units in each layer are sufficiently large, multilayer perception (the most popular architecture) can model functions of arbitrary complexity [12] to [15]. For both systems (biological and artificial) the learning process is achieving by altering the "strength" of synaptic connections (weights). ANN learns the relationship between input and output through training. In supervised learning a set of training data needs to be collected. The training data contains examples of input/output pairs. Once the number of layers, and number of units in each layer, has been selected, the weights and thresholds of network must be adjusted, using one of the training algorithms, so as to minimize the prediction error made by the network. The error of the network is determined by comparing the outputs of the network with the targets and then calculating an error function. The most common error function is the sum-squared error, where the individual errors of output units on each training pair are squared and summed together [14]. The network error is used to adjust the weights, and then the process repeats. The learning algorithm progresses through a number

Table 1. *Physical values and coded indexes of input factors*

Input factors	**Coded values of input parameters**				
	$x_{-i\alpha}$	$x_{-i,\min}$	x_{-i0}	$x_{i,\max}$	$x_{+i\alpha}$
	-1.682	-1	0	+1	+1.682
$x_1 = v_c$, **m/min**	115.9	150	200	250	284.1
$x_2 = a_p$, **mm**	0.4	0.6	0.9	1.2	1.4
$x_3 = f$, **mm/rev**	0.12	0.16	0.22	0.28	0.32

of epochs. The training process stops when a given number of epochs is exceeded, or when the error reaches a desirable value, or when the error stops improving. The most desirable property of a network is its ability to generalize to new (unseen) cases. A network with more weights models a more complex function, and is therefore prone to over-fitting. A network with fewer weights may not be sufficiently powerful to model the underlying function [12], [13] and [15].

In order to mathematically model the influence of cutting parameters on the cutting force components and the surface roughness a three layer feed-forward ANN has been chosen. In accordance with the aim of this research the chosen ANN model had three neurons in the input layer, twenty neurons in the hidden layer and one neuron in the output layer (Fig. 5).

The same network architecture has been used for modelling the each of four physical relations separately. Namely, in this way the three cutting parameters (cutting speed, depth of cut and feed) are related with the tangential component of cutting force, feed component of cutting force, radial component of cutting force and surface roughness. The network models are named as follows:

- Model 1 - relates cutting parameters and tangential component of cutting force,
- Model 2 - relates cutting parameters and feed component of cutting force,
- Model 3 - relates cutting parameters and radial component of cutting force,
- Model 4 - relates cutting parameters and surface roughness.

In the hidden and output layer sigmoid and linear activation function has been used, respectively. The resilient back-propagation (Rprop) learning algorithm [16] and [17], with supervised learning mechanism, was used for all models. During the training, the initial weight change value for Rprop learning algorithm was taken 0.07 for all models. Before training, input and output variables were normalized within the range of –0.9 and 0.9. In order to avoid over-fitting or under-fitting the weight decay regularization [18] have been applied to all models. The choice of appropriate values for the regularization parameter is essential since it determines the degree of fitting. The leave-one-out cross-validation procedure was used to estimate the regularization parameter of all models. Data set for training and testing the network consisted of 22 data pairs for each of the models. The 15 data pairs were taken from the conducted design of experiment and 7 additional data pairs were measured separately. Out of the data set 4 data pairs were selected randomly and the testing data set was obtained. Training data set consisted of 18 training pairs. After the training, all models were tested to their generalization ability. Testing was performed with the testing data that had not been used in the training process. Results of training and testing, in the form of regression analysis, for Model 1 are shown in Figure 6.

R is a measure of agreement between the outputs and targets. The aim is to get R-value very close or equal to 1. In the example on Figure 6, R-values are very close to 1 and that indicates very good fit. For the other models the R-values are 0.98 or higher for both training and testing. In order to conduct the training, testing and simulation of the neural network models, a neural network toolbox embedded in MATLAB [19] was used.

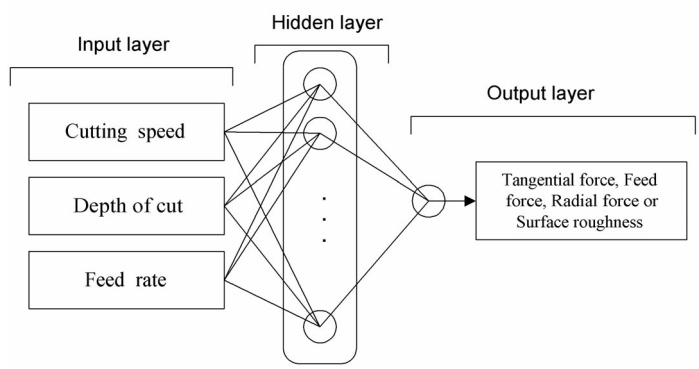

Fig. 5. *Neural network model*

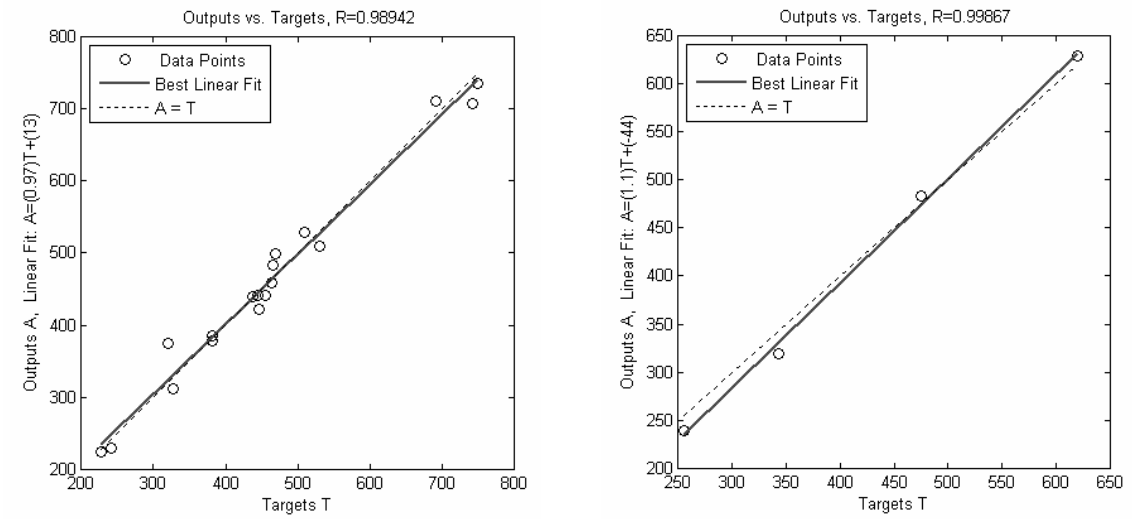

a) b)

Fig. 6. Result of training (a) and testing for generalization ability (b) of Model 1

5 EXPERIMENT PERFORMANCE

The experiments for measuring the cutting force components and surface roughness were carried out on the universal lathe "Prvomajska" D-420/1500. The cutting force components were measured utilizing force transducer KISTLER (Type: 9257 A) produced in Winterthur Switzerland. The roughness measurements were performed with the "SURTRONIC 3+" instrument, produced by Rank Taylor Hobson. Before the measurements had been carried out all the measuring instruments were calibrated. The longitudinal turning experiments were performed by a tool for the external machining. The tool has been composed of the tool holder PTGNR2020K16 and the cutting insert TNMG160408–PF4015, produced by SANDVIK Coromant. The material of workpiece was carbon steel Ck45. The workpiece was in a form of axle with bored centering holes. On the lathe the workpiece was prepared in order to remove rust, grooves and all damages from the surface and to obtain the workpiece with wanted dimensions. All experiments were carried out without the cooling and lubrication agents.

Altogether 33 experiments were conducted. Twenty experiments were conducted in order to allow performing ANOVA and regression analysis, and additional 13 experiments to obtain additional data for neural network training and verification of modelling.

6 RESULTS OF BOTH STATISTICAL ANALYSIS AND NEURAL NETWORKS SIMULATION

The twenty measured values of cutting force components and surface roughness, (Table 2), are input data for the second-order regression models and ANOVA. The ANOVA and regression analysis have been carried out using program package "Design Expert 6". The ANOVA has shown which factors and interactions had an important influence on the cutting force components and the surface roughness.

Applying the regression analysis the coefficients of regression, multi-regression factors, standard false evaluation and the value of *t*-test have been determined. After omitting insignificant factors and interactions the mathematical models for the tangential component of cutting force, feed component of cutting force, radial component of cutting force and surface roughness are obtained as follows:

Tangential component of cutting force:

$$F_c = -144.76 + 0.595 \cdot v_c + 198.91 \cdot a_p + \\ +559.714 \cdot f - 2.526 \cdot v_c \cdot f + 366.041 \cdot a_p \cdot f \quad (4).$$

Feed component of cutting force:

$$F_f = 353.15 - 0.808 \cdot v_c - 180.064 \cdot a_p - \\ - 817.523 \cdot f + 152.182 \cdot a_p^2 + 3047.996 \cdot f^2 \quad (5).$$

Radial component of cutting force:

Table 2. *Experimental data*

Exp. number	v_c (m/min)	a_p (mm)	f (mm/rev)	F_c (N)	F_f (N)	F_p (N)	Ra (μm)
1	284.1	0.90	0.224	456	175	155	2.23
2	250	0.60	0.160	242	94	120	1.81
3	250	1.20	0.280	743	260	230	3.65
4	250	1.20	0.160	466	210	170	1.96
5	250	0.60	0.280	382	126	178	3.13
6	200	0.90	0.125	327	162	145	1.43
7	200	0.40	0.224	227	78	163	2.39
8	200	1.40	0.224	692	300	234	2.44
9	200	0.90	0.315	620	209	225	4.43
10	200	0.90	0.224	464	184	165	2.38
11	200	0.90	0.224	459	181	160	2.34
12	200	0.90	0.224	465	185	168	2.41
13	200	0.90	0.224	468	188	162	2.40
14	200	0.90	0.224	466	182	164	2.39
15	200	0.90	0.224	460	180	169	2.36
16	150	1.20	0.280	750	320	250	3.60
17	150	0.60	0.160	255	105	150	1.65
18	150	0.60	0.280	447	160	218	3.44
19	150	1.20	0.160	470	230	208	1.71
20	115.9	0.90	0.224	475	193	178	2.39

$$F_p = 17.237 - 0.184 \cdot v_c + 2.599 \cdot a_p + \\ + 769.93 \cdot f + 1560.196 \cdot a_p \cdot f \quad (6).$$

Surface roughness:

$$Ra = 2.67 - 1.81 \cdot a_p - 14.875 \cdot f + \\ + 73.662 \cdot f^2 - 0.0285 \cdot v_c \cdot f \quad (7).$$

The squares of regression coefficient (r^2) for F_c, F_f, F_p and Ra are 0.9827, 0.978, 0.9935 and 0.993 respectively.

Table 3 shows 13 additional measured experimental data. Data marked with asterisk (*) were not used either in the network training or in the regression analysis. These data were utilized for the validation of both regression analysis and ANN modelling.

Table 4 shows the values of cutting force components and surface roughness obtained from the both type of modelling, i.e. from the regression

Table 3. *Additional measured experimental data*

Exp. number	v_c (m/min)	a_p (mm)	f (mm/rev)	F_c (N)	F_f (N)	F_p (N)	Ra (μm)
21*	300	1.60	0.400	1105	392	425	5.80
22*	280	0.50	0.315	355	95	201	3.97
23	240	0.70	0.200	343	123	128	2.04
24	230	1.10	0.160	445	200	160	1.63
25*	225	1.00	0.250	555	207	190	2.90
26	220	0.85	0.280	510	194	198	3.43
27	210	0.65	0.250	320	120	185	2.63
28*	190	1.00	0.280	610	230	216	3.48
29	170	0.80	0.200	381	161	173	2.05
30	160	1.00	0.180	438	204	170	1.82
31*	150	0.70	0.180	325	130	160	1.80
32	140	1.30	0.140	530	250	205	1.45
33*	100	0.30	0.125	117	29	110	1.60

Table 4. *Values obtained by regression analysis and neural network models*

Exp. numb.	Regression				Neural network			
	F_c (N)	F_f (N)	F_p (N)	Ra (µm)	F_c (N)	F_f (N)	F_p (N)	Ra (µm)
21	1272.31	367.04	447.5	7.76	1064.67	399.87	433.77	6.19
22	336.2	91.64	218.53	3.84	369.67	100.02	196.8	3.91
23	333.79	130.22	134.05	2	329.18	112.88	124.91	2
24	434.55	198.12	161.69	1.78	441.88	198.36	162.86	1.77
25	560.81	211.76	181.17	2.83	549.4	213.94	215.04	2.82
26	532.53	188.92	192.28	3.39	529.11	188.47	208.72	3.4
27	385.12	136.47	166.73	2.73	374.59	132.79	172.47	2.7
28	624.43	236.62	209.64	3.51	629.88	235.51	224.3	3.52
29	391.57	160.48	155.61	2.02	377.71	159.32	173.88	2.06
30	434.76	196.57	169.31	1.79	440.09	199.39	182.81	1.84
31	324.89	131.77	153.81	1.81	316.97	135.58	161.39	1.83
32	444.41	239.51	222.44	1.42	510.06	254.3	219.86	1.47
33	143.18	17.78	188.84	1.68	111.22	37.85	125.63	1.58

Table 5. *Relative error for data taken within interval limited with the min and max values of cutting parameters*

Exp. number	Relative error using regression (%)				Relative error using neural network (%)			
	F_c	F_f	F_p	Ra	F_c	F_f	F_p	Ra
25	1.05	2.30	4.65	2.41	1.01	3.35	13.18	2.76
28	2.37	2.88	2.94	0.86	3.26	2.40	3.84	1.15
31	0.03	1.36	3.87	0.56	2.47	4.29	0.87	1.67
Average:	1.15	2.18	3.82	1.28	2.25	3.35	5.96	1.86
	Total average: 2.11 %				Total average: 3.35 %			

Equations (4) to (7) and from the simulation of neural network models.

In order to test which modelling method gives better prediction, a relative error of deviations from measured values have been calculated. In these calculations only experimental data that were not used for modelling either the regression equations or neural network models were utilized.

These experimental data have been also divided into two sets. The first data set consists of three randomly chosen experiments (experiments 25, 28 and 31) for which the values of the cutting parameters (Table 4) have been taken from the interval limited with maximum and minimum values (Table 1) used in this study. The second data set consists of randomly chosen experiments 21, 22 and 33 for which the cutting parameters have been taken outside the min/max interval. In this way the both methods of modelling have been tested for the possibility of both interpolation and extrapolation. The reason for choosing the only three experiments in both sets is the costs reduction and the attention to show that with the small number of experiments neural network modelling is able to give similar results as the DOE approach. The results of relative error calculations for the values of the cutting parameters inside and outside the interval are shown in Table 5 and Table 6, respectively.

From the presented results it can be seen that the modelling with regression analysis gives the lesser total average relative error for the data taken within the interval. Although the total error for both modelling is quite low, the regression analysis is able to give somewhat better prediction when the interpolation is considered. It should be noticed that ANN models have learned and tested from only 22 data pairs. This implies that more data pairs would give better results. Regarding the extrapolation, the neural network modelling gives much better results, although the total average relative error is much larger when comparing to the results obtained in the interpolation.

Fig. 7 shows the tangential component of cutting

Table 6. *Relative error for data taken outside the interval limited with the min and max values of cutting parameters*

Exp. number	Relative error using regression (%)				Relative error using neural network (%)			
	F_c	F_f	F_p	Ra	F_c	F_f	F_p	Ra
21	15.14	6.37	5.29	33.79	3.65	2.01	2.06	6.72
22	5.30	3.54	8.72	3.72	4.13	5.28	2.09	1.51
33	22.38	38.69	71.67	5.00	4.94	30.52	14.21	1.25
Average:	14.27	16.20	28.56	14.02	4.24	12.60	6.12	3.16
	Total average: 18.26 %				Total average: 6.53 %			

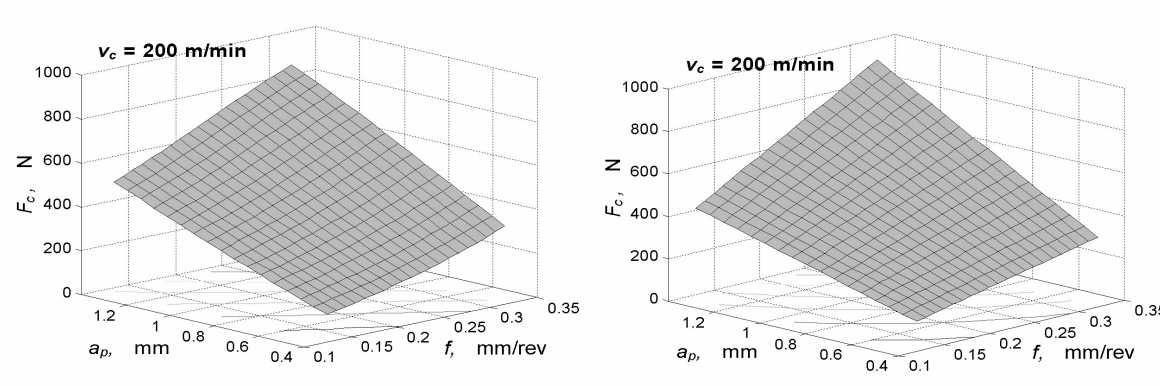

a) b)

Fig. 7. *Response surface for tangential component of cutting force as a function of feed rate and depth of cut obtained from neural network (a) and regression analysis (b); for constant cutting speed of 200 m/min*

force as a function of feed rate and depth of cut. The shown results have been obtained from neural network simulation (Fig. 7a) and regression analysis (Fig. 7b) with the constant cutting speed of 200 m/min. Response surfaces on Fig. 7 show that in both cases similar results are obtained. Namely, both modelling predict the minimum value of the tangential component of cutting force when both feed rate and depth of cut are minimized.

Figure 8 shows the results obtained from neural network simulation (Fig. 8a) and regression analysis (Fig. 8b) for the feed component of cutting force and its dependence on feed rate and depth of cut. Again it can be seen that both methods predict that the feed component of cutting force linearly depends on both, feed rate and depth of cut. The minimum value of the feed component of cutting force is achieved at minimum both feed rate and depth of cut.

On Figure 9 it can be seen the response surfaces for radial component of cutting force as a function of feed rate and depth of cut obtained from neural network (Fig. 9a) and regression analysis (Fig. 9b). Cutting speed has been kept constant at 200 m/min. Both modelling methodologies predict similar behaviour of the radial component of cutting force with change in feed rate and depth of cut. Again the minimum value of the radial component of cutting force is achieved when feed rate and depth of cut reach their minimum values.

Figure 10 shows the dependence of surface roughness on feed rate and depth of cut for neural network (Fig. 10a) and regression analysis (Fig. 10b) modelling methodology when cutting speed is constant 200 m/min. Both methodologies give the similar results. They both predict that dept of cut has no at all or has slight influence on the surface roughness. Feed rate has dominant influence on *Ra*. It is evident that the minimum surface roughness is obtained at minimum feed rate.

From the conducted optimization the optimum values of cutting parameters that give the minimum values for the cutting force components and surface roughness were obtained. The optimization was carried out using Genetic algorithm [20] and the results of optimization are presented in Table 7.

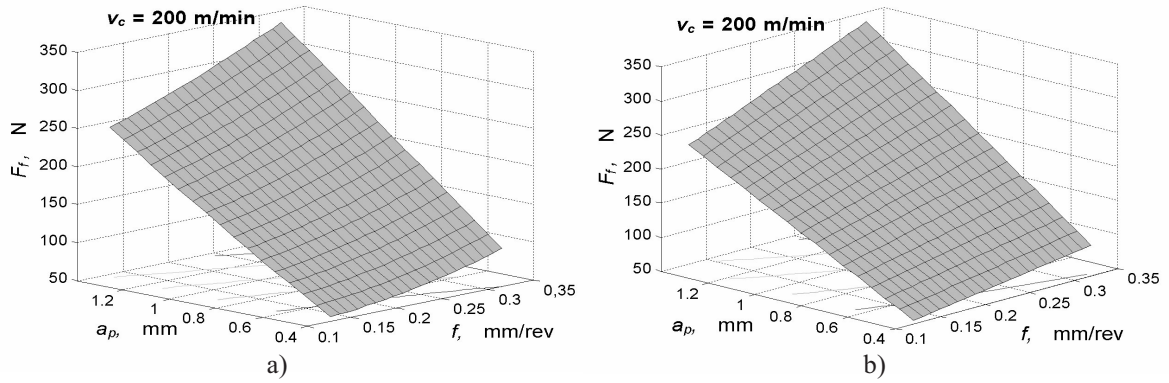

Fig. 8. Response surface for feed component of cutting force as a function of feed rate and depth of cut obtained from neural network (a) and regression analysis (b); for constant cutting speed of 200 m/min

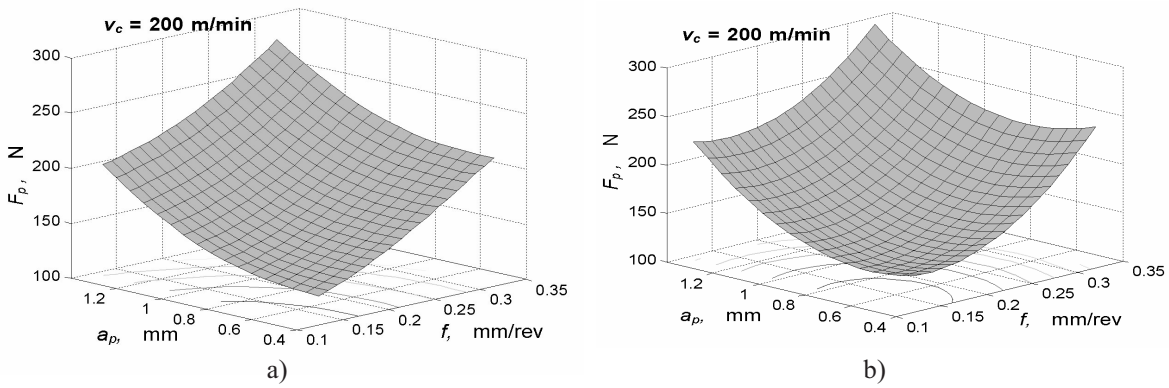

Fig. 9. Response surface for radial component of cutting force as a function of feed rate and depth of cut obtained from neural network (a) and regression analysis (b); for constant cutting speed of 200 m/min

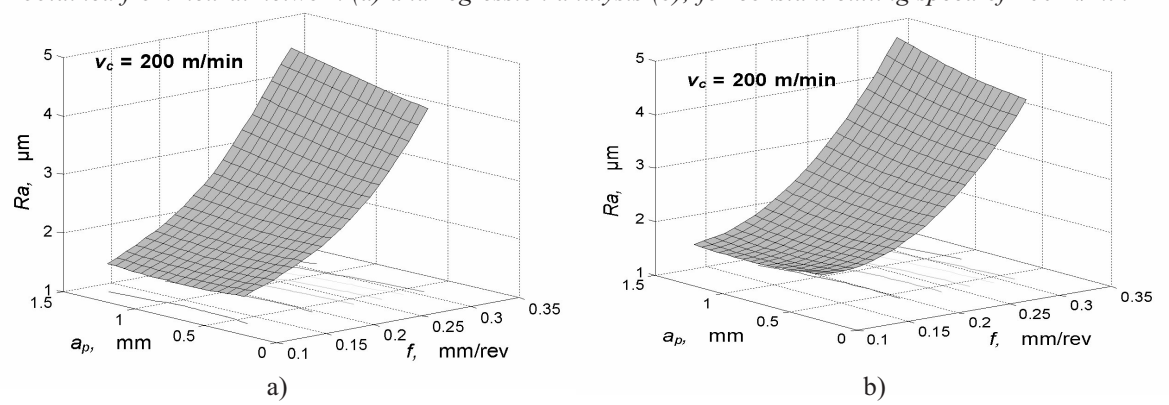

Fig. 10. Response surface for surface roughness as a function of feed rate and depth of cut obtained from neural network (a) and regression analysis (b); for constant cutting speed of 200 m/min

7 CONCLUSION

The aim of this paper is the examination of possibility of the cutting force components and the surface roughness modelling. In order to model dependency of the cutting force components and the surface roughness on the cutting speed, the depth of cut and the feed rate, regression analysis and neural network methodology were used. Both methodologies were tested for interpolation and extrapolation capability. Regarding the interpolation, both methodologies are found to be capable for accurate predictions (approximately relative error of 3%) of the cutting force components and the surface roughness, although regression models give somewhat better predictions. In the case of the extrapolation neural

Table 7. *Optimum cutting parameters*

Optimum cutting parameters			Minimum values of output parameters
v_c (m/min)	a_p (mm)	f (mm/rev)	
206.3	0.6	0.16	F_c = 249.2 N
192	0.6	0.16	F_f = 102 N
250	0.6	0.16	F_p = 120 N
150	1.11	0.16	Ra = 1.59 μm

network models give significantly better predictions. Neural network models were trained with 18 experimental data so even with the small data set ANNs are capable to achieve predictions nearly as accurate as regression models.

8 REFERENCES

[1] Chang-Xue, F., Xianfeng, W. Development of empirical models for surface roughness prediction in finish turning. *International Journal of Advanced Manufacturing Technology*, vol. 20, no. 5, 2002.

[2] Cukor, G., Kuljanić, E. A genetic programming approach for developing the machinability models. *9th International Scientific Conference on Production Engineering CIM 2003*, Lumbarda, 2003, p. I-031-038.

[3] Cukor, G., Kuljanić, E., Barišić, B. Optimisation of machining process using evolutionary algorithms. *AMST'05 - Advanced Manufacturing Systems and Technology, CISM Courses and Lectures No. 486*, Wien, New York: Springer, 2005, p. 135-142.

[4] Bajić D., Majce, I., Optimization of parameters of turning process. *International Scientific Conference on Production Engineering,* Lumbarda, 2006, p. 129-136.

[5] Bajić, D., Špar, I., Veža, I. Mathematical modelling of surface roughness in turning process. *5th DAAAM International Conference on Advanced Technologies for Developing Countries*, Rijeka, 2006, p. 113-118.

[6] Bajić, D., Gjeldum, N., Zulim, R. Modelling of cutting power and cutting resistance in turning process. *11th International Scientific Conference on Production Engineering CIM 2007*, Biograd, 2007, p. 61-68.

[7] Čuš, F. *Modeling and optimization of metal cutting*. University o Maribor, Faculty of Mechanical Engineering, Maribor, 2005.

[8] Šavar, Š. *Chip-forming metal machining*, Part I and II, Zagreb: School book, 1991. (In Croatian).

[9] Bernados, P.G., Vosniakos, G.C. Predicting surface roughness in machining: a review. *International Journal of Machine Tools & Manufacture*, 43 (2003), p. 833-844.

[10] Ekinović, S. *Chip-forming machining*. Zenica: Dom štampe, 2001.

[11] Montgomery, D.C. *Design and analysis of experiments*. New York: John Wiley & Sons, Inc., 1997.

[12] Korošec, M., Balič, J., Kopač, J. Neural network based manufacturability evaluation of free form machining. *Int. j. mach. tools manuf.*, January 2005, vol. 45, iss. 1, p. 13-20.

[13] Župerl, U., Čuš, F., Kopač, J. Cutting force modelling in end milling with multilevel perceptron. *Annals of DAAAM for 2003 & proceedings of the 14th International DAAAM symposium "Intelligent manufacturing & Automation: focus on reconstruction and development"*, 22-25th October 2003, Sarajevo, Bosnia and Hercegovina. Vienna: DAAAM International, 2003, str. 517-518.

[14] Fausett, L. *Fundamentals of neural networks*. New York: Prentice Hall, 1994.

[15] Bishop, C. *Neural networks for pattern recognition*. Oxford: University Press, 1995.

[16] Riedmiller, M., Braun, H. A direct adaptive method for faster backprogagation learning: The RPROP algorithm. *Proceedings of the IEEE International Conference on Neural Networks (ICNN)*, San Francisco (1993), p. 586–591.

[17] Anastasiadis, D.A., Magoulas, D.G., Vrahatis, N.M. New globally convergent training scheme based on the resilient propagation algorithm. *Neurocomputing*, 64 (2005), p. 253–270.

[18] Krogh, A., Hertz, J. A. A simple weight decay can improve generalization. *Advances in Neural Information Processing Systems*, vol. 4, San Mateo, CA: Morgan Kaufmann, 1992, p. 950-957.

[19] *MATLAB User's Guide: The Mathworks*, 2003, Neural Network Toolbox.

[20] Balič, J. *Inteligent manufacturing systems*, University o Maribor, Faculty of Mechanical Engineering, Maribor, 2004.

Strojniški vestnik - Journal of Mechanical Engineering 54(2008)5, 334-346
UDC 625.739
UDC 656.142
Paper received: 19.7.2007
Paper accepted: 19.12.2007

The Use of Micro-Simulation in Determining the Capacity of a Roundabout with a Multi-Channel Pedestrian Flow

Tomaž Tollazzi[1] - Tone Lerher[2] - Matjaž Šraml[1,*]
[1]University of Maribor, Faculty of Civil Engineering, Slovenia
[2]University of Maribor, Faculty of Mechanical Engineering, Slovenia

The main purpose of this paper is to analyse the influence of the multi-channel pedestrian flow on the capacity of the one-lane roundabout, using discrete simulation methods. The proposed model is based on the theory of the expected time void between the units of pedestrian traffic flow, which have the priority when crossing the arm of the roundabout. The proposed model represents an upgrade of the previous research in the field of modelling traffic flows in the one-lane roundabout. While the previous model of the pedestrian crossing is handled as the single-channel system in which the pedestrians arrive randomly from one side of the pedestrian crossing only, the proposed model deals with the multi-channel system in which the pedestrians arrive randomly from both sides of the pedestrian crossing. In this way the mathematical model can better illustrate the real conditions. The previous model considers only the disturbances of entry traffic flow of motorised vehicles caused by the pedestrian flow crossing the roundabout arm. The proposed model considers the disturbances caused by the circular traffic flow of motorised vehicles as well. A simulation analysis has been conducted on the roundabout at Koroška Street in Maribor, in which the counting of the motorised traffic flow and the pedestrian flow has been performed in the morning peek hour. The results of the analysis have indicated a high reserve of the capacity for pedestrians who arrive from the left and right sides of the roundabout with regard to motorised vehicles in the analysed arm of the roundabout. The real reserve of the capacity would otherwise be smaller in case of enlargement of the motorised vehicle flow in the future. Nevertheless it would be high enough for an undisturbed traffic flow of motorised vehicles through the roundabout to be possible. The presented methodology represents a practicable and adaptable tool for planning the roundabout capacity in practice and for the sensitivity analysis of individual variables on the throughput capacity of the roundabout.

Keywords: roundabout, pedestrian flow, traffic flow modeling, simulation models

0 INTRODUCTION

In one-lane roundabouts difficulties with the throughout capacity of the roundabout can occur due to a strong pedestrian traffic flow. Vehicles on entries and exits should as a rule give priority to pedestrians. Due to this fact disturbances occur in the main vehicle flow [1] to [3].

The possibility of a blockage of the roundabout can be determined in several ways. In the past, authors [4] and [5] have used different ways of determining the capacity of roundabouts and different approaches of determining the influence of the non-motorised flow on the capacity of a roundabout. The common features of all these approaches are mathematical models and a definite simplification for the calculation of the roundabout capacity [6]. Among simple methods where only a diagram or one equation is used are the German method for determining the pedestrian influence [7] and the Dutch method for determining the cyclist influence [8] on the throughout capacity of the one-lane roundabout.

Two major groups of methods for determining the capacity of a roundabout and the resulting influences of pedestrian and cyclist flows on the roundabout capacity have been dominant lately. The first group consists of deterministic and the second group of stochastic methods. The significance of simulation methods is also increasing, with most credit going to more and more capable computers and numerous possibilities of creating complex mathematical models that enable a good comparability of results with authentic

*Corr. Author's Address: University of Maribor, Faculty of Civil Engineering, Smetanova 17, SI-2000 Maribor, sraml.matjaz@uni-mb.si

models. Several analytical and micro-simulation models offer variants of the roundabout analysis based on either the gap acceptance or empirical approaches. Examples of such codes are RODEL [9], PARAMICS, VISSIM, SYNCHRO [9], SIDRA [10] to [12], etc. For the presented problem the computer tool AutoMod [13] has been used. Although the chosen code is not specialised for traffic simulation, the discrete simulation algorithm is very efficient for analysing different situation events of traffic flows. The proposed model derives from the theory of the expected time void in the pedestrian traffic flow, used by vehicles for entering and exiting the roundabout, presuming that pedestrians always have priority. The geometry of the roundabout was copied in the simulation model, whereby all the necessary data are taken into account. For the model calibration with real conditions in practice, the counting of the motorised traffic flow and the pedestrian flow in the analysed arm of the roundabout has been performed (Fig. 2). The cyclists are not discussed in this model. The arrivals of motorised vehicles in the roundabout are based on the *Poisson statistical distribution*, whereby the mean value (λ_3) has been obtained on the basis of the conducted counting in the morning peek hour. Additionally, the circular flow of motorised vehicles in the roundabout was considered, which also presents an additional disturbance for the main flow of motorised vehicles on the entry. The pedestrian flows are defined as a multi-channel flow with the *Poisson statistical distribution* with mean values (λ_1 and λ_2), which have been obtained on the basis of the conducted counting in the morning peak hours. In the model we also consider definite restrictions such as: the constant mean velocity of pedestrians $v_{1,2}$ and the constant mean velocity of motorised vehicles $v_{3,4,5}$ without any respect to the driver behaviour. The main purpose of this paper is to analyse the influence of the pedestrian flow and consequently the capacity of the one-lane three-armed roundabout, using the discreet numeric simulation modelling.

1 PROBLEM DESCRIPTION

When defining the reduction of the roundabout capacity because of the pedestrian flow crossing the arm of the roundabout, two different samples can be distinguished. In the first case, the traversing pedestrian flow influences the capacity of the roundabout, but the traffic still flows normally. In the second case, the influence of the pedestrian flow is so large that bottlenecks on the roundabout entry and exit are possible, which then influences the queues upon the adjacent roundabout arms [3]. If the vehicle queue is so long that it reaches the previous entry, problems with the occupation of the roundabout arise and a blockage of the entire roundabout can occur. In reality, the abovementioned problems of entering and exiting a roundabout normally appear simultaneously. It is also common for the intensive pedestrian flow to traverse only one arm of the roundabout, although in some cases the pedestrian flow traverses all arms at once. In these

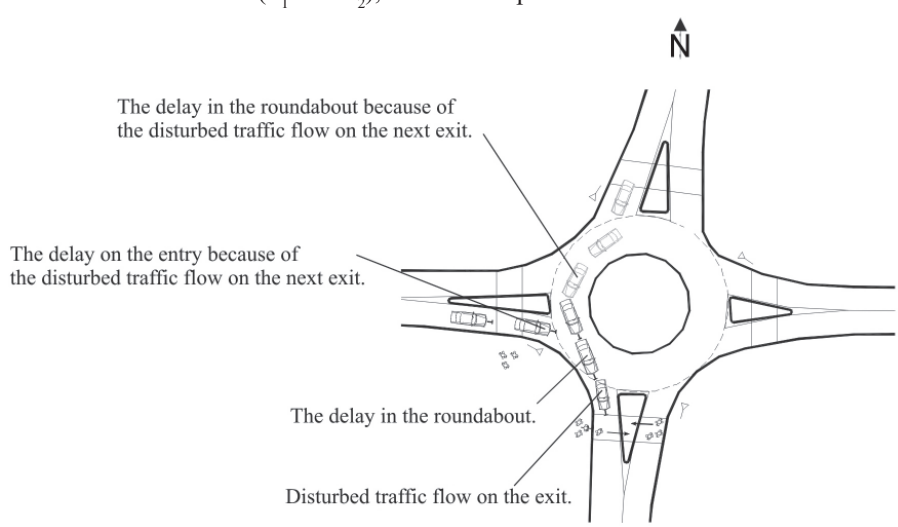

Fig. 1. *Queue formation in a roundabout [3]*

cases the blockage of the roundabout is easier to occur. In the following paragraph, an example of the roundabout where a strong pedestrian flow traverses only one arm is described in order to make it easier to explain.

The priority pedestrian flow traverses the southern arm of the roundabout (Fig. 1). Time interspaces between two consecutive pedestrians are long enough; therefore the vehicles exiting the roundabout make use of them and exit the roundabout without disruption. The vehicle flow on the exit is stable in this case.

In the one-lane roundabout with the waiting space for one vehicle only the following three situations can generally occur in the waiting place between the pedestrian crossing and the outer edge of the circulatory roadway:

- time interspaces between individual units of the traversing pedestrian flow are sufficient for the vehicle flow, therefore there are no waiting vehicles in the waiting place;
- time interspaces between individual units of the traversing pedestrian flow are still sufficient for the vehicle flow, although vehicles do wait in the waiting place;
- time interspaces between individual units of the traversing pedestrian flow are not large enough, the waiting line is occupied all the time and every next vehicle waits in the circulatory roadway.

How many times these situations occur, what are the conditions for the occurrence of these situations, what conditions have to be fulfilled for a blockage of one roundabout arm and at what traffic load of the pedestrian or motorised traffic flow the disturbance is transferred from one to another arm are the questions, the answers to which determine the influence of the pedestrian flow on the throughput capacity and the efficiency of the one-lane roundabout. It is obvious that so complex influences and mutual actions of different variables cannot be solved without appropriate mathematical models or discreet simulations of the traffic flows of motorised vehicles, pedestrians and/or cyclists. In the following chapter the basic theoretical background for the analysis of the traffic flow in the roundabout is given. The simulation model and the simulation analysis of real and variable data which are presumed to be the case in the future (the enlargement of the motorised vehicle and pedestrian flows) are given.

2 THE SIMULATION OF THE TRAFFIC FLOW IN THE ROUNDABOUT

The analysis of the traffic flow using discreet event simulations presents a successful way of analysing complex intersections for determining capacity, as presented in [10] to [16]. According to discreet models and traffic movement, simulation methods can be generally divided into two groups, (*i*) macroscopic and (*ii*) microscopic models. With macroscopic models the emphasis is laid on the traffic flows. Unlike microscopic models, macroscopic models focus on a long-term planning period. With microscopic models every vehicle, pedestrian, cyclist, etc. can be described with real characteristics (dimension, velocities, accelerations, decelerations, etc.).

Considering the complexity of the analytical model of the roundabout and the application of the discreet simulation technique, the discreet event simulation was used for the analysis of the flow capacity of the observed area of the roundabout. In this contribution, the program tool AutoMod [13] has been used for the capacity analysis of the roundabout. AutoMod is mostly used to implement discreet numeric simulations of internal logistic systems and all other logistic discreet systems [1] and [17]. The programming tool consists of individual programming modules that construct the AutoMod as integrity. When modelling a general system, the already built-in elements (continuous transporters, automated transport vehicles, etc.) that present certain complexes in the chosen process can be used. With the help of command lines in the source file the implementation of the simulation is determined. On the basis of the acquired results of the simulation analysis and its statistical processing in AutoStat [13], the success and the efficiency of the system are analysed.

In the following section the steps of the simulation and the analysis of the traffic flow of the motorised vehicles in the three-armed, one-lane roundabout with a strong pedestrian flow on Koroška Street in Maribor (Fig. 2) are shown. Actual geometrical and kinematics data are acquired from a sample of pedestrian and motorised vehicle traffic flows on the observed area of the roundabout, established by counting traffic and statistically evaluating the acquired data (Table 2).

2.1 Input Data for Building the Simulation Model – An Analysis of the Actual Situation of the Traffic Flow Performed by Counting Pedestrians and Vehicles

When building the simulation model for a definite area of the one-lane three-armed roundabout (Fig. 2), the actual geometry of the roundabout and the velocity characteristics of motorised vehicles and pedestrians (Table 1) were considered. The measured data was used for the calibration of the simulation model. The counting – the areas where counting was performed are labelled with MP_i (Fig. 2) and are presented in Table 2. The mean velocity of the Personal Car Unit (PCU) before entering the roundabout equals 40 *km/h*, in the area of the roundabout it equals 20 *km/h*; the mean velocity of pedestrians equals 5 *km/h*. The arrivals of pedestrians are based on the multi-channel system from both sides with probability density functions $f_{P1}(t)$ and $f_{P2}(t)$ (Fig. 2). The influence of cyclists is neglected. The influence of the roundabout circulation is taken into account (MP_3), with the presumed mean velocity 20 *km/h*. For all motorised vehicles (the main traffic flow MP_4, the circulating flow in the roundabout MP_3 and the traffic flow from the roundabout in the direction of Koroška Street – East MP_5), the personal car unit model (PCU) is applied.

A three-hour (6.30 to 9.30 AM) counting has been performed on the observed area for the requirements of the analysis, separately for the traffic flow of the motorised vehicles and pedestrian traffic. Based on the traffic count of motorised vehicles and pedestrians of the roundabout on Koroška Street, the acquired data have been statistically evaluated. The results of the statistical evaluation of the traffic of motorised vehicles and pedestrian traffic that are used in this work are presented in Table 2. The data in table 2 refers to the period from 6.30 to 9.30 AM.

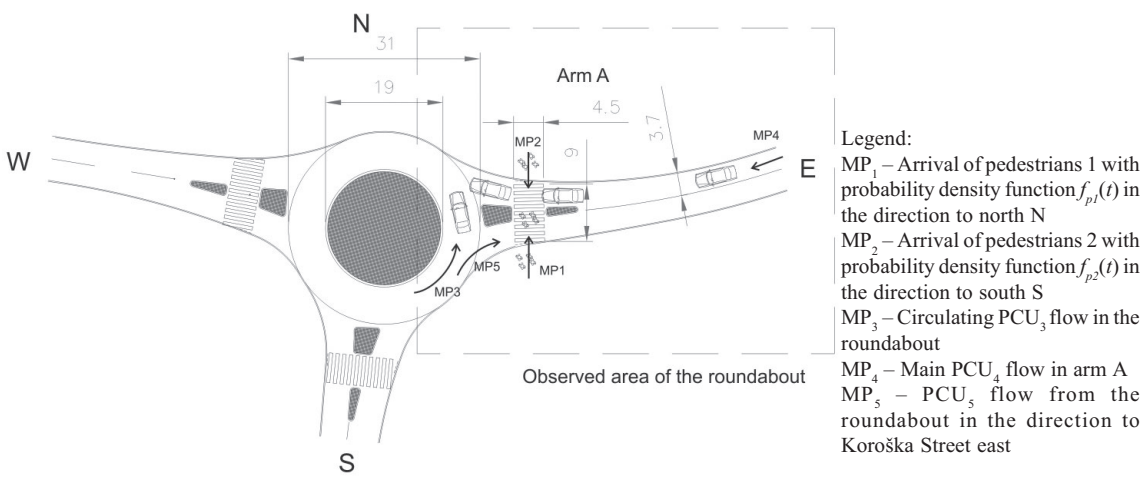

Fig. 2. *Geometry of the roundabout (distances are measured in meters)*

Table 1. *Geometrical and kinematics input data*

Geometrical input data	
Outside diameter of the roundabout	31 m
Inside diameter of the roundabout	19 m
Width of the road	3.7 m
Width of the pedestrian crossing	4.5 m
Length of entrance road of observed area	Arm A – 115 m
Length of pedestrian crossing	10 m
Kinematics input data	
Velocity $v_{1,2}$ of a pedestrian	5 km/h
Velocity v_3 of a PCU in the roundabout	20 km/h
Velocity v_5 of a PCU near the pedestrian crossing	20 km/h
Velocity v_4 of a PCU on the arm	40 km/h

Table 2. *Counting of PCU and pedestrians i for the time interval of 3 hours at* MP_i

Time interval AM	Observed area of roundabout				
	MP_1 Pedestrians 1 (Q_1)	MP_2 Pedestrians 2 (Q_2)	MP_3 PCU's $_3$ (Q_3)	MP_4 PCU's $_4$ (Q_4)	MP_5 PCU's $_5$ (Q_5)
6.30 to 6.35	27	2	27	48	43
6.35 to 6.40	18	8	29	60	49
6.40 to 6.45	21	6	27	50	48
6.45 to 6.50	30	10	28	63	53
6.50 to 6.55	64	4	33	70	52
6.55 to 7.00	26	5	44	61	48
7.00 to 7.05	22	4	38	64	50
7.05 to 7.10	24	4	38	57	60
7.10 to 7.15	43	6	37	64	38
7.15 to 7.20	20	5	28	52	41
7.20 to 7.25	39	8	31	55	41
7.25 to 7.30	42	7	34	48	45
7.30 to 7.35	39	10	30	60	53
7.35 to 7.40	61	5	26	67	48
7.40 to 7.45	38	7	45	58	46
7.45 to 7.50	45	9	40	59	53
7.50 to 7.55	36	5	39	64	51
7.55 to 8.00	41	7	34	63	53
8.00 to 8.05	21	7	38	56	50
8.05 to 8.10	35	8	32	58	44
8.10 to 8.15	26	7	32	55	48
8.15 to 8.20	37	5	26	57	43
8.20 to 8.25	22	8	33	61	43
8.25 to 8.30	27	3	23	50	42
8.30 to 8.35	23	6	29	53	49
8.35 to 8.40	25	9	24	52	41
8.40 to 8.45	44	5	27	54	51
8.45 to 8.50	24	8	26	58	47
8.50 to 8.55	29	13	18	53	48
8.55 to 9.00	25	7	23	53	50
9.00 to 9.05	20	9	25	60	56
9.05 to 9.10	22	11	20	48	42
9.10 to 9.15	25	9	22	53	41
9.15 to 9.20	29	9	20	63	47
9.20 to 9.25	24	6	29	58	43
9.25 to 9.30	23	11	21	49	44
SUM	1120	254	1073	2053	1697
Frequency λ_i [Q_i/sec.]	$\lambda_1 = 0.1037$	$\lambda_2 = 0.02352$	$\lambda_3 = 0.09935$	$\lambda_4 = 0.19$	$\lambda_5 = 0.1571$
Mean time between two arrivals *exp*. ($1/\lambda_i$) [sec./Q_i]	*exp.* (9.65)	*exp.* (42.58)	*exp.* (10.06)	*exp.* (5.26)	*exp.* (6.37)

The experimentally acquired input data present the input data for the traffic flow of motorised vehicles and pedestrians in the simulation model. Since the measurements were taken using counting on an individual arm of the roundabout, the presumption has been made that the traffic flow of PCU_i and pedestrian flow j (j = 1, 2) match with *Poisson's statistical distribution*. In this case the time between the arrivals of two PCU and pedestrians is distributed according to the *exponent statistical distribution*.

The time between two arrivals of pedestrians or PCU is defined according to the relation presented in the next case. *Case:* the number of PCU_3 arrivals within the time interval from 6.30 to 6.35 is 27, which is presumed to be distributed according to *Poisson statistical distribution*, with an average degree of arrivals per time unit $\lambda = 27/5 = 5{,}4$ [PCU_3/min]; the time between two consecutive arrivals of PCU_3 can then be determined by using the *exponential statistical distribution* with the mean value of $t = 1/\lambda = 0{,}185$ [min/ PCU_3].

2.2 The Theoretical Background of the Simulation Model

When planning a roundabout, its capacity in relation to the traffic flow (*i*) of PCU and (*ii*) pedestrians is predominantly the main point of interest. The general rule of all roundabouts is that pedestrians are always given priority over the PCU traffic flow. When determining the capacity of a roundabout, the rates of PCU (λ_3, λ_4, λ_5) and pedestrian flows (λ_1, λ_1), crossing each other on an individual arm of the roundabout, are used. The total capacity of PCU and pedestrian flows in an individual arm of the roundabout can be presented with the following simplified relation dependence. The arrivals of PCU and pedestrian flows in the individual arm of the roundabout can be treated as a system of a waiting queue with one serving place. When determining the appropriate system of the waiting queue, the basic condition that the arrivals of PCU are distributed according to *Poisson's statistical distribution* is taken into account. The condition that the time between two arrivals of pedestrians is distributed according to *exponent statistical distribution* is also considered. Due to the connection between *Poisson*'*s* and *exponential statistical distribution*, the following relation has to be defined. If the number of PCU and pedestrian arrivals in a given time interval t is distributed according to *Poisson*'*s statistical distribution* with an average degree of arrivals in a time unit λ and a medium value $\lambda \cdot t$, then the time intervals between the arrivals of two consecutive PCU and pedestrians are distributed according to the *exponent statistical distribution* with a medium value of $1/\lambda$. The relations in the roundabout can be represented with the following expressions:

M – refers to *Poisson*'*s* distribution of PCU and pedestrian arrivals in a given time unit,

M – refers to *Poisson*'*s* distribution of time, required for the driving of PCU over the

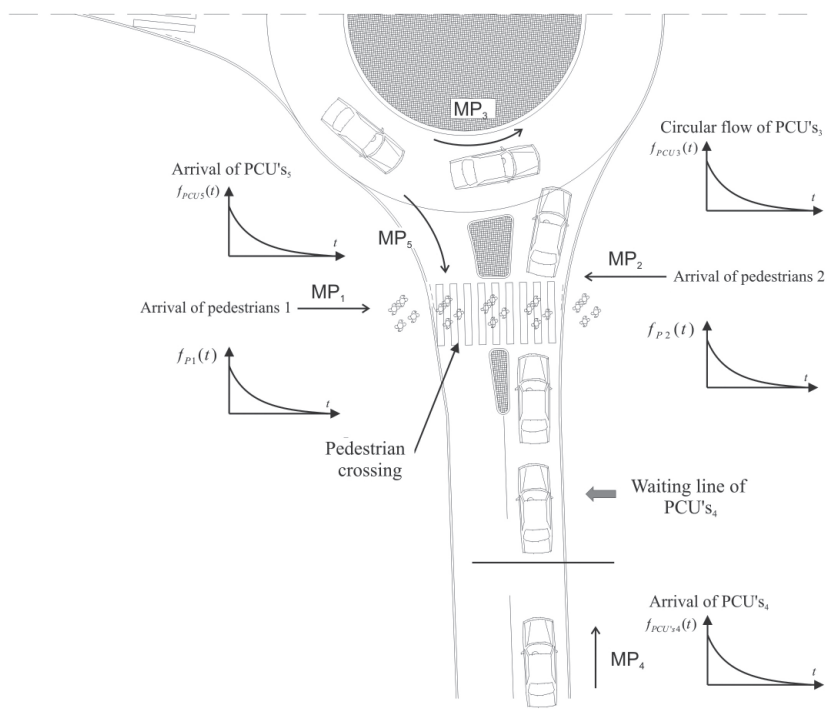

Fig. 3. *An individual roundabout arm (for the observed area see Figure 2)*

pedestrian crossing and the crossing of pedestrians to the other side of the roadway,

s – only one serving station exists the system, which is connected to the pedestrian crossing,

∞ – arrival in the roundabout is determined by an infinite flow of PCU and pedestrians,

FIFO – when coming into the system, PCU and pedestrians are first served according to the first-in-first-out (FIFO) selection rule.

The *M*/*M*/1/∞/*FIFO* system for the traffic flow of PCU and the system for the pedestrian traffic flow are schematically shown in the Figure 3 for the example of the roundabout arm in question.

Because of three independent traffic flows PCU_i (i = 1, 2, 3) and the pedestrian j (j = 1, 2) flow, an individual arm in the roundabout presents a combination of two mutual dependent systems, that is:

- The combination of *M*/*M*/1/∞/*FIFO* for the PCU_4 main traffic flow and pedestrian j (j = 1, 2) flow *M*/*M*/1/∞/*FIFO*.
- The combination of *M*/*M*/1/∞/*FIFO* for the PCU_3 circulating flow and the PCU_4 main flow *M*/*M*/1/∞/*FIFO*.

While the PCU traffic flow presents a typical *M*/*M*/1/∞/*FIFO* system, the pedestrian traffic flow system *M*/*M*/1/∞/*FIFO* is modified, since the waiting time periods and the waiting line never occur. This statement can be explained by the fact that pedestrians in the roundabout are always given priority over the motorised flow. Because of the complexity and non-determination of the system, the capacity of the traffic flow of an individual arm of the roundabout and the entire roundabout is impossible to be analytically treated. A possible solution to the problem is the use of discreet numeric simulations method, which is presented in the following section.

2.3 Simulation Model of the Roundabout

On the basis of the real roundabout in Koroška Street in Maribor the simulation model has been created (Figure 4 presents a detailed draft of the simulation model). The simulation model in the programming tool AutoMod [13] is illustrated with paths, on which the motorised vehicle (PCU) and pedestrian traffic flows are entwined. The simulation model has been created on the basis of real geometrical data presented in the CAD drawing and kinematics values, which are presented in Table 1, as well as from a sample of PCU and pedestrian traffic flows (Table 2). The operation of the simulation model is governed by a program code in the source file according to the following algorithm (Fig. 5).

The simulation begins with a process based on user determined functions in the source file of the program. The functions in the source file start the operation of the roundabout. When the function »*Begin model initialization function*« equals »true«,

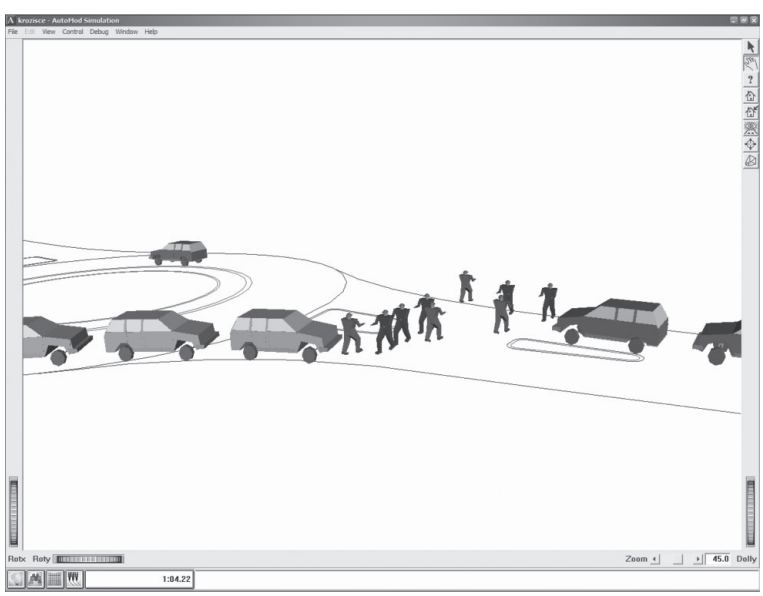

Fig. 4. *Micro-simulation model of the roundabout [13]*

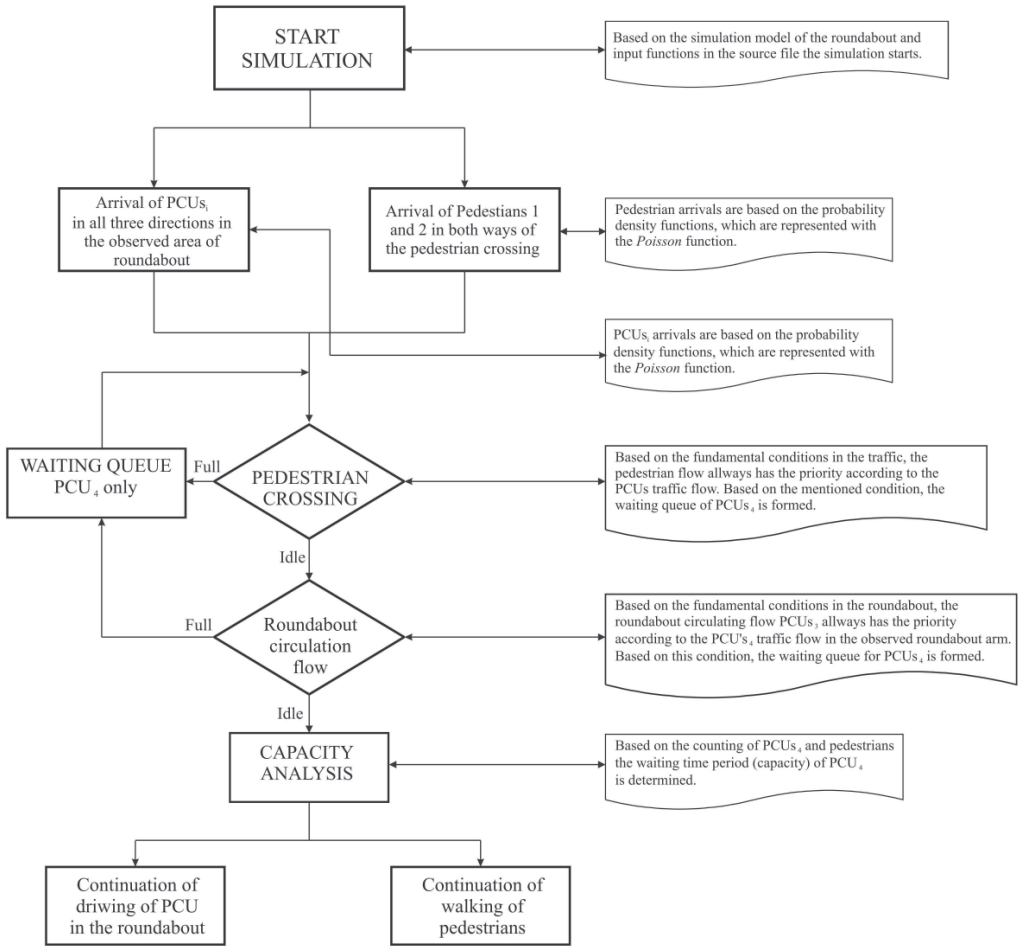

Fig. 5. *Algorithm of the course of operating the simulation model of the roundabout*

the process »*P_roundabout_start*« begins. The process consists of project variables, pedestrians and PCU attributes of type integer and real, subroutines and individual program loops. The model is built according to the defined geometrics construction of the roundabout from the CAD file and kinematics characteristics for pedestrians and PCU. The mean time between two consecutive arrivals of PCU and pedestrians is programmed according to the experimentally acquired values, presented in Table 2. It is presumed that the arrivals of PCU and pedestrians are uneven; therefore the *Poisson statistical distribution* has been used for generating the traffic flow.

• **The gap acceptance model**

The gap acceptance model of the roundabout has been modelled using the »*Block claim and Block release functions*« and the »*Order list*«. The »*Block claim function*« for the arrival of PCU_4 on the considered pedestrian crossing verifies whether there is already a pedestrian on the pedestrian crossing or not. If there is a pedestrian on the pedestrian crossing (the function »*B_block_1 current claims <> 0*«), the PCU_4 immediately stops and waits until the pedestrian leaves the pedestrian crossing. During the waiting period, the PCU_4 is inscribed into the *order list wait for path* (»*wait to be ordered on Ol_waitForPath_1*«). When the pedestrian flow is extremely heavy, waiting queues of PCU_4 occur. The moment the pedestrian crossing is free the »*B_block_1 current claims = 0*«, PCU_4 continues with driving in the first-in-first-out (FIFO) consequence according to their waiting queue. The driving of PCU_4 takes place until the next pedestrian appears on the pedestrian crossing, which again stops the driving of PCU_4. In the case of roundabout circulating flow PCU_3 and the main traffic flow PCU_4, the same approach with the »*Block claim and Block release functions*« and the

»*Order list*« has been used. For every passing of PCU_4 and pedestrians the program registers the basic information variables »*V_waiting_time*« for PCU_4, »*V_no._of_ PCU*$_4$« and »*V_no._of_ pedestrians*« as follows: the number of passing PCU_4 and the number of pedestrian crossings in the roundabout, the period an individual PCU_4 has been in the observed arm of the roundabout (the waiting time period) and the number of successfully passed PCU_4 and pedestrians in the defined time.

The main goal of the simulation analysis is to establish the PCU_4 capacity on the observed arm when the waiting queue in front of the pedestrian crossing and consequently the waiting time for crossing the observed arm is still acceptable.

2.4 Analysis of Results

The results of the performed analysis for determining the mean waiting time and the capacity of the PCU_4 main traffic flow depending on the pedestrian flows give basic conclusions, presented in Tables 3, 4 and 5.

With regard to the performed counting of the traffic flow of motorised vehicles and pedestrian flow (Table 2) it can be stated that the frequency of pedestrians (λ_1) presents the biggest influence on the capacity of the PCU_4 main traffic flow (Fig. 4). Assuming that the pedestrian frequency will only get bigger in the future (closure of the "Old bridge", increase in the public transportation), it is necessary to find out what level of increase in the number of pedestrians in both directions with regard to the main traffic flow of PCU_4 would still be admissible. When analysing the capacity of the treated arm of the roundabout, we deal with a number of independent variables, i.e. different frequencies of the motorised vehicle traffic flow (λ_3, λ_4, λ_5) and pedestrian flow (λ_1, λ_2). To determine the influence of a variable on the system's response (waiting time and roundabout capacity) it is therefore necessary to fix individual variables and change the value of only one variable or both variables at the same time. Since we are mainly interested in the influence of pedestrians on the capacity of the roundabout arm, the frequency of pedestrians 1 (λ_1) and the frequency of pedestrians (λ_2) in the roundabout arm present the main variables. Due to a different frequency of pedestrians in both directions (λ_1 = 0,1037 ped./sec. and λ_2 = 0,02352 ped./sec.) the influences on the waiting time and capacity of the roundabout for PCU_4 have been analysed in the following way:

a) beside the fixed variables (λ_3, λ_4, λ_5) the frequency of pedestrians 2 (λ_2) has been fixed. In the analysis, values λ_1 have been changed or increased to the level that the mean waiting time

Table 3. *The influence of increasing arrivals of pedestrians 1 on the mean waiting time and mean capacity for the main traffic flow of PCU_4*

PCUs arrivals ($1/\lambda_3$ = 10.06) ($1/\lambda_4$ = 5.26) ($1/\lambda_5$ = 6.36)	Arrivals of pedestrians 1 (sec./pedestrian)				
	Pedestrians 1 ($1/\lambda_1$ = 9.65) λ_1 = 100 %	Pedestrians 1 ($1/\lambda_1$ = 7.72) λ_1 = 120 %	Pedestrians 1 ($1/\lambda_1$ = 5.79) λ_1 = 140 %	Pedestrians 1 ($1/\lambda_1$ = 3.86) λ_1 = 160 %	Pedestrians 1 ($1/\lambda_1$ = 2.895) λ_1 = 170 %
	Pedestrians 2 ($1/\lambda_2$ = 42.58) λ_2 = 100 %	Pedestrians 2 ($1/\lambda_2$ = 42.58) λ_2 = 100 %	Pedestrians 2 ($1/\lambda_2$ = 42.58) λ_2 = 100 %	Pedestrians 2 ($1/\lambda_2$ = 42.58) λ_2 = 100 %	Pedestrians 2 ($1/\lambda_2$ = 42.58) λ_2 = 100 %
Mean wait. time T (sec.)	**3.62**	**4.49**	**6.81**	**18.58**	**266.67**
SD	0.25	0.34	0.74	3.06	117.92
Confidence Interval (95 %)	(3.58 to 3.67)	(4.27 to 4.56)	(6.67 to 6.96)	(17.97 to 19.18)	(243.27 to 290.06)
Mean capacity for the time interval of 3^h Q_4 (PCU's$_4$)	**2048**	**2048**	**2048**	**2046**	**1956**
SD	48	48	48	47	35
Confidence Interval 95 %	(2039 to 2058)	(2039 to 2058)	(2039 to 2058)	(2037 to 2056)	(1949 to 1963)

Table 4. *The influence of increasing arrivals of pedestrians 2 on the mean waiting time and mean capacity for the main traffic flow of PCU_4*

PCUs arrivals ($1/\lambda_3 = 10.06$) ($1/\lambda_4 = 5.26$) ($1/\lambda_5 = 6.36$)	Arrivals of pedestrians 2 (sec./pedestrian)				
	Pedestrians 2 ($1/\lambda_2 = 42.58$) $\lambda_2 = 100$ %	Pedestrians 2 ($1/\lambda_2 = 34.064$) $\lambda_2 = 120$ %	Pedestrians 2 ($1/\lambda_2 = 25.548$) $\lambda_2 = 140$ %	Pedestrians 2 ($1/\lambda_2 = 17.032$) $\lambda_2 = 160$ %	Pedestrians 2 ($1/\lambda_2 = 12.774$) $\lambda_2 = 170$ %
	Pedestrians 1 ($1/\lambda_1 = 9.65$) $\lambda_1 = 100$ %	Pedestrians 1 ($1/\lambda_1 = 9.65$) $\lambda_1 = 100$ %	Pedestrians 1 ($1/\lambda_1 = 9.65$) $\lambda_1 = 100$ %	Pedestrians 1 ($1/\lambda_1 = 9.65$) $\lambda_1 = 100$ %	Pedestrians 1 ($1/\lambda_1 = 9.65$) $\lambda_1 = 100$ %
Mean wait. time T (sec.)	**3.62**	**3.8**	**4.15**	**4.94**	**5.87**
SD	0.25	0.28	0.33	0.46	0.6
Confidence Interval (95 %)	(3.58 to 3.67)	(3.75 to 3.86)	(4.09 to 4.21)	(4.85 to 5.03)	(5.76 to 5.99)
Mean capacity for the time interval of 3^h Q_4 ($PCU's_4$)	**2048**	**2048**	**2048**	**2048**	**2048**
SD	48	48	48	48	48
Confidence Interval (95 %)	(2039 to 2058)	(2039 to 2058)	(2039 to 2058)	(2039 to 2058)	(2039 to 2058)

Table 5. *The influence of increasing arrivals of pedestrians 1 and pedestrians 2 on the mean waiting time and mean capacity for the main traffic flow of PCU_4*

PCUs arrivals ($1/\lambda_3 = 10.06$) ($1/\lambda_4 = 5.26$) ($1/\lambda_5 = 6.36$)	Arrivals of pedestrians 1 and pedestrians 2 (sec./pedestrian)				
	Pedestrians 1 ($1/\lambda_1 = 9.65$) $\lambda_1 = 100$ %	Pedestrians 1 ($1/\lambda_1 = 7.72$) $\lambda_1 = 120$ %	Pedestrians 1 ($1/\lambda_1 = 5.79$) $\lambda_1 = 140$ %	Pedestrians 1 ($1/\lambda_1 = 3.86$) $\lambda_1 = 160$ %	Pedestrians 1 ($1/\lambda_1 = 2.895$) $\lambda_1 = 170$ %
	Pedestrians 2 ($1/\lambda_2 = 42.58$) $\lambda_2 = 100$ %	Pedestrians 2 ($1/\lambda_2 = 34.064$) $\lambda_2 = 120$ %	Pedestrians 2 ($1/\lambda_2 = 25.548$) $\lambda_2 = 140$ %	Pedestrians 2 ($1/\lambda_2 = 17.032$) $\lambda_2 = 160$ %	Pedestrians 2 ($1/\lambda_2 = 12.774$) $\lambda_2 = 170$ %
Mean wait. time T (sec.)	**3.62**	**4.76**	**7.83**	**36.92**	**929.52**
SD	0.25	0.38	1.0	10.15	165.05
Confidence Interval (95 %)	(3.58 to 3.67)	(4.68 to 4.83)	(7.63 to 8.03)	(34.91 to 38.94)	(896.77 to 962.27)
Mean capacity for the time interval of 3^h Q_4 ($PCU's_4$)	**2048**	**2048**	**2048**	**2043**	**1694**
SD	48	48	48	47	37
Confidence Interval (95 %)	(2039 to 2058)	(2039 to 2058)	(2038 to 2057)	(2033 to 2052)	(1687 to 1701)

and capacity of the main traffic flow of PCU_4 are still admissible (Table 3);

b) beside the fixed variables (λ_3, λ_4, λ_5) the frequency of pedestrians 1 (λ_1) has been fixed. In the analysis, values λ_2 have been changed or increased to the same level as the frequency of pedestrians 1 (Table 4);

c) the variables (λ_3, λ_4, λ_5) have been fixed. In the analysis, values of frequency λ_1 and λ_2 have been changed or increased to the level that the mean waiting time and capacity of the main traffic flow of PCU_4 are still admissible (Table 5).

Analysis results for every mean waiting time and the roundabout capacity shown in Tables 3, 4, and 5 have been carried out on the basis of 100

consecutively performed simulations in the AutoStat programming tool [13]. Consequently, a good enough representative average is obtained, which would not be in the case of probability functions with a small number of performed simulations.

2.4 Discussion – Interpretation of the Simulation Results

In the case of fixing the values of the variables for the traffic flow (λ_3, λ_4, λ_5) and the pedestrian flow 2 (λ_2) it can be noticed that the pedestrian flow 1 in the direction of "Old bridge" towards "Main square" has a major influence on the mean waiting time of the main traffic flow of PCU_4. When increasing the frequency λ_1 from 20 % to 40 % one can notice a rather small increase in the mean waiting time, whereby the PCU_4 capacity remains the same all the time. For this purpose the frequency of pedestrians 1 was increased for 60% and it has been found out that the mean waiting time has enormously increased in comparison with the previous increases of frequency, whereby the capacity of PCU_4 remains unchanged. It has been determined that with constant – linear increase of the frequency λ_1 the mean waiting time of PCU_4 does not increase evenly. In the continuation of analysis, the frequency λ_1 was increased from 60 % to 70 %. We have established that the mean waiting time of PCU_4 has increased to 266.67 seconds, which is unacceptable for the traffic flow in the roundabout. On the basis of results in Table 3 it can be concluded that theoretically there is a 60 % reserve of the capacity in the case of increase of pedestrian 1 frequency. This statement is valid under the condition that the frequencies of traffic flow (λ_3, λ_4, λ_5) of PCU are fixed and unchangeable. The same holds true for the frequency (λ_2) of the pedestrian flow 2.

In the continuation of the analysis, when operating with the pedestrian flow 2, the influence of increasing the frequency λ_2 on the mean waiting time of the main traffic flow of PCU_4 was compared. Due to the simultaneous treatment with several variables the values of variables (λ_1, λ_3, λ_4, λ_5) were fixed. In Table 4 it can be observed that the increase of the pedestrian frequency 2 does not have a major influence on the mean waiting time and capacity of the main traffic flow of PCU_4. This finding is reasonable since the pedestrian frequency (λ_2 = 0.02352 ped/sec) is relatively small considering the pedestrian frequency (λ_1 = 0.1037 ped/sec) and consequently has a smaller influence on the mean waiting time of PCU_4. This means that theoretically there is a relatively great reserve of capacity in the case of the increase of pedestrian frequency.

The actual roundabout capacity is definitely dependent on the simultaneous consideration of pedestrian frequencies λ_1 and λ_2 as well as on other fixed variables (λ_3, λ_4, λ_5) of PCU. For this reason Table 5 shows dependencies of the mean waiting time and PCU_4 capacity with a simultaneous increase of pedestrian frequencies (λ_1, λ_2) for pedestrians 1 and pedestrians 2. Because of the simultaneous influence of both pedestrian flows 1 and 2, the mean waiting time is higher than in previous cases. The dependency of the mean waiting time and capacity of the main traffic flow PCU_4 is similar to the dependency in the case of only increasing the pedestrian frequency λ_1 and fixed values of other variables (λ_2, λ_3, λ_4, λ_5). Due to a relatively small influence of pedestrians 2 and a great influence of pedestrians 1 there is a theoretical 60 % reserve of capacity at a simultaneous increase of pedestrian frequencies λ_1 and λ_2.

3 CONCLUSION

In this paper the influence of the strong pedestrian traffic flow on the capacity of the one-lane three-armed roundabout using the discreet numeric simulations modelling is presented. The analysis presented in this paper provides a new complex confirmation of the traffic flow (the simultaneous use of the main and the circulating flow) and the influence of the strong pedestrian flow (the use of multi-channel system) on the capacity of the roundabout.

First, the main theoretical background for the analysis of the traffic flow of motorised vehicles – personal car units (PCU) and pedestrians in the roundabout is presented. Since in roundabouts the pedestrian traffic flow is given priority, the vehicles on entries/exits have to give way to pedestrians. Consequently, disturbances at entering/exiting of motorised vehicles occur and the motorised vehicle flow is disrupted. The more disrupted the motorized vehicle flow is, the lower the capacity of the roundabout. In case the flows towards the entry of

the roundabout are disturbed, the minimum capacity is not reached. In case the flows towards the exit of the roundabout are disturbed, the maximum capacity can get exceeded. Under real conditions, the entering and exiting of the motorised traffic flow are simultaneously disturbed and congestions are transferred from arm to arm, in clock-wise direction. For this purpose, the mathematical modelling of traffic flows with the use of discreet simulations has been used for the analysis of the influence of the pedestrian flow on the capacity of the roundabout, considering the statistically evaluated input data of the PCU and pedestrian traffic flows.

The main part of this paper consists of the discreet numeric simulation of the roundabout. The simulation model of the roundabout is general, i.e. it can be extended for every individual implementation according to the chosen geometrical and kinematics sizes. The mathematical model derives from legalities of acceptable time voids in the pedestrian traffic flow, used by the vehicles for entering/exiting a roundabout, using the exponent and Poisson statistical distribution. For determination of the traffic flow of motorised vehicles and pedestrians the real input data acquired by the traffic counting on Koroška Street in Maribor have been used. The results (the capacity of motorised vehicles Q_4) acquired with measurements of the traffic flow and simulation analyses match well (Tables 4, 5 and 6), which means that simulation analysis results give a good prediction for the evaluation of the waiting period and waiting queues of motorized vehicles in an individual arm of a roundabout. It has been determined that the current situation of the traffic flow is acceptable for the roundabout capacity. With an increase of the pedestrian flow (in both directions) a major influence on the roundabout capacity is not expected. On the basis of analysis results it can be established that there is a relatively great reserve available in relation to the capacity of pedestrians 1 and 2 (up till 60 % of current frequencies λ_1 in λ_2). Since the traffic flow of PCU is going to increase in the future, we assume that the capacity reserve will get lower, but it will still be great enough to allow an undisturbed traffic flow of PCU. It should be mentioned that the analysis results refer to the counting of traffic flow carried out in the morning peak hour, only on the treated part of the roundabout. In the continuation of this research it would be reasonable to analyse the influence of the mean waiting time and PCU capacity on the whole roundabout and in the afternoon peak hour, considering a different pedestrian speed. Different types of motorised vehicles and pedestrians (dimensions, reaction times, velocities, accelerations, etc.) should be taken into account.

4 REFERENCES

[1] Tollazzi, T., Lerher, T., Šraml, M. An analysis of the influence of pedestrians' traffic flow on the capacity of a roundabout using the discreet simulation method. *Journal of Mech. Eng.* (2006), vol. 52, p. 359-379.

[2] Tollazzi, T., Kralj, B., Destovnik, S. Analysis of the influence of pedestrian flow on roundabout capacity by using the simulation method. *Suvremeni promet*, (2005), vol. 25.

[3] Tollazzi, T., Lerher, T., Šraml, M. Simulation of the pedestrians' influence to the capacity of motorised vehicles in a roundabout. *Am. j. appl. sci.*, 2008, 5, 1, p. 34-41. http://www.scipub.org/fulltext/ajas/ajas5134-41.pdf.

[4] Stone, J.R., Chae, K. Roundabouts and pedestrian capacity: A simulation analysis. *Transportation Research Board*, Annual Meeting CD-ROM, 2003.

[5] Hagring, O. A further generalization of Tanner's formula. *Transportation Research Part B: Methodological*, Elsevier Science, Exeter, England, vol. 32 b, no. 6, 1998.

[6] Wu, N. A universal procedure for capacity determination at unsignalized priority controlled intersections. *Transportation Research Part B: Methodological*, Elsevier Science, Exeter, England, volume 35 b, no. 6, 2001.

[7] Federal Ministry for Economy: *Guidelines: Using area and design elements of roundabouts on federal roads*, Chapter VI/2. Berlin, 1996. (In German).

[8] Information and Technology Platform for Transport, Infrastructure and Public space: Roundabouts, publication 79, Ede, 1993. (In Dutch).

[9] Oketch T., Delsey M., Robertson D. Evaluation of performance of modern roundabout using Paramics micro-simulation model. *TAC Conference* 2004.

[10] Akçelik R. Roundabout model calibration issues and a case study. *TRB National Roundabout Conference*, Colorado, 2005.

[11] Akçelik R., Besley M. Microsimulation and analytical methods for modelling urban traffic. *Conference of Advanced Modelling Techniques and Quality of Service in HCA, truckee*, California, USA, July 2001.

[12] Akçelik R. Operating cost, fuel consumption and pollutant emission savings at a roundabout with metering signals. *7th Congress on Advanced in Civil Eng.* (ACE 2006), Turkey 2006.

[13] BROOKS Automation, *AutoMod-User manual V 12.0*, Utah, December 2005.

[14] Wiedermann, R., Reiter, U. Microscopic traffic simulation. *The Simulation System Mission*, 1970.

[15] Fellendorf, Vortisch. *Integrated modelling of transport demand, route choice, traffic flow and traffic emissions*, January 2000.

[16] Dowling Associates, Inc. *Guidelines for applying traffic microsimulation modelling software*. Federal Highway Administration, August 2003.

[17] Potrč, I., Lerher, T., Kramberger, J., Šraml, M. Simulation model of multi-shuttle automated storage and retrieval systems. *Journal of material processing technology*, (2004), vol. 157/158, p. 236–244.

Strojniški vestnik - Journal of Mechanical Engineering 54(2008)5, 347-355
UDC 007.52
Paper received: 6.6.2007
Paper accepted: 28.9.2007

PI+PD Type Fuzzy Logic Controlled Dual-Arm Robot in Load Transfer

Yuksel Hacioglu - Yunus Ziya Arslan - Nurkan Yagiz*
Istanbul University, Faculty of Engineering, Department of Mechanical Engineering, Turkey

This paper presents a PI+PD type fuzzy logic control method for simultaneous cooperative motion of a dual arm robot in load transfer tasks. First, physical model of dual arm robot with the load are presented and dynamic equations of the system are derived while constrained conditions are also taken into account. Since fuzzy logic controllers can successfully be designed even if the exact mathematical model of the system is unknown, this control method is preferred in many applications. Therefore, PI+PD type fuzzy logic controller is introduced to achieve cooperative coordination of dual arms. In order to verify the safety performance of the proposed controller, unexpected disturbances are introduced to the system. These are noise components, which are thought as disturbance torques, and an elastic element unintentionally catching the first robot arm. Finally, numerical results are presented and the performance of the control method is discussed.

Keywords: fuzzy logic, dual-arm robot, cooperative motion control, load transfer

0 INTRODUCTION

Using dual arm robots instead of single arm robots offers many advantages, especially with their greater capability in handling large objects with higher precision than single arm robots [1] to [4]. Therefore, cooperative dual arm robots have a wide range of application area in industrial automation such as holding heavy and large welding machines; in medical applications such as physical rehabilitation [5]; in dangerous environment tasks such as transporting of radioactive materials in nuclear power plants, disposing of explosive ordnances [6], and in aerospace robotics [7]. These sophisticated tasks require solving complex problems such as analysis of closed kinematic chain [8] and motion synchronization of the robot arms [9].

The motion control problem of cooperative dual arm robots has been studied by many investigators in recent years [10] to [14]. The main problem in controlling such systems is that unless the robot arms are carefully coordinated, conflicting motions among them may cause undesired extra stresses on the manipulated object [15] that may cause breakage or dropping of the object.

Fuzzy logic control is a knowledge-based control method and it is based on the fuzzy set theory which was first presented by Zadeh in 1965 [16]. This control method has become widespread within automatic control research community since it has applicability to systems with unknown mathematical model. Another important reason for its wide use is its rule-based structure. In this system, the knowledge coming from human operators or experts can be expressed by fuzzy rules and they are used directly during the control signal calculations. Because of these attractive properties, fuzzy logic controllers are used in wide range of applications such as in robotic manipulator control [17], control of unmanned underwater vehicles [18], vehicle active suspension control [19], power systems [20], and so on.

In general, there are two main types of fuzzy logic controllers, namely, PD-type and PI-type fuzzy logic controllers [21]. Generally, in both types the error and its derivative are used as inputs. The output for the PD-type fuzzy logic controller is control signal whereas the output for the PI-type fuzzy logic controller is the incremental change in control signal. It is well known that PD-type fuzzy logic controller has good transient performance but sometimes steady state error cannot be eliminated. On the other hand PI-type fuzzy logic controllers can remove steady state error but it gives poor transient performance [22] and [23]. In fact, it is possible to design a PID-type fuzzy logic controller, but constructing a 3-D rule base is difficult and

*Corr. Author's Address: Istanbul University, Faculty of Engineering, Department of Mechanical Engineering, 34320 Avcilar, Istanbul, Turkey, nurkany@istanbul.edu.tr

this type of controllers are rarely used if compared with PD-type and PI-type fuzzy logic controllers [24] and [25].

Therefore, in order to bring together the advantages of the PD type and PI type fuzzy logic controllers, a PI +PD type fuzzy logic controller is designed and applied to the dual arm robot system in load transfer.

1 PHYSICAL MODEL

The physical model of the dual arm robot consisting of two planar robot arms with actuating motors at revolute joints is seen in Figure 1. Without being contact of the robot arms with the load, the robot system would have four degrees of freedom (DoF). Since the robots handle the object, because of the constraints, the DoF of the system reduces to two. It should be noted that the load is not allowed to rotate. In physical model of the robot system, m_i, I_i and L_i represents the mass, mass moment of inertia and length of the related links. a_i is the distance of the mass center and α_i is the joint angle of the related links. Also, there are viscous frictions on all of the joints denoted by b_{ti}. M is the load mass. Numerical values of the parameters are given in the Appendix. The spring which is represented by stiffness k stands for an undesired elastic element catching the first arm at a certain moment during the transportation process.

The dual arm robot works in xy-plane and gravity acts in negative z-direction. There are two phases in motion task of the robots. First, robots start from their home position and move towards the load. Then, in the second part, robots handle the load and move it to its new position while tracking the given trajectory as seen in Figure 2.

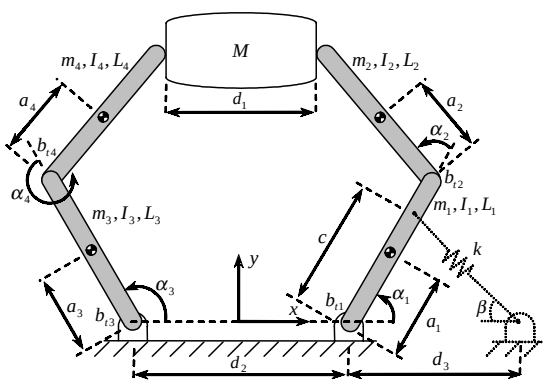

Fig. 1. *The dual arm robot handling the load*

Handling and transportation task of the load are carried by the forces F_1, F_2 applied from arm tips to the load. The vector representations of the force interactions are shown in Figure 3. Friction-assisted handling prevents slipping of the load from the contact points during motion. Friction forces F_{s1}, F_{s2} and their components $F_{s1y}, F_{s1z}, F_{s2y}, F_{s2z}$ between arm tips and load surface are shown in Figure 3. μ is the coefficient of dry friction. In this paper it is aimed that the load is moved without rotation. Thus, F_{s1y} and F_{s2y} are equal preventing the rotation about z-axis. Similarly, F_{s1z} and F_{s2z} are equal since there is no rotation about y-axis, too. Then:

$$F_{s1y} = F_{s2y} \tag{1}$$

$$F_{s1z} = F_{s2z} = Mg/2 \tag{2}.$$

Equations of motion after handling the load are:

$$\begin{aligned} &\ddot{\alpha}_1(A_1 + A_2 + 2A_3\cos\alpha_2) + \ddot{\alpha}_2(A_2 + A_3\cos\alpha_2) - \\ &-A_3\sin\alpha_2(\dot{\alpha}_2^{\,2} + 2\dot{\alpha}_1\dot{\alpha}_2) + b_1\dot{\alpha}_1 \\ &= u_1 - F_1[L_1\sin\alpha_1 + L_2\sin(\alpha_1+\alpha_2)] - \\ &-F_{s1y}[L_1\cos\alpha_1 + L_2\cos(\alpha_1+\alpha_2)] + T_e(t) + T_{d1}(t) \end{aligned} \tag{3}$$

$$\begin{aligned} &A_2\ddot{\alpha}_2 + \ddot{\alpha}_1(A_2 + A_3\cos\alpha_2) + A_3\dot{\alpha}_1^{\,2}\sin\alpha_2 + b_2\dot{\alpha}_2 = \\ &= u_2 - F_1L_2\sin(\alpha_1+\alpha_2) - F_{s1y}L_2\cos(\alpha_1+\alpha_2) + T_{d2}(t) \end{aligned} \tag{4}$$

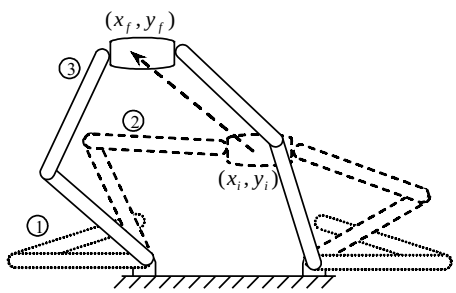

Fig. 2. *The dual arm robot in action*

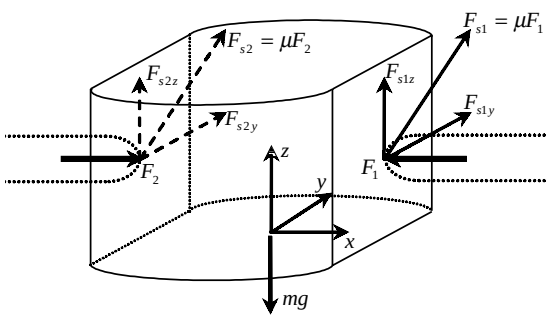

Fig. 3. *The forces on the load*

$$\begin{aligned}&\ddot{\alpha}_3(A_4+A_5+2A_6\cos\alpha_4)+\ddot{\alpha}_4(A_5+A_6\cos\alpha_4)-\\&-A_6\sin\alpha_4(\dot{\alpha}_4{}^2+2\dot{\alpha}_3\dot{\alpha}_4)+b_3\dot{\alpha}_3\\&=u_3+F_2[L_3\sin\alpha_3+L_4\sin(\alpha_3+\alpha_4)]-\\&-F_{s2y}[L_3\cos\alpha_3+L_4\cos(\alpha_3+\alpha_4)]+T_{d3}(t)\end{aligned} \quad (5)$$

$$\begin{aligned}&A_5\ddot{\alpha}_4+\ddot{\alpha}_3(A_5+A_6\cos\alpha_4)+A_6\dot{\alpha}_3{}^2\sin\alpha_4+b_4\dot{\alpha}_4=\\&=u_4+F_2L_4\sin(\alpha_3+\alpha_4)-F_{s2y}L_4\cos(\alpha_3+\alpha_4)+T_{d4}(t)\end{aligned} \quad (6),$$

where A_i are constant coefficients given in the Appendix. The u_i in governing equations are the torque inputs induced by PI+PD type fuzzy logic controller. $T_e(t)$ represents an unexpected problem such that, the first arm is caught by an elastic element which was supposed not to exist in the actual transfer operation:

$$T_e(t)=\begin{cases}0 & ; \quad t<2.2\\ -k\,x_k(t)\,c\sin(\alpha_1+\beta) & ; \quad t\geq 2.2\end{cases} \quad (7).$$

Here $x_k(t)$ is the extension in elastic element. Note that the load transfer starts at 2nd second. In these equations, all of the $T_{di}(t)$ represent the undesired noise acting on related robot arms. As, the x, y coordinates of the load mass center are the same in designing trajectory of the arms, the DoF of the overall system becomes two:

$$\begin{aligned}x_M&=\frac{d_2}{2}+L_1\cos\theta_1+L_2\cos(\theta_1+\theta_2)-\frac{d_1}{2}=\\&=-\frac{d_2}{2}+L_3\cos\theta_3+L_4\cos(\theta_3+\theta_4)+\frac{d_1}{2}\end{aligned} \quad (8)$$

$$y_M=L_1\sin\theta_1+L_2\sin(\theta_1+\theta_2)=L_3\sin\theta_3+L_4\sin(\theta_3+\theta_4) \quad (9).$$

The dynamic equations of the load are:

$$M\,\ddot{x}_M=F_2-F_1 \quad (10)$$

$$M\,\ddot{y}_M=2F_{s1y}=2F_{s2y} \quad (11),$$

and the constraints for the friction forces:

$$F_{s1y}{}^2+(\frac{Mg}{2})^2<(\mu F_1)^2 \quad (12)$$

$$F_{s2y}{}^2+(\frac{Mg}{2})^2<(\mu F_2)^2 \quad (13).$$

2 PI+PD FUZZY LOGIC CONTROLLER DESIGN

Fuzzy logic control is a knowledge-based control system, and it gives the ability to use linguistic expressions during the controller design. These heuristic decision rules generally include the intuition of human operators or experts, and they are generally in the following form for a system with two inputs and single output:

$$\textit{if}\ \ (x\ \textit{is}\ X)\ \textit{and}\ \ (y\ \textit{is}\ Y)\ \ \textit{then}\ \ (u\ \textit{is}\ U) \quad (14).$$

There are three important steps in fuzzy logic control applications, namely, fuzzification, inference and defuzzification. In the first step, membership functions and their ranges are defined for the variables used. In the second step, the controller output is determined according to predefined rules which are based on the knowledge about system characteristics coming from human operators or experts. In the last step, the output is converted to a crisp value by a suitable defuzzification method, since the output values could not be used directly. There are different defuzzification methods available in the literature such as, max membership principle, weighted average method, centroid method, while the last one is often preferred by the researchers and it is used in this paper.

In order to bring the useful properties of the PD-type and PI-type fuzzy logic controllers, a PI +PD type fuzzy logic controller is used in this paper. Structure of the controller is given in Figure 4. The controller consists of two parts, which are the PD-type fuzzy logic controller and PI-type fuzzy logic controller. Both of the fuzzy logic controllers use the error e_N and its derivative $\dot{e}_N$ as inputs. The output of the PD-type fuzzy controller is the control signal u_N and the output of the PI-type fuzzy logic controller is the incremental change in control signal Δu_N. For the PI type controller the resulting output is calculated as:

$$u(t)_{PI}=\Delta u(t)_{PI}+u(t-\delta t)_{PI} \quad (15),$$

where δt is the sampling time. Since the incremental control signal is added up to the control signal belonging to the previous step, the PI part of the PI+PD type fuzzy logic controller ensures that there is no steady state error. On the other hand, PD part of the PI+PD type fuzzy logic controller gives faster response ability to the controller. That is by combining them an efficient controller is obtained. Thus, the control signals $u(t)_{PD}$ and $u(t)_{PI}$ are added up in order to obtain the final control input $u(t)_{PD+PI}$ to the system as given below:

$$u(t)_{PD+PI}=u(t)_{PD}+u(t)_{PI} \quad (16).$$

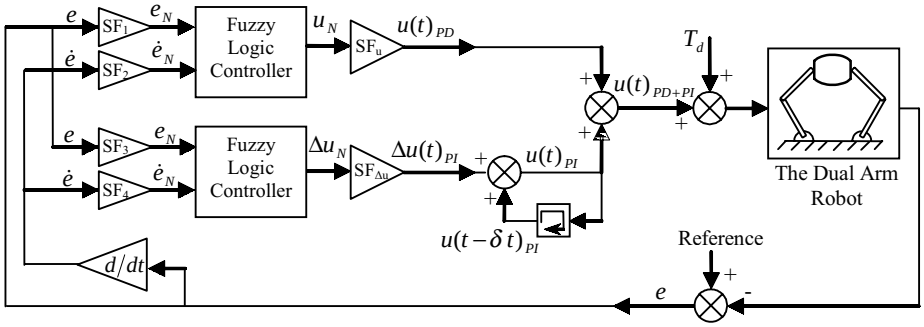

Fig. 4. *General structure of the controller*

Gaussian membership functions are used for the fuzzification of the input and output variables. Membership functions for the error e_N and its derivative $\dot{e}_N$ are given in Figure 5a and membership functions for the outputs u_N and Δu_N are given in Figure 5b. For the membership functions used, *NB*, *NM*, *NS*, *Z*, *PS*, *PM* and *PB* denotes negative big, negative medium, negative small, zero, positive small, positive medium and positive big, respectively. All the membership functions are defined on the [-1,1] closed interval. SF_1, SF_2, SF_3 and SF_4 are the input scaling factors. SF_u and $SF_{\Delta u}$ are the output scaling factors of the PD-type and PI-type fuzzy logic controllers, respectively. All these scaling factors are used in order to map the related crisp values to their fuzzy universe of discourse. Relations between the input and output variables for the PD type controller are:

$$e_N = SF_1\, e \tag{17}$$

$$\dot{e}_N = SF_2\, \dot{e} \tag{18}$$

$$u(t)_{PD} = SF_u\, u_N \tag{19}$$

In the Equations (17 to (19), the subscript N denotes the normalized variable. Relations between the input and output variables for the PI type controller are:

$$e_N = SF_3\, e \tag{20}$$

$$\dot{e}_N = SF_4\, \dot{e} \tag{21}$$

$$\Delta u(t)_{PI} = SF_{\Delta u}\, \Delta u_N \tag{22}.$$

The rule table, for computing u_N for the PD-type fuzzy logic controller and for computing Δu_N for the PI-type fuzzy logic controller, is given in Table 1.

The following manner is used for the construction of rule base:

Suppose that the system output is far from the desired output i.e. e_N is *PB* and $\dot{e}_N$ is *Z* (Fig. 6, case 1) then u_N or Δu_N is selected to be *PM* in order to decrease the error value and bring the system state to the desired value rapidly. In case 2,

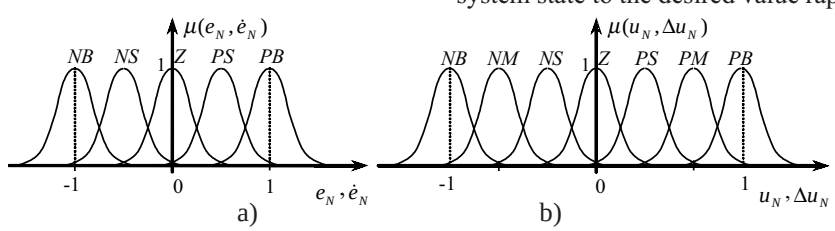

Fig. 5. *Membership functions for a) input variables b) output variables*

Table 1. *Rule table for* u_N *and* Δu_N

e_N \ $\dot{e}_N$	***NB***	***NS***	***Z***	***PS***	***PB***
NB	*NB*	*NB*	*NM*	*NS*	*Z*
NS	*NB*	*NM*	*NS*	*Z*	*PS*
Z	*NM*	*NS*	*Z*	*PS*	*PM*
PS	*NS*	*Z*	*PS*	*PM*	*PB*
PB	*Z*	*PS*	*PM*	*PB*	*PB*

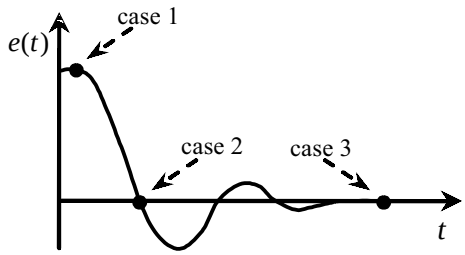

Fig. 6. *Graphical representations for the sample rules*

the e_N is *Z* but it tends to increase due to the nonzero $\dot{e}_N$ thus, u_N or Δu_N should not be zero and it is selected to be *NM*. In case 3, both e_N and $\dot{e}_N$ are *Z*, which is the desired case and the system does not need any control input therefore, u_N or Δu_N is selected to be *Z*. The rules are in the following form for the PD-type fuzzy logic controller:

$$\begin{aligned} &\textit{If } (e_N \textit{ is } PB) \textit{ and If } (\dot{e}_N \textit{ is } Z) \\ &\textit{Then } (u_N \textit{ is } PM) \qquad \text{case 1} \end{aligned} \tag{23}$$

$$\begin{aligned} &\textit{If } (e_N \textit{ is } Z) \textit{ and If } (\dot{e}_N \textit{ is } NB) \\ &\textit{Then } (u_N \textit{ is } NM) \qquad \text{case 2} \end{aligned} \tag{24}$$

$$\begin{aligned} &\textit{If } (e_N \textit{ is } Z) \textit{ and If } (\dot{e}_N \textit{ is } Z) \\ &\textit{Then } (u_N \textit{ is } Z) \qquad \text{case 3} \end{aligned} \tag{25}.$$

And for the PI-type fuzzy logic controller:

$$\begin{aligned} &\textit{If } (e_N \textit{ is } PB) \textit{ and If } (\dot{e}_N \textit{ is } Z) \\ &\textit{Then } (\Delta u_N \textit{ is } PM) \qquad \text{case 1} \end{aligned} \tag{26}$$

$$\begin{aligned} &\textit{If } (e_N \textit{ is } Z) \textit{ and If } (\dot{e}_N \textit{ is } NB) \\ &\textit{Then } (\Delta u_N \textit{ is } NM) \qquad \text{case 2} \end{aligned} \tag{27}$$

$$\begin{aligned} &\textit{If } (e_N \textit{ is } Z) \textit{ and If } (\dot{e}_N \textit{ is } Z) \\ &\textit{Then } (\Delta u_N \textit{ is } Z) \qquad \text{case 3} \end{aligned} \tag{28}.$$

3 NUMERICAL RESULTS

In this section, numerical results for dual arm robot system are presented. The parameters of the designed PI+PD type fuzzy logic controller are given in the Appendix. In order to reveal the performance of the designed controller better, the conventional (PD type) fuzzy logic controller is also included in the numerical analysis and numerical parameters for the conventional fuzzy logic controller are same as the PD part of the designed PI+PD fuzzy logic controller.

Normally distributed noise components which are thought as random disturbing torques acting on the related joints and unexpected non-linear torque disturbance because of the elastic element catching the first arm are shown in Figure 7a and b, respectively. These disturbances are introduced to the system in order to test the robust behavior of the controller used.

During the motion of the robot arms, there are two stages, namely approaching and transportation stages. Transportation stage consists of two periods. First, the first arm is free; in second period the first arm is caught by an unexpected elastic element. In the beginning, the robot arms are at rest and the corresponding initial values of the joints are $\theta_1(0)=0$, $\theta_2(0)=9\pi/10$, $\theta_3(0)=\pi$ and $\theta_4(0)=-9\pi/10$. In the first part of the motion, the robots are approaching to the load and in the second part of the motion the robot arms handle the load and transfer it to its new location. The reference trajectories for the coordinates of the load center during the transportation are defined by:

$$x_{Mr}(t) = x_f + (x_i - x_f)\exp\left(-20(t-2)^2\right) \tag{29}$$

$$y_{Mr}(t) = y_f + (y_i - y_f)\exp\left(-20(t-2)^2\right) \tag{30}.$$

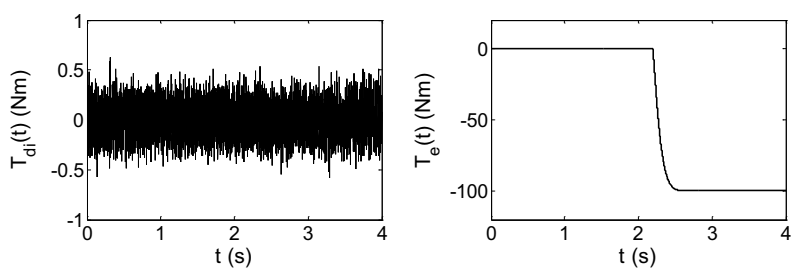

a) b)

Fig. 7. *a) Noise acting on links b) The resulting torque disturbance of the elastic element on first link*

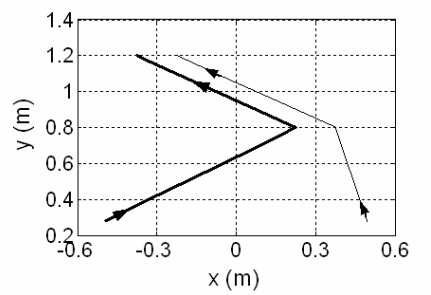

Fig. 8. *Robot arm trajectories (—— First robot arm , —— Second robot arm)*

The initial and final coordinates of the load are given in the Appendix. The approaching motion is accomplished until 2nd second and the transportation starts after that moment. The actual trajectories of the robot arm tips during approaching and transportation motion are given in Figure 8.

It should be noted that for all subsequent figures, the first two seconds correspond for the approaching motion and the second two seconds correspond for the transportation motion of the robot arms. The reference angles for the controllers, which are given in Figure 9, are obtained by inverse kinematics using the desired trajectory for the load. It is clear from Figure 9 that, both conventional fuzzy logic controller and proposed PI+PD controller ensured that both of the robot arms track their trajectory successfully in spite of the external disturbances since the reference and actual angle values are the same.

In order to evaluate and clarify the performance of the proposed controller, tracking errors of the related joints for the conventional and designed PI+PD fuzzy logic controller are shown in Figure 10. It is observed that the proposed controller successfully overcomes the effect of the undesired noise components and unexpected nonlinear torque disturbance whereas the conventional fuzzy logic controller could not remove the steady state errors and the steady state error for the first joint angle of the first robot arm is fairly big due to the unexpected nonlinear torque disturbance. Additionally, the magnitudes of the error values for the PI+PD type controller are smaller and they converge to zero, rapidly. Thus, it is concluded that the tracking performance of the proposed PI+PD type fuzzy logic controller during the approaching and transportation motions is highly acceptable.

Figure 11 depicts the time history of the interaction forces F_1 and F_2 for the PI+PD type fuzzy logic controller. Since there is no interaction between the robot arms and load during the approaching motion, the magnitudes of those forces are identically zero until 2nd second. After that moment the load is handled and transportation begins. Thus, the magnitudes of the forces increase at the beginning of the transportation and thereafter smoothly changes. Also, it should be noted that at the end of the motion there are residual forces both for F_1 and F_2 due to the weight of the load and they are both equal to $Mg/2\mu$.

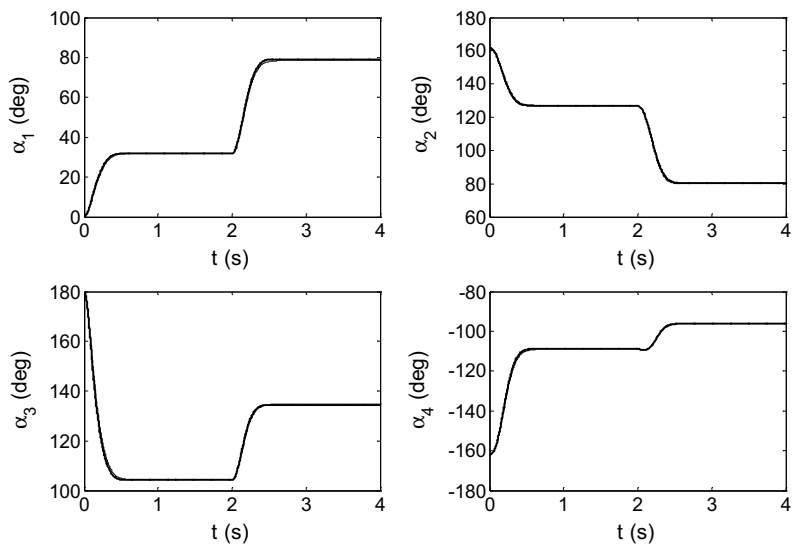

Fig. 9. *Joint angles (reference ····· , conventional fuzzy controlled ——, PI+PD type fuzzy controlled ——)*

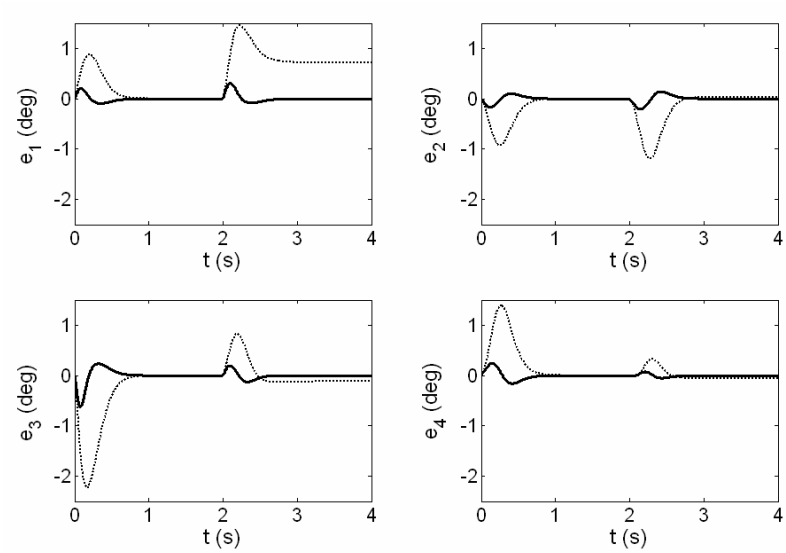

Fig. 10. *Joint angle tracking errors (PD type fuzzy logic controlled ····· , PI+PD type fuzzy logic controlled ——)*

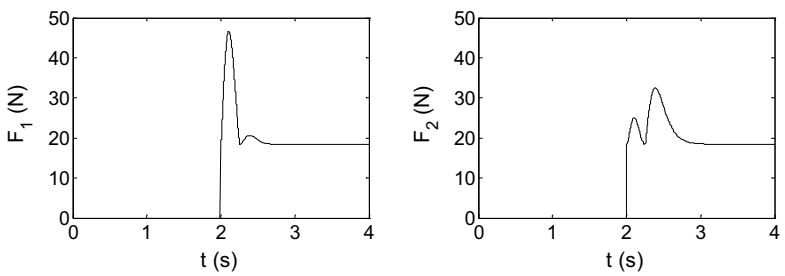

Fig. 11. *Interaction forces*

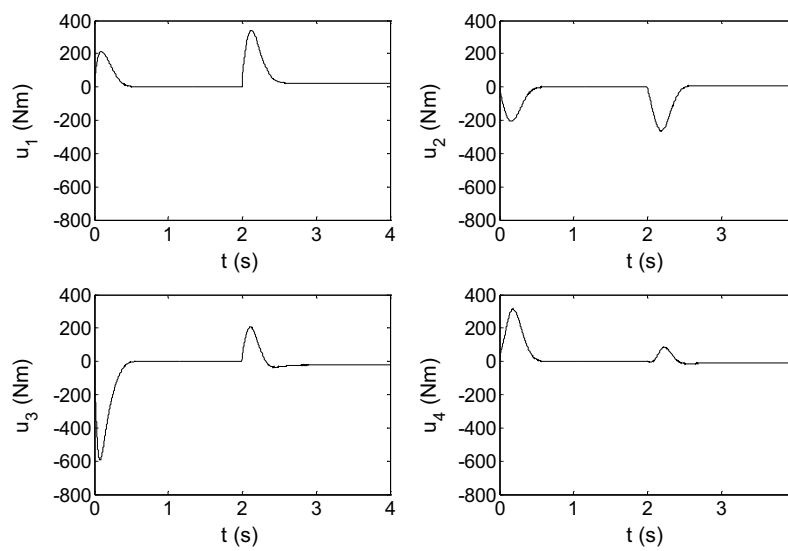

Fig. 12. *Applied joint torques*

Figure 12 presents the control torque inputs to joints which are induced on the related joints by the proposed PI+PD type fuzzy logic controller. The load handling produces interaction forces at the contact points between the load and robot arm tips resulting in changes in control torque inputs.

4 CONCLUSION

Kinematics, dynamics and control scheme of a dual arm robot handling and transferring a load were investigated in this paper. First, dynamic equations of the robot arms and the load were derived. In order to maintain the desired cooperative motion trajectory, PI+PD type fuzzy logic controller was designed for the dual arm robot system. The disturbances such as noise components and an unexpected elastic obstacle were introduced to the system to test the success of the controller. Numerical results showed that PI+PD type fuzzy logic control method showed a satisfactory performance such that the trajectory tracking errors were too small despite the unexpected disturbances. It is concluded that this control method can be used in dangerous environment tasks safely as well as in the applications of industrial automation, medical, and aerospace robotics.

5 APPENDIX

i) Numerical parameters of the two-arm robot system:

$m_i = 2$ [kg]	$\mu = 0.4$
$I_i = 0.135$ [kgm^2]	$k = 1000$ [N/m]
$L_i = 0.9$ [m]	$d_1 = 0.15$ [m]
$b_{ti} = 90$ [Nms]	$d_2 = 0.9$ [m]
$a_i = 0.36$ [m]	$d_3 = 1.35$ [m]
$M = 1.5$ [kg]	

i = 1,2,3,4

ii) Constant coefficients used in the equations of motion of the robot arms:

$$A_1 = m_1 a_1^{\,2} + m_2 L_1^{\,2} + I_1$$
$$A_2 = m_2 a_2^{\,2} + I_2$$
$$A_3 = m_2 L_1 a_2$$
$$A_4 = m_3 a_3^{\,2} + m_4 L_3^{\,2} + I_3$$
$$A_5 = m_4 a_4^{\,2} + I_4$$
$$A_6 = m_4 L_3 a_4$$

iii) Numerical parameters of the controller:

$SF_1 = 10$	$SF_4 = 1$
$SF_2 = 1$	$SF_u = 1500$
$SF_3 = 10$	$SF_{\Delta u} = 20$

Controller parameters are the same for all joints

iv) The initial and final coordinates of the load:

$(x_i, y_i) = (0.3,0.8)$ [m]; $(x_f, y_f) = (-0.3,1.2)$ [m]

6 REFERENCES

[1] Carignan, C.R., Akin, D.L. Cooperative control of two arms in the transport of an inertial load in zero gravity. *IEEE Transactions on Robotics and Automation*, 4(4), 1988, p. 414-419.

[2] Meier, W., Graf, J. A two-arm robot system based on trajectory optimization and hybrid control including experimental evaluation. *Proceedings of the IEEE International Conference on Robotics and Automation*, 1991, p. 2618-2623.

[3] Xue, Q., Maciejewski, A.A., Sheu, P.C.-Y. Determining the collision-free joint space graph for two cooperating robot manipulators. *IEEE Transactions on Systems, Man, and Cybernetics*, 23(1), 1993, p. 285-294.

[4] Yamano, M., Kim, J.S., Konno, A., Uchiyama, M. Cooperative control of a 3D dual-flexible-arm robot. *Journal of Intelligent and Robotic Systems*, no. 39, 2004, p. 1-15.

[5] Khalili, D., Zomlefer, M. An intelligent robotic system for rehabilitation of joints and estimation of body segment parameters. *IEEE Transactions on Biomedical Engineering*, 35(2), 1988, p. 138-146.

[6] Kron, A., Schmidt, G. Haptic telepresent control technology applied to disposal of explosive ordnances: Principles and experimental results. *IEEE International Symposium on Industrial Electronics*, Croatia, 2005, p. 1505-1510.

[7] Tarn, T.J., Bejczy, A.K., Yun, X. New nonlinear control algorithms for multiple robot arms. *IEEE Transactýons on Aerospace and Electronic Systems* 24(5), 1988, p.571-583.

[8] Tarn, T.J., Bejczy, A.K., Yun, X. Design of dynamic control of two cooperating robot arms: closed chain formulation. *Proceedings of the IEEE International Conference on Robotics and Automation*, Raleigh, NC, 1987, p.7-13.

[9] Uchiyama, M., Dauchez, P. A symmetric hybrid position/force control scheme for the coordination of two robots. *Proceedings of the IEEE International Conference on Robotics and Automation*, Philadelphia, 1988, p. 350-356.

[10] Laroussi, K., Hemami, H., Goddard, R.E. Coordination of two planar robots in lifting. *IEEE Journal of Robotics and Automation*, 4(1), 1988, p. 77-85.

[11] Liu, Y.H., Arimoto, S. Distributively controlling two robots handling an object in the task space without any communication. *IEEE Transactions on Automatic Control*, 41(8), 1996, p. 1193-1198.

[12] Yim, W., Selvarajan, M., Wells, W.R. Sliding mode cooperative motion control of dual arm manipulators. *Artif. Life Robotics*, 3, 1999, p.166-159.

[13] Liu, J.F., Abdel-Malek, K. Robust control of planar dual-arm cooperative manipulators. *Robotics and Computer-Integrated Manufacturing*, vol. 16, no. 2-3, 2000, p. 109-120.

[14] Nagchaudhuri, A., Garg, D.P. Adaptive control and impedance control for dual robotic arms manipulating a common heavy load. *International Conference on Advanced Intelligent Mechatronics Proceedings*, Italy, 2001, p.683-688.

[15] Hsu, P. Coordinated control of multiple manipulator systems. *IEEE Transactions on Robotics and Automation*, 9(4), 1993, p. 400-410.

[16] Zadeh, L.A. Fuzzy sets. *Information and Control*, 8, 1965, p. 338-353.

[17] Emami, M.R., Goldenberg, A.A., Turksen, I.B. Fuzzy-logic control of dynamic systems: from modeling to design. *Artificial Intelligence*, 13, 2000, p.47-69.

[18] Zanoli, S.M., Conte, G. Remotely operated vehicle depth control. *Control Engineering Practice*, 11, 2003, p. 453-459.

[19] Taskin, Y., Hacioglu, Y., Yagiz, N. The use of fuzzy-logic control to improve the ride comfort of vehicles. *Strojniski Vestnik-Journal of Mechanical Engineering*, 53(2007)4, p. 233-240.

[20] Yesil, E., Guzelkaya, M., Eksin, I. Self tuning fuzzy PID type load and frequency controller. *Energy Conversion and Management*, 45, 2004, p. 377-390.

[21] Lee, J. On methods for improving performance of PI-type fuzzy logic controllers. *IEEE Transactions on Fuzzy Systems* 1(4), 1993, p. 298-301.

[22] Woo, Z.W., Chung, H.Y., Lin, J.J. A PID type fuzzy controller with self-tuning scaling factors. *Fuzzy Sets and Systems*, 115, 2000, p. 321-326.

[23] Guzelkaya, M., Eksin, I., Yesil, E. Self-tuning of PID-type fuzzy logic controller coefficients via relative rate observer. *Engineering Applications of Artificial Intelligence*, 16, 2003, p. 227-236.

[24] Mudi, R.K., Pal, N.R. A robust self-tuning scheme for PI- and PD-type fuzzy controllers. *IEEE Transactions on Fuzzy Systems*, 7(1), 1999, p. 2-16.

[25] Xu, J. X., Hang, C.C., Liu, C. Parallel structure and tuning of a fuzzy PID controller. *Automatica*, 36, 2000, p. 673-684.

Strojniški vestnik - Journal of Mechanical Engineering 54(2008)5, 356-363
UDC 620.92
UDC 629.3.021.2
Paper received: 20.7.2007
Paper accepted: 19.12.2007

Fuelling the Car of the Future

Paul McGuiness
Jožef Stefan Institute, Slovenia

Whether you worry about man-made global warming due to the burning of fossil fuels, or not, you have to face up to the fact that the supply of crude oil that we convert to petrol and diesel is finite, and the time when it will no longer be possible to match supply with demand is not so far away. Projections vary, but even the most optimistic do not predict much more than 20 years. For this reason we need to start looking very seriously at ways we can fuel our vehicles in a post-crude-oil future. Hydrogen is a popular option, but is it a realistic one? Don't the Brazilians run their cars on alcohol? Is that a strategy we could apply world wide? And what about battery-powered vehicles? Is that just for golf carts? The answer, as it turns out, is not to go for a single option, rather we will have to employ a combination of some of these technologies to keep us on the road.

Keywords: automobiles, internal combustion engine, hybrid electric vehicle, fuels, renewable energy sources

0 INTRODUCTION

In the industrialised world, approximately 97% of the energy consumed by cars, vans, lorries and airplanes comes from refined crude oil [1]. With the end of plentiful supplies of cheap crude oil in sight we need to look closely at alternative ways of powering our transport systems. In simple terms we appear to have two choices, either we find an alternative to the refined petroleum product we use now, for example, biodiesel, ethanol or hydrogen, and so keep vehicles with internal combustion engines (albeit with a different fuel), or we look at a radical change to the way we store the energy in the vehicle, for example, hydrogen-storage materials or batteries, and go for vehicles that are driven by electric motors. In this article we will look at how realistic these choices are and attempt to predict how the engines of vehicles will change over the next 20 years or so, based on the best information available now.

1 STAYING WITH THE INTERNAL COMBUSTION ENGINE

The internal combustion engine (ICE) has been the main power unit of the motorcar for more than 100 years. Despite a mechanical efficiency of just 20% or so [1] it has seen off, among others, gas engines, the Hornsby-Ackroyd oil engine and the rotary Wankel engine. Although the classic four-stroke cycle has remained largely unaltered, engineers and scientists have continued to improve the design in terms of power output and fuel economy, and it is very likely that the ICE will continue to be the mainstay of the car's power-production unit for a long time yet. In the first half of this paper we look at alternatives to petrol that we can put in the tank.

1.1 Ethanol

Ethanol is an alternative fuel popular with farmers, who anticipate healthy profits, and car companies, who will not have to make any major changes to the engines they are already producing. The world's total production of ethanol in 2006 amounted to 51 billion litres, with 69% of this coming from Brazil and the United States [2] (Fig. 1). Ethanol can be used as both a motor fuel and as a fuel additive. In Brazil, for example, 50% of cars can run on 100% ethanol; this figure includes ethanol-only engines and what are called "flex-fuel" engines, which can run on any mixture of ethanol and gasoline. In the United States, however, only 6m of the country's 237m cars and lorries can be described as "semi-flex-fuel" vehicles, able to use a fuel called E85 (85% ethanol). In Brazil the ethanol is produced from sugar cane; this makes Brazilian ethanol easier and cheaper to make than American ethanol, which is normally produced from maize. The maize-based fuel has two main

*Corr. Author's Address: Jozef Stefan Institute, Department for Nanostructured Materials, Jamova 39, SI-1000 Ljubljana, Slovenia, paul.mcguiness@ijs.si

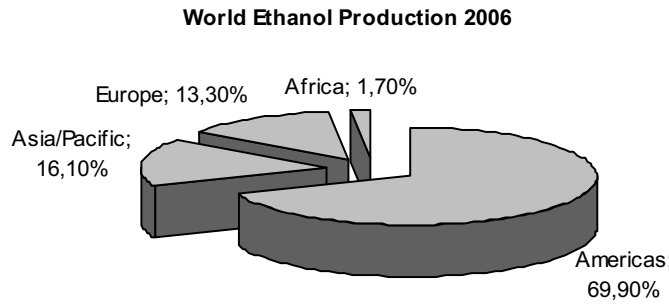

Fig. 1. *A breakdown of global ethanol production for 2006*

disadvantages. Firstly, it is expensive; its price at a gas station in the US is only competitive with petroleum because the country's taxpayers subsidise production to the tune of $6 billion a year. Secondly, corn ethanol has dubious green credentials. Researchers in California [3] have reported that maize-based ethanol is only some 10–15% better than gasoline in terms of greenhouse-gas emissions. There are, however, alternative ways of producing ethanol under investigation; one of the most promising involves making it from straw, woodchips or anything containing cellulose. This idea has proved popular with the American president, who has pledged $385m in government subsidies to bring cellulose-based ethanol to the market [4]. One additional problem with ethanol is that it is less energy intensive than petrol (about 30% less energy per unit volume [5]), which means accepting lower performance, a shorter range between fill ups or a larger fuel tank, taking up passenger space in the vehicle. However, a recent report in Nature [6] suggests that the problems associated with the lower energy density of ethanol can be overcome by producing it straight from fructose, which is present in fruits such as apples, pears, berries and melons as well as some vegetables. The resulting fuel is not only energy rich, it is also water repellent, so overcoming another problem associated with ethanol.

1.2 Biodiesel

Biodiesel is a diesel-equivalent fuel produced from biological sources, such as vegetable oils, and can be used in an unmodified diesel engine. This property distinguishes it from vegetable oils, which require the vehicle's engine to be modified. In contrast to the situation regarding ethanol, when it comes to biodiesel, Europe is the dominant player (Fig. 2). Biodiesel is both non-toxic and biodegradable, and produces only 40% as much CO_2 as conventional diesel because most of the CO_2 released during the combustion process was absorbed from the atmosphere by the crops that were later processed to produce the biodiesel. One of the most attractive features of biodiesel is that it can be produced from a very wide range of oils. These include rapeseed and soyabean oils,

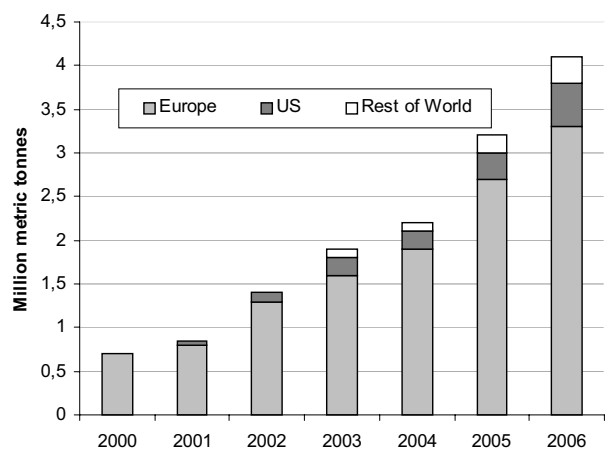

Fig. 2. *World biodiesel production from 2000 to 2006*

sunflower, canola and palm oils, waste vegetable oils, animal fats, and some forms of sewage [7]. The most obvious problem associated with a shift away from fossil-fuel-based petroleum to biofuels is the huge amounts of farmland required to grow the plant feedstock. Best estimates suggest that the US could produce only 25% of the 80 billion US gallons of diesel fuel it consumes every year if it was to use all its fallow, set-aside and export-crop lands [8]. Conservationists are also very worried about how the chopping down of tropical forests to clear space for growing biofuel feedstock could threaten the existence of the natural habitat of enormous numbers of animal species, including our close relatives, the great apes [9]. However, it would also be foolish to overlook the politically sensitive issue of rich Western countries growing food for fuel while poorer parts of the world struggle to grow enough food to feed their populations [10]. In the US, estimates of the total amount of fuel used for heating and transportation put the figure at about 230 billion US gallons [11]. This figure dwarfs the total amount of vegetable oils used for all purposes (3 billion US gallons) [12], which means that at best, biodiesel will fill a niche market as just one of the fuels that will begin to replace petroleum over the next 20 years.

1.3 Vegetable Oils

Many vegetable oils have similar properties to diesel, which means that with simple engine modifications they can be used to fuel a wide range of vehicles. Two grades are available: straight vegetable oils (SVOs) and waste vegetable oils (WVOs). It is ironic that Rudolf Diesel, who invented the diesel engine, originally designed it to run on peanut oil; however, it was soon discovered that the engine would also run on the cheaper petroleum oil, and as a result the diesel engine has been a heavy polluter throughout most of its history. Today, most diesel cars can run on SVO with a few simple modifications costing less than €500. Viscosity is SVO's main drawback, which means that it must be preheated in the fuel tank or blended with straight diesel during the winter months. The legal situation with regard to using vegetable oil to fuel your car is far from clear. In the US, for example, the conversion of an automobile to run on vegetable oil is illegal under United States Environmental Protection Agency guidelines. Taxation also remains a mostly unresolved issue, although Germany, Canada, and Ireland have decided to impose a 0% tax. In the UK, Her Majesty's Revenue & Customs have decided to impose the full diesel excise rate of £0.47 per litre [13].

WVOs are widely available as they are a waste product from the food-processing industry and the restaurant industry, in particular fast-food outlets; however, the collection and cleaning costs are likely to keep this form of oil from ever becoming a profitable product.

1.4 Hydrogen

Internal combustion engines (ICEs) designed to run on hydrogen are only slightly modified versions of the petroleum engines in most of today's cars. The introduction of the hydrogen ICE is often seen as a way of moving quickly towards a hydrogen-fuel economy without having to wait for fuel cells (necessary to generate electricity from the hydrogen) to become a practical and economic reality for fully electric-powered vehicles. Of the world's major car manufacturers, Ford and BMW have been most active in the pursuit of the hydrogen ICE, and in an attempt to publicise the success of their work on hydrogen vehicles, BMW built the BMW H2R. Designed and developed in only 10 months, this 6-litre V12 generates 232 HP and has a top speed of over 187 mph. BMW have also announced the Hydrogen 7, a derivative of the 7 Series 12-cylinder engine, which will be able to run on liquid hydrogen or gasoline. Plans were to begin sales to customers in Europe and the US in 2007 [14].

At first glance the hydrogen-powered ICE is a compelling solution, but although it gets around the fuel-cell problem (of which more later) it does not solve many intractable problems associated with hydrogen as a fuel. First off, how do we make the hydrogen? There is little or no hydrogen gas in the atmosphere, which means we need to create the hydrogen by breaking the chemical bonds in water, or methane or some other compound. All this takes energy, and this energy has to come from somewhere. With the prospects for solar panels covering the world's deserts still a long way off, the only realistic solutions involve using fossil fuels, but then that negates any benefit of using hydrogen in the first place, or renewables, but they

would be better used displacing coal-fired power stations than replacing gasoline. Using hydrogen from renewable sources has a carbon-dioxide avoidance cost of $600/tonne, which is a factor of 10 higher than most other avoidance strategies under consideration [15]. Secondly, how would the hydrogen be distributed? There is a tendency in the pro-hydrogen lobby to talk in terms of millions of mass-produced low-cost fuel-cell cars being refuelled by hydrogen from a Europe- or US-wide system of super-insulated pipelines carrying liquid hydrogen. But who is going to fund the building of this pipeline, especially when the advantages of hydrogen as a viable fuel for vehicles are far from clear? And what about the energy costs of making liquid hydrogen? Turning hydrogen gas into liquid hydrogen costs you a third to a half of the energy in the resulting liquid hydrogen [16], and then because you have to keep it in an un-pressurised fuel tank in the car at -241°C a quarter of the hydrogen will boil away every week. Analyses looking at hydrogen-powered vehicles have suggested that hydrogen will not play any sort of role in transport until after 2035 [17], and a report by the National Research Council in the US suggested that the DOE should stop funding research on high-pressure tanks and liquid hydrogen because they have little promise of any long-term practicality [18].

1.5 Other Fuels

Although much of Europe now has a single currency, European drivers are likely to face a wide variety of filling-up options in the near future. As well as the ethanol, biodiesel and oils described above there will be the opportunity to buy compressed natural gas, known as CNG, liquefied petroleum gas (LPG) and there will also be plug-in points for electric cars. Car manufacturers are responding to this multi-fuel situation by making their cars more flexible in terms of the fuels they can use. Fiat, for example, has introduced its Tetrafuel [19] system, which means that some of its cars can run on four different fuels: petrol, a mixture of petrol and ethanol, pure ethanol, and CNG. Not wishing to be left out, GM Europe has an Opel Zafira that can run on natural gas and some Saabs, the 9-5 and 9-3, can use ethanol mixes. Which of these fuels will win out depends as much on the policies of governments when it comes to taxation as on anything else. However, if supplies of crude oil from the oil fields of the world were to start drying up more quickly than currently anticipated there must be serious doubts as to whether the gaps in supply that would appear could be filled by any or all of these alternative fuels without introducing price increases that would see the mass abandonment of private vehicles and the serious problems that that would pose to governments.

2 SWITCHING TO VEHICLES WITH ELECTRIC MOTORS

Everyone in the automotive industry agrees that one day all cars will be electric vehicles. What they do not agree on is when that will be and how will the energy to drive the electric motors be stored in the vehicle. Right now the industry is divided into two camps: those who think that hydrogen combined with fuel cells will produce the electricity, and those who see batteries as the future. In the second half of this paper we take a closer look at these technologies.

2.1 Hydrogen-Powered Fuel-Cell Vehicles

The fuel cell is a device for combining hydrogen or hydrogen-containing gases with the oxygen in the atmosphere to produce electricity. This electricity can then be used to do work, like powering the wheels of a car. Much of the attraction of such a car comes from the rather narrow perspective of a car with a store of hydrogen, converting hydrogen to electricity, and then using this electricity to power the car while pure water drips from the "exhaust pipe". The broader reality is quite different. Not only is hydrogen awkward to produce in a clean process and enormously expensive to transport, by whatever method we choose, storing it in the car as a gas or in a storage material also presents us with massive problems – and that is before we get to the cost of fuel cells.
We have already looked at the problems associated with liquid hydrogen, but hydrogen could also be stored in the car as a gas under high pressure or in solid-state form, for example, as a metal hydride. Unfortunately, hydrogen's volumetric energy density is very low (Fig. 3), which means we would have to use very high pressures to store on board about 4–5 kg of hydrogen to give a range of about

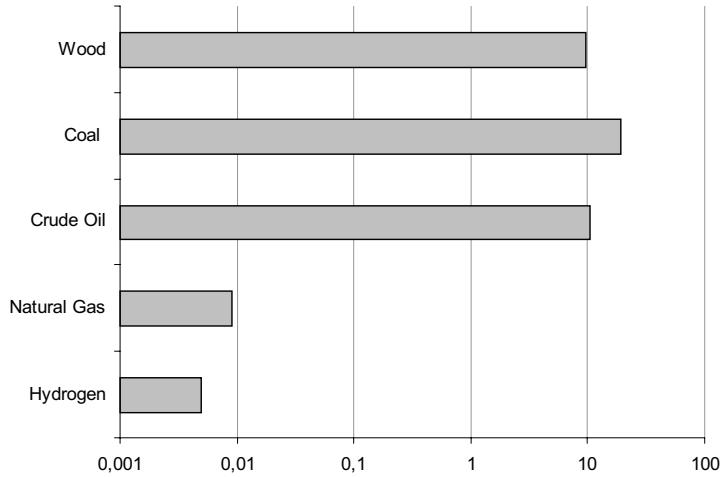

Fig. 3. *Volumetric energy density of some common fuels*

400–500 km. Maintaining gases safely at pressures up to 500 bar is a realistic possibility, albeit a very expensive one. A 500-bar hydrogen fuel tank would probably cost $2100 per kilogram of capacity [20]. Another problem with high-pressure tanks is their shape. The strength of the shell demands a cylinder; the last thing a car designer wants is to find a way of absorbing such a shape into the layout of the car.

So what about storing the hydrogen in solid-state form, in a hydrogen-storage material? The best known and most intensively researched hydrogen-storage materials are the metal hydrides. Put simply, the metal or alloy acts like a sponge, absorbing the hydrogen in atomic form into the matrix of the metal or alloy. The hydrogen atoms then occupy the interstitial sites between the metal atoms in a thermodynamically metastable system. The best of such systems can store up to a maximum of about 2 weight percent hydrogen [21] and [22], but that is not enough. Remembering that we need 4 to 5kg of hydrogen, that means our "fuel tank" would weigh at least 250kg – about the same weight as a large Harley Davidson motorcycle. This extra weight would hurt the fuel efficiency, one of the main reasons for having a hydrogen-powered vehicle in the first place. In spite of the fact that there have been no real breakthroughs in this area for 20 or 30 years, a lot of scientists, particularly in Europe, continue to plug away in this field. As part of its 5th Framework Programme the EU funded three projects – HYSTORY, FUCHSIA and HYMOSSES – with at least one more – STORHY – as part of the 6th Framework, with little sign of a major breakthrough in hydrogen-storage materials. Indeed, the surprising enthusiasm for funding hydrogen-storage research shown by oil companies like BP [23], Shell [24] and Chevron [25] would almost suggest they are attempting to improve their green credentials while knowing they are running little risk of being put out of business by hydrogen any time soon.

Researchers are also struggling with other issues relating to the onboard storage of hydrogen in a metal-hydride-type system. One problem that seems particularly tricky to solve is that of refuelling. Reversible metal-hydride systems are refuelled with a supply of pure hydrogen, but this refuelling period could take hours rather than a few minutes, making refuelling stops on a long journey something more than a quick stop at the petrol station.

Now let us turn to fuel cells. The first fuel cell was developed by the Welsh scientist Sir William Robert Grove in 1843, making this technology quite some years older than the ICE. A fuel cell differs from a battery in that it consumes reactant, which has to be replenished, while batteries store electrical energy chemically in a closed system. As far as automotive applications are concerned the most promising type of fuel cell is known as the proton-exchange-membrane (PEM) fuel cell, which uses hydrogen as the fuel and oxygen from the atmosphere as the oxidant. One of the most positive aspects of a hydrogen fuel-cell car is the so-called tank-to-wheel efficiency.

Under small loads this can be as high as 45%, with average values of about 36% on a driving cycle like the New European Driving Cycle [26]. The comparable value for a diesel-engined vehicle is about 22%. A more realistic figure, however, is the power-plant-to-wheel efficiency. In this case the values are reduced to 22 and 17%, respectively, when the hydrogen is stored as a high-pressure gas or as a liquid. A detailed investigation of the efficiencies of various fuel paths can be found in a 2004 review in Scientific American [27].

Fuel cells also suffer from being extremely expensive. Prices vary, but for a PEM fuel cell you would expect to pay anywhere from $1000 to $5000 per kW for a 10-kW to 100-kW motor. For a fuel cell to become competitive with an ICE these costs will have to tumble to less than $50 per kW. Mass production alone will not suffice; a technological breakthrough is required.

2.2 Battery-Powered Electric Vehicles

Whenever battery-powered vehicles are mentioned, most people instinctively think of a milk float or a golf cart. However, the reality of a modern battery electric vehicle (BEV) is very different. Many such vehicles are capable of accelerating faster than conventional gasoline-powered cars, they are also quiet, and they do not produce noxious fumes from an exhaust pipe. Over most of their history BEVs have had problems with the high costs of batteries, a limited range between "refuelling" stops, charging times and battery lifetimes. However, while hydrogen vehicles have been grabbing all the publicity, ongoing battery-technology developments have gone a long way to solving these problems. As of 2004, there were more than 55,000 BEVs in the US, with an annual growth rate of almost 40% [28] (Fig. 4).

There are, of course, still problems associated with BEVs. The purchase price of a BEV is typically 80% more than a comparable petrol or diesel car or van. Battery-replacement costs are also high, which means that leasing, at a cost of about €100 per month, is a popular option among owners. Running costs for a BEV are in the region of €0.01–0.02 per km, which means a saving of €1200 per year in fuel costs for a typical 15,000 km per year. However, if battery leasing costs are included, these cancel out the fuel savings. Whether BEVs are more environmentally friendly and reduce the consumption of fossil fuels depends on the source of the electricity used to charge them up. Like with the energy needed to produce hydrogen: if it is a clean source, we should be using that clean electricity to displace the electricity that comes from the dirtiest sources like coal, and if it is a dirty source, then we are really fooling ourselves if we say that a BEV is an emissions-free or environmentally friendly vehicle.

The Achilles' heal of a purely electric vehicle is the battery; the current technologies for electric motors are more than good enough. BEVs use many different types, e.g., lead-acid, NiCd,

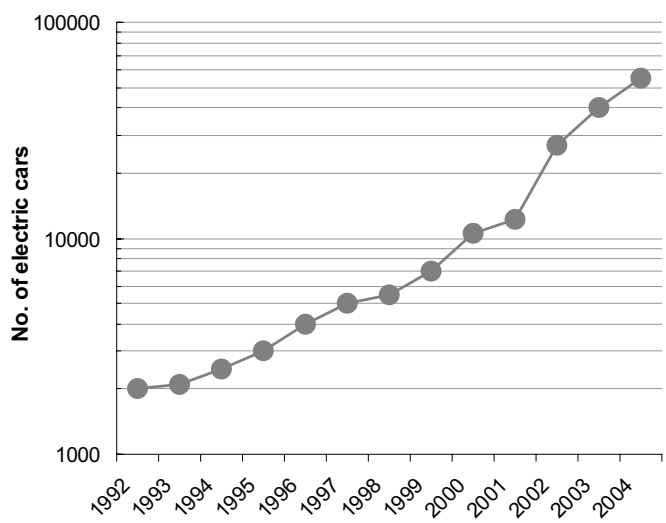

Fig. 4. *Growth in the number of electric cars in the US (1992 to 2004)*

nickel metal hydride, lithium ion, and Li-ion polymer. Of these, lead-acid batteries are the cheapest, most familiar and easily available. A typical lead-acid-battery-based car has a range of 30–80km, depending on a number of factors, like the use of headlights and the temperature. General Motors' EV1, the most famous all-electric car, never performed well in cold weather. However, new research [29] suggests that the use of foam grids in lead-acid batteries could significantly improve the range of such cars. Nickel metal hydride batteries can deliver up to 200 km of range, and vehicles fitted with lithium-ion batteries can drive as far as 400 to 500 km on a single charge, and although these figures represent ideal rather than real driving conditions it is clear that batteries are closer to being good enough than any hydrogen-storage material.

3 WHICH WAY DO WE GO FROM HERE?

So, having looked at a lot of alternatives, can we now predict what will be powering our cars 20 years from now? The truth is that none of the alternatives above – on their own – provide the answer. However, the beginnings of a solution are already with us, in the form of hybrid vehicles, the most popular example of which is the Toyota Prius. Hybrid vehicles combine a small, but fairly conventional, diesel or petrol engine with an electric motor. This electric motor runs from a battery, which is charged by regenerative braking, and used primarily at low speeds, when the petrol or diesel engine is at its most inefficient. It is this combination of saving energy during braking and optimising performance that makes hydrids very efficient vehicles, particularly on low-speed, stop-start urban cycles. The latest-model Prius, for example, has a City Fuel Economy figure of 4 litres/100km; about half what you would expect from a similar-sized petrol-driven car. However, these are early days; the next five years should see car showrooms displaying what are known as plug-in hybrids. A plug-in hybrid has the rechargeable batteries, the electric motor and the petrol or diesel engine, but it also has the option to charge these batteries from the electricity grid while the car is parked, so giving the car a significant all-electric range. As of 2007 there are no plug-in hybrid passenger vehicles in production [30], but both Toyota and General Motors, with its new Volt concept car, have signalled their intension to introduce them soon. GM claim that after being charged from a domestic power outlet for six hours the Volt will be able to drive about 65 km on the batteries alone, without consuming a drop of petrol from the tank. They are also boasting that the Volt could save an average motorist 500 (US) gallons (1850 litres) of petrol per year [31]. In other words, the plug-in hybrid is a stepping stone to the all-electric vehicle. But what makes it particularly attractive is that it can be done in many small steps without running the risk of introducing a disruptive technology – like hydrogen-powered vehicles – that would be both enormously expensive and far from certain to succeed. Then, as battery technology improves, each new generation of plug-in hybrids will have a smaller and less frequently required petrol engine until eventually the vehicle will have sufficient range in its batteries to dispense with the petrol engine altogether. But does that mean the hydrogen-powered car will never be a mainstream reality? We would have to conclude that the answer is almost certainly no. When it comes to storing energy in a mobile device, however we look at it – safety, cost, weight, recharging – batteries are likely to be as good or better than any hydrogen-storage techniques, and when it comes to transporting this energy, hydrogen can never match the ease with which we can distribute electricity through ordinary copper wires.

4 REFERENCES

[1] Romm, J. The car and the fuel of the future. *Energy Policy*, 34 (2006), p. 2609–2614.

[2] Heywood, J.B. *Internal combustion engine fundamentals*. McGraw-Hill series in mechanical engineering, 1988.

[3] *Renewable fuels association industry statistics*, http://www.ethanolrfa.org/industry/statistics/#E, July 2007.

[4] Farrell, A.E., Plevin, R.J., Turner, B.T., Jones, A.D., O'Hare, M., Kammen, D.M. Ethanol can contribute to energy and environmental goals. *Science* 311 (5760), p. 1747–1748.

[5] The drive for low emissions, *The Economist*, (2007) 29–30 (supplement).

[6] US Department of Energy, Alternative Fuels Data Center, http://www.eere.energy.gov/afdc/progs/ddown.cgi?afdc/FAQ/5/0/0, July 2007.

[7] Schmidt, D.L., Dauenhauer, J.P. Hybrid routes to biofuels. *Nature*, vol. 447, 21 June (2007), p. 914–915.
[8] Kiong, E., NZ firm makes bio-diesel from sewage in world first. *The New Zealand Herald*, 12 May (2006). http://www.nzherald.co.nz/section/1/story.cfm?c_id=1&ObjectID=10381404.
[9] *BiodieselAmerica.org*, http://www.biodieselamerica.org/node/2784.
[10] Adam, D. Great apes face disaster. *The Guardian Weekly*, 15 June 2007, p. 29.
[11] Vidal, J. *Global rush to energy crops threatens to bring food shortages and increase poverty, says UN. The Guardian*, 9 May 2007. http://environment.guardian.co.uk/energy/story/0,,2075292,00.html.
[12] Briggs, M. Biofuels: Re-thinking our approach to alternative fuels. *Chemical Engineer*, 765 (2005), p. 47–49.
[13] Van Gerpen, J. Biodiesel processing and production. *Fuel Processing Technology*, 86 (10) 2005, p. 1097–1107.
[14] *HM Revenue & Customs*, http://customs.hmrc.gov.uk/, July 2007.
[15] Vanzieleghem, B. *BMW officially announces the BMW Hydrogen 7*, http://www.autobloggreen.com/2006/09/12/bmw-officially-announces-the-bmw-hydrogen-7/, July 2007.
[16] Romm, J. The hype about hydrogen. *Island Press*, 2005, p. 156–157.
[17] Bossel, U. The hydrogen "illusion". *Cogeneration and On-Site Power Production*, March-April, 2004, p. 55–59.
[18] Geffen, C., Edmonds, J., Kim, S. Transportation and climate change: the potential for hydrogen systems. *Technology and Business Challenges, SAE World Congress*, Detroit. Mich., vol. 1865 (2004) p. 13–20.
[19] *The hydrogen economy*. National Research Council, National Academy Press, Washington DC, 2004.
[20] *Fiat Brazil launches tetrafuel Sienna*. http://www.ngvglobal.com/market-developments/fiat-brazil-launches-tetrafuel-sienna.html, July 2007.
[21] Simbeck, D., Chang, E. *Hydrogen supply: Cost estimate for hydrogen pathways–scoping analysis*. US Department of Energy, National Renewable Energy Lab, 2002.
[22] *Hydride.* Wikipedia, http://en.wikipedia.org/wiki/Metal_hydride, July 2007.
[23] Zuttel, A. Materials for hydrogen storage. *Materials Today*, September, 2003.
[24] Mbugua, M. *BP awards UD multimillion-dollar renewable energy research grants*. http://www.udel.edu/PR/UDaily/2004/BP051804.html, July 2007.
[25] *Plans to establish hydrogen storage joint venture unveiled*, http://www.shell.com/home/content/media-en/news_and_library/press_releases/2001/planstoestablish_10101302.html, July 2007.
[26] *Texaco and energy conversion devices, inc. form hydrogen storage joint venture*. http://www.chevron.com/news/archive/texaco_press/2000/pr10_31.asp, July 2007.
[27] von Helmolta, R., Eberle, U. Fuel cell vehicles: Status 2007. *Journal of Power Sources*, vol. 165, issue 2 (2007), p. 833–843.
[28] Ward, L.M. Questions about a hydrogen economy. *Scientific American*, May, 2004, p. 42–47.
[29] *Energy Information Administration, Official Energy Statistics from the U.S. Government.* http://www.eia.doe.gov/cneaf/alternate/page/datatables/aft1-13_03.html, July 2007.
[30] Dai, C.S., Zhang, B., Wang, D.L., Yi, T.F., Hu, X.G. Preparation and performance of lead foam grid for negative electrode of VRLA battery. *Materials Chemistry and Physics*, 99 (2-3), (2006), p. 431–436.
[31] *Plug-in hybrid*. Wikipedia, http://en.wikipedia.org/wiki/Plug-in_hybrid, July 2007.
[32] Power struggle. *The Economist*, 2 February 2007.

Strojniški vestnik - Journal of Mechanical Engineering 54(2008)5, 364-371
UDC 528.02
Paper received: 20.6.2007
Paper accepted: 28.9.2007

Modern Deformation Measurement Techniques and their Comparison

Boštjan Kovačič[1,*] - Rok Kamnik[1] - Miroslav Premrov[1] - Nenad Gubeljak[2] - Jožef Predan[2] - Zdravko Tišma[2]
[1]University of Maribor, Faculty of Civil Engineering, Slovenia
[2]University of Maribor, Faculty of Mechanical Engineering, Slovenia

Deformation measurement experiment has been undertaken where a concrete structure was subject to controlled loading. Concrete plate was loaded with hydraulic cylinder PZ 100 up to 42 kN. Nikon total station ser. 720 and camera Fuji Pro S3 have been used to make measurements at critical points during each additional load. A hydraulic computer operated cylinder was used for load increase. The use of total stations for deformation measurements is quite often, but the combination with digital photography is rather new and very suitable technique. It offers the capability of simultaneous monitoring of a large number of signalized or non-signalized points with very low root mean square error of 0.16 mm in geodetic method 0.7 mm in photogrammetry, respectively. The concrete plate was modeled and the comparison with the geodetic, photogrammetric and hydraulic method was made.

Keywords: deformation measurements, geodesy, digital photogrammetry

0 INTRODUCTION

The monitoring of structures has a high importance with regard to the assessment of the reliability, availability, health diagnostics, damage detection, load rating, condition assessments, load carrying capacity estimation and model updating [1]. Control measurements can be performed in a variety of ways depending on the structures. In practice, control measurements are performed with the help of geodetic measurements, the basic goal of which is to capture any geometric changes in the measured object. Displacements and deformations are determined. This means defining the position of changes and the object's shape, with respect to the environment and time. Increasing attention to predictive maintenance and health monitoring of existing structures has prompted more and more research work back to laboratories.

Geodetic deformation measurements are quite often for such tasks [2]. Building monitoring is usually carried out with classic geodetic methods such as trigonometric heights, leveling and nowadays, also with classic or digital photogrammetry, GPS and laser scanners.

The method for fastest and easiest monitoring the points on the structure, with the very good accuracy is a trigonometric height. The step forward is to combine that method with other non-conventional methods such as photogrammetry. Photogrammetric measurement has been, till now, usually used for the needs of architecture (façade), cultural heritage (archaeological sites), medicine (face, body, skin, eyes studies etc.) and industry (quality check). With the development of accuracy in digital photography [3] it is possible to precisely monitor the deformations of objects of interest like concrete plate, bridge, building etc. [4] and [5].

This paper presents the comparison of geodetic deformation measurements with the analitical model, photogrammetric technique and the results of the vertical deflections got from the hydraulic cylinder.

1 THEORETICAL BASICS OF MEASUREMENT METHODS

1.1 Trigonometric Heights

Trigonometric height is the classic geodetic task where the altitude difference between two points is given by [6]:

$$\Delta H = S \cdot ctgZ_A + i_A - l_B + \left(\frac{1-k_a}{2}\right)\cdot\left(\frac{S^2}{R}\right) \quad (1),$$

where:

*Corr. Author's Address: University of Maribor, Faculty of Civil Engineering, Smetanova 17, SI-2000 Maribor, bostjan.kovacic@uni-mb.si

S - horizontal measured distance between A and B
Z_A - vertical distance
i_A - height of instrument at point A
l_B - height of prism at point B
k_a - coefficient of refraction (for Slovenia $k_a = 0.13$) [6]
R - Earth radius as a sphere ($R = \sqrt{M \cdot N}$; M - radius of curvature along the meridian, N - radius of curvature along the prime vertical (transverse radius of curvature); R = 6370,04 km)

In this case the height of instrument i_A can be omitted from the Eq. (1), because measurements were in a relative coordinate system and all measurement were of a fully local nature. The height of prisms l_B can also be omitted from Eq. (1), because reflective tape targets have negligible thickness.

Equation (1) can be simplified:

$$\Delta H = S \cdot ctgZ_A + \frac{S^2}{2R} - k_a \frac{S^2}{2R} \qquad (2).$$

The zenith distance can be replaced by the vertical angle (α); the refraction coefficient can be omitted (because of the laboratory conditions) so the final equation is:

$$\Delta H = S \cdot tg\alpha + \frac{S^2}{2R} - k_a \frac{S^2}{2R} \qquad (3).$$

A post-processing of all recorded data was carried out before the analysis (filtering). In this way all possible errors were eliminated, such as double observation of the same point, wrong order of sightings, etc. The observations were arranged according to individual epoch. Every load test epoch was compared with the zero state, which was recorded from the start of measurements and controlled by the control points on the wall.

The precise processing of the measured data and its analyses were performed after the field measurement. For every target the standard deviation was calculated. Ten readings were performed for each target (distance, horizontal and vertical angle) in the precise measurement mode of the instruments. The arithmetic mean values of the distance readings were calculated. For each target, the standard deviation was calculated [7]:

$$s = \sqrt{\frac{\sum v^2}{(n-1)}} \qquad (4),$$

where:
s - standard deviation,
v^2 - squared deviation from arithmetic mean
n - number of observations.

A measurement precision in distance of ± 0.16 mm, horizontal angle of ± 3.0'', vertical angle of ± 3.4'', Y coordinate of 0.13 mm, X coordinate of 0.13 mm and of Z coordinate of 0.11 mm was achieved.

This method is very fast and accurate with option of getting some of the results already on the field. To get a strong reflected signal small in incident angles should be avoided. Distance measurement represents the essential component of instrument accuracy [8].

The costs of this method increases with the number of surveyed spots. On the field, we usually must use prisms instead of tape targets (there is high installation expense).

1.2 Photogrammetric Method

Stereo-photogrammetry is an optical measuring method which has become a standard method in geodesy, civil engineering and architecture in past few decades. Measuring object is recorded using a high resolution CCD camera after which a digitalisation and computer processing of stereo-couples is made. Picture coordinates of measuring points are being searched with numerical procedures and then calculated in 3D object coordinates using a principle of triangulation. This method is suitable for accurate measuring of the position in space, three-dimensional displacement and with high number of points even measuring of object shape and deformation.

For performing a measurement, two sets of coordinates have to be defined – object (space) coordinates, which are bound to outer coordinate system and picture coordinates which define a position of measuring points on film plane and are bound to camera coordinate system. Dependency between these two coordinate sets with respect to measuring object is shown in Figure 1.

Determination of dependency between object coordinates and picture coordinates of an arbitrary point P begins with setting up a coordinate system in projective center of camera objective O (X_0, Y_0, Z_0) so that its X* and Y* axis are parallel to camera axis x and y. Z* axis is opposite to the optical axis H-O. Object coordinates of point P in this coordinate system are calculated with transformation matrix, whose elements are transformation coefficients based on angles

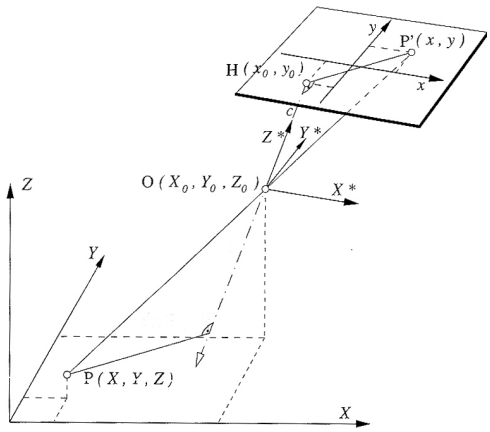

Fig. 1. *Dependency between two coordinate sets*

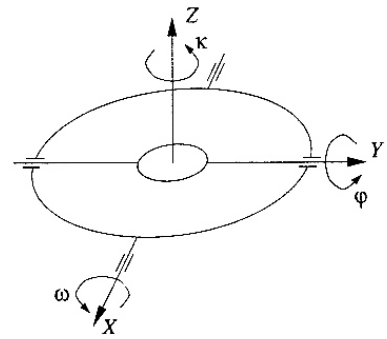

Fig. 2. *Three angles of rotation (ω, φ, κ)*

between coordinate axis. Rotation around coordinate system can be described with three independent angles of rotation (ω, φ, κ) around coordinate axis (X, Y, Z) – Figure 2.

The relation between picture coordinates (x, y) and transformed object coordinates comes from co-linearity condition [8]:

$$\begin{bmatrix} x \\ y \end{bmatrix} = \begin{bmatrix} x_O \\ y_O \end{bmatrix} - \frac{c}{Z_P^*} \begin{bmatrix} X_P^* \\ Y_P^* \end{bmatrix} + \begin{bmatrix} \Delta x \\ \Delta y \end{bmatrix} \quad (5),$$

where x_0, y_0 denotes main point's picture coordinates of snap-shot H and $\Delta x, \Delta y$ denotes deviation from central projection as a consequence of objective distortion. In general the picture coordinates can be written as:

$$\begin{aligned} x &= f\left(c, X_O, Y_O, Z_O, \omega, \varphi, \kappa, X, Y, Z, x_O, \Delta x\right) \\ y &= f\left(c, X_O, Y_O, Z_O, \omega, \varphi, \kappa, X, Y, Z, y_O, \Delta y\right) \end{aligned} \quad (6).$$

It follows that the picture coordinates are a function of six parameters of external orientation – projection center coordinates O (X_0, Y_0, Z_0) and rotation angles (ω, φ, κ) – and three parameters of internal orientation – camera constant c and picture coordinates of snap-shot's main point H (x_0, y_0). Thus if external and internal orientation of camera is known we can calculate a picture coordinate x, y for every object point.

The problems appear, if we would like to calculate object coordinates from picture coordinates. Three unknown object coordinates X, Y, Z can be calculated from two measured picture coordinates only taking extra presumption like observing a flat object which is perpendicular to recording direction so that Z coordinate is constant and known for all measuring points. For object measuring in space it is necessary to take at least one more snap-shot from different angle so that for every measuring point three or more picture coordinates can be measured. For this purpose the stereoscopic effect and method of triangulation is being used.

This principle has been used from the very beginning of stereo-photogrammetry when the measuring object was recorded with cameras from multiple positions after which the pictures (stereocouples) were being processed by using special devices called stereocomparators. Object (space) coordinates of measuring points were determined directly by using so called opto-mechanical reconstruction procedure.

In today's stereophotogrammetric measurement, an automatic – analytical procedure is being used. On stereocouples, which are recorded with CCD cameras, picture coordinates of measuring points are measured with software and for every picture coordinate one equation can be set. Provided that the number of measuring points (and by that the number of extra equation) is bigger than the number of total unknown camera parameters the system of equation becomes overdefined. Thus an exact solution doesn't exist but it needs to be found with a method of minimum deviation.

In classic stereophotogrammetry the measuring points are defined with the help of known details on measuring object or by measuring marks. If measuring marks are well recorded, the accuracy of the method is very high. For measuring position in space, movement tracking, deflection measurement and in application where high point density is not necessary the stereophotgrametric method is the most powerfull among optical methods.

Photogrammetry offers the advantages of a versatile and efficient full field three-dimensional measurement technique, offering a high precision potential at reasonable cost [9].

1.3 Hydraulic Method

There was 14 epochs where the load increased for 3 kN at a time. Each epoch was held for 400 s (static load) for measurement to be made and in the next 100 s the hydraulic cylinder PZ 100 increased the load for 3 kN. The hydraulic cylinder was controlled with a LabVIEW software. Vertical deformation, for central point 5, was measured with a very precise measuring rod attached to the main cylinder. To measure the vertical displacement, measuring rod has an electrical output with the incremental counter.

2 RESULTS

2.1 Test Configuration

In order to compare the above described measurement methods, the prefabricated prestressed concrete plate beam was made (Figure 3). Such concrete beam is frequently used for industrial buildings. Predicted vertical displacements are analytical calculated using the presented static design with the vertical force at the middle of the span. Schematic view of concrete beam is shown in Figure 4.

Deflection of the plate depends on the geometrical and material characteristics of the test sample.

Fig. 3. *Prefabricated prestressed concrete plate with measured marks*

Geometrical characteristics:
Calculated static length: *L = 3750 mm*
Width: *b = 500 mm*
Height: *h = 150 mm*
Effective depth of a cross-section: *d = 120 mm*
Cross sectional area of tensile reinforcement:
A_{s1}^{+} = 7.70 cm² (5∅14)
A_{s2}^{+} = 0.724 cm² (3×3∅3.2)
Cross sectional area of compressive reinforcement:
A_{s}^{-} = 3.93 cm² (5∅10)

Material characteristics:
Concrete:
Strength class: *C 30/37*
Mean tensile strength: $f_{ctm} = 2.9$ *MPa*
Secant modulus of elasticity: E_{cm}*=32* GPa
Mean shear modulus: G_{cm}
Reinforcement:
Strength class: *S 400* (A_{s1}^{+}, A_{s}^{-}*), S 1680* (A_{s2}^{+}*)*
Characteristic yield strength: $f_{yk} = 400$ *MPa*
Design value of modulus of elasticity:
E_s*=200* GPa

2.2 Analytical Results

The well known analytical methods can be used for calculation of non-cracked cross-section displacements. Further problems are encountered at cracked cross-sections where cracks occur in the tensile area due to the low tensile strength of a concrete. This results in reduction of the second moment of area of concrete section and consequently in deflection increasing. As it is difficult to exactly determine the location as well as the size of the cracks they are usually approximately stated using different national codes. Recently Eurocode 2 [11] has been most frequently applied in Europe and therefore considered in our analysis.

According to the presented characteristics the second moment of area of the un-cracked cross-section is $I_y^{(I)}$*=15345.478 cm⁴*.

The bending moment forming the first crack in the tensile concrete section ($M_y^{(I)}$) is calculated in the form of:

$$M_y^{(I)} = f_{ctm} \cdot \frac{2 \cdot I_y^{(I)}}{h} = 5.9336 \text{ kNm} \qquad (7).$$

For the un-cracked cross-section (M_{y0} *d"* $M_y^{(I)}$) the maximum vertical displacement (w_{inst}) is the sum of bending moment (M_{y0}), shear force (V_{z0})

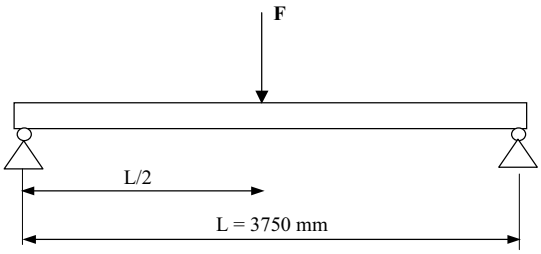

Fig. 4. *Static design of the test sample*

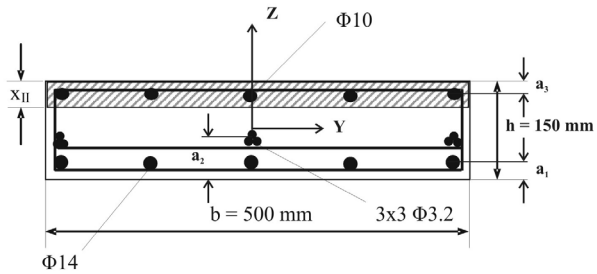

Fig. 5. *Considered elements for the cracked cross section*

and contribution (N_0):

$$w_{init} = w_{init,M} + w_{init,V} + w_{init,N} = \\ = \int_S \frac{M_{y0}(x) \cdot M_{y1}(x)}{E_{cm} \cdot I_{y,eff}^{(II)}} dx + \int_S \frac{V_{z0}(x) \cdot V_{z1}(x)}{G_{cm} \cdot A_{cs,eff}^{(II)}} dx + \int_S \frac{N_0(x) \cdot N_1(x)}{E_{cm} \cdot A_{c,eff}^{(II)}} dx \quad (8),$$

where:

A_c - cross-section area

For the treated static design (Fig. 2) Eq. (1) results in:

$$w_{init} = \frac{F \cdot L^3}{48 \cdot E_{cm} \cdot I_{yI}} + \frac{1.2 \cdot F \cdot L}{4 \cdot G_{cm} \cdot A_{cs}} \quad (9),$$

where $G_{cm} = E_{cm} / 2 \cdot (1 + \nu_c)$, $A_{cs} = A_c / 1.2$ and ν_c Poisson concrete coefficient, for which it was taken $\nu_c = 0.2$.

For the cracked cross-section ($M_{y0} > M_y^{(I)}$) the maximum vertical displacement (w_{inst}) is calculated in the form of:

$$w_{init} = w_{init,M} + w_{init,V} + w_{init,N} = \\ = \int_S \frac{M_{y0}(x) \cdot \bar{M}_{y1}(x)}{E_{cm} \cdot I_y^{(I)}} dx + \int_S \frac{V_{z0}(x) \cdot \bar{V}_{z1}(x)}{G_{cm} \cdot A_{cs}} dx + \int_S \frac{N_0(x) \cdot \bar{N}_1(x)}{E_{cm} \cdot A_c} dx \quad (10),$$

where $A_{cs,eff}^{(II)} = bx_{II} / 1.2$ and $A_{c,eff}^{(II)} = bx_{II}$.

The effective second moment of area of the cracked cross-section ($I_{y,eff}^{(II)}$) is determinated according to *Eurocode 2* in the form of:

$$I_{y,eff}^{(II)} = \xi \cdot I_y^{(II)} + (1 - \xi) \cdot I_y^{(I)}$$

$$\xi = 1 - \beta_1 \cdot \beta_2 \cdot \left(\frac{M_{yI}}{M_{y0,max}}\right)^2 \quad (11).$$

$$M_{y0,max} = \frac{F \cdot L}{4}; \quad \beta_1 = 1.0, \ \beta_2 = 1.0$$

The value of $I_y^{(II)}$ is calculated according to the neutral axis position (x_{II}) using the scheme from Figure 5 and $n = E_s / E_{cm}$:

$$\frac{b \cdot x_{II}^2}{4} + (n-1) \cdot A_s^- \cdot (x_{II} - a_3) - \\ - n \cdot A_{s1}^+ \cdot (h - a_1 - x_{II}) - n \cdot A_{s2}^+ \cdot (h - a_2 - x_{II}) = 0$$

$$x_{II} = 4.948 cm \quad (12).$$

$$I_y^{(II)} = \frac{b \cdot x_{II}^3}{3} + (n-1) \cdot A_s^- \cdot (x_{II} - a_3)^2 + n \cdot A_{s1}^+ \cdot (h - a_1 - x_{II})^2 + \\ + n \cdot A_{s2}^+ \cdot (h - a_2 - x_{II})^2 = 4757.344 cm^4$$

2.3 Measured Results Using Different Methods

For characteristic point observations trigonometric height was used. Measurements were performed from one station point (stabilised one day in advance). The measurements were made from tripod that was glued to the ground. Between each load phase a station point position was checked for stability (measurements of control points on the wall). Potential shifts of the instrument didn't occur. Before measurement the instrument was calibrated and data about air temperature and pressure were entered (both were stable during the test). First, the zero state was recorded and then one individual phase after another. Nikon series 800 instrument and precise measurement mode (PMRS) was used for the trigonometric heighting.

210 sight points on the concrete plate were observed in a local (object) coordinate system. Each point was observed with 10 iterations. Leica's reflective tape targets of dimensions 1 x 1 cm were used on each target point. In Figure 6 reflective tape targets 4, 5 and 6 in the middle of the concrete plate (where the breakage was expected) are shown.

Reference points (targets) have been used in vicinity of Leica reflective tape targets so that the deflection has been measured in the same position with both methods. A reference point is represented as a white circle of 18 mm diameter on black surface. For determination of camera position and position of reference points, the coded marks have been used. Each of them had a 15-bit type code presented by circle sectors which identifies them in every snap-shot. The correct distance between measuring points is determined

with scale bars whose distance is known and doesn't change during the measurement.

For presented measurement a stereo-photogrammetry system TRITOP was used (manufacturer GOM mbH, Braunschweig, Germany) with high resolution CCD camera Fuji Pro S3 (4256 x 2848 pixels) and software for calculation and analysis of object coordinates (Fig. 5). In each loading stage minimum 8 snap-shots from different angles and position were made so that all the points were visible. Camera positions were not stabilized. Snap-shots of each loading stage have been processed during the measurement so that the deflections from previous stages were already known. Maximum standard deviation of measuring results was 0.08 mm.

2.4 Comparison of Results

A comparison of the calculated analytical and (measured) geodetic, (measured) photogrammetric vertical displacements and (measured) hydraulic cylinder vertical displacements was made. Table 2 shows vertical displacements by epochs for point 5 in the middle of the concrete plate (because only point 5 was monitored with all three methods). In practice there is an unwritten rule that the ratio between calculated and measured value should not be less then 75 %. We neglected the first two epochs that the mean ratio between calculated and measured values was 88.5 %.

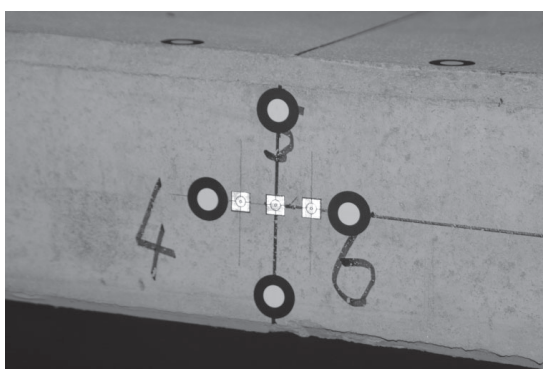

Fig. 6. *Reflective tape targets 4, 5 and 6 in the middle of the concrete plate*

The comparison of measurements of vertical displacements for the whole concrete plate was made. The geodetic and photogrammetric results were comparable (some tenth of mm) for point 5 (Fig. 8). It can be seen that the surveyed vertical displacement was always smaller then the calculated values. There is a small deviation in the first two epochs because of local contact surface under hydraulic piston was undefined.

3 CONCLUSION

Load deformation of a concrete plate can be monitored with a variety of different methods. We can choose the method by a construction dimensions, presumed displacements, access to the construction and also field and weather conditions. In practice, it is reasonable to use at least two independent methods for pretentious constructions. In that way we increase cost and duration of measurements but on the other hand we can get more trustworthy and non uniform results. If we measure more data that is needed for uniform results, we can make all sorts of statistical analyses at the time of data processing.

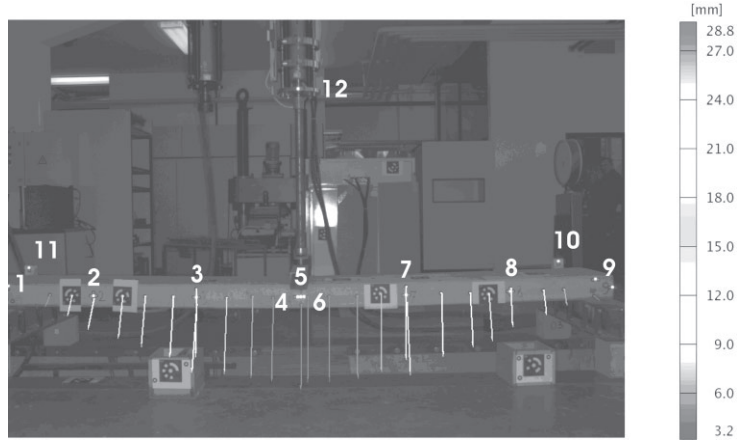

Fig. 7. *Reference points, coded marks, scale bars and displacement vectors of a concrete plate*

Table 1. *Vertical displacement by epochs for point 5 in the middle of the concrete plate*

[kN]	Point	Vertical displacement			
		Analytical	Hydraulic	Photo	Geodetic
3	5	-0.7	-1.5	-0.9	-1.0
6	5	-1.3	-2.3	-1.8	-1.8
9	5	-6.4	-4.1	-3.5	-3.6
12	5	-8.6	-6.0	-6.7	-6.9
15	5	-10.8	-9.2	-8.6	-8.7
18	5	-13.0	-11.6	-11.4	-11.6
21	5	-15.2	-14.1	-13.8	-14.0
24	5	-17.3	-16.7	-16.4	-16.4
27	5	-19.5	-18.7	-18.2	-18.4
30	5	-21.7	-21.6	-21.2	-21.3
33	5	-23.9	-23.4	-22.4	-22.8
36	5	-26.1	-25.6	-24.6	-25.2
39	5	-28.2	-27.8	-26.6	-27.1
42	5	-30.4	-30.1	-28.7	-29.1
Average ratia analitycal/ measured			90.5 %	86.8 %	88.2 %

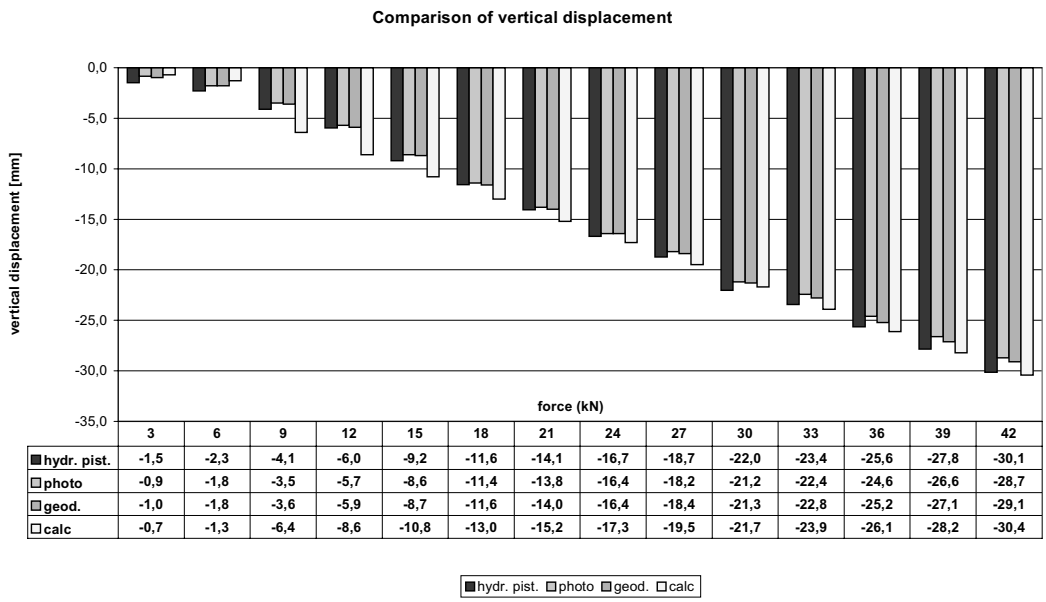

Fig. 8. *Comparison of vertical displacement in point 5*

In our case we used four independent methods. Three measurement methods and one analytical. The goal of all measurements was comparison of methods and find out which method is most comparable with calculated results. One of goals was also to test photogrammetric results which are rather new for that kind of testing in Slovenia. The results are showing that al methods are suitable and accurate what can be seen in *Table 1* and *Figure 8*. The results show that the agreement between hydraulic piston and analytical calculation was 90 %, photogrammetric 86 % and geodetic 88 %. In practice the agreement is usually taken over 75 %. Closer look at the results shows, that we used too few photogrammetric measurements, geodetic method is very sensitive to outer conditions meanwhile hydraulic piston is most accurate with 1/100 mm but suitable only for indoor laboratory testing. In field, there is a good combination of photogrammetric and geodetic methods but only if the access and the construction is suitable. The problem with access is in the case of bridges where water prevents to take photos from the middle of the

span, meanwhile geodetically we can measure even those points.

From results we can conclude that we got very good accuracy with comparison of results, so in practice we can use each one.

We will continue with our tests and compare these methods with other. Further research will be on the field of redundant measurement analyses, motorized geodetic measurements and better algorithms for calibration, snap-shot processing and the calculation of three-dimensional coordinates, which, in combination with development of new cameras, will lead to even better accuracy and use of the method.

4 REFERENCES

[1] Ataei, S., et al. Sensor fusion of a railway bridge load test using neural networks. *Expert Systems with Applications*, 29, 2005, p. 678-683.

[2] Kovačič, B., Kamnik, R. Measurement of displacement and deformations on the biggest Slovenian viaduct, with particular stress on accuracy calculations. *Allgemaine Vermessungs Nachrichten*, 10/2006, p. 322-328.

[3] Dörstel, C., Jacobsen K., Stallmann D. DMC - Photogrammetric accuracy - Calibration aspects and generation of synthetic DMC images. *Proceedings of Optical 3D Measurements Symposium*, Zürich, 2003.

[4] Albert, J., Maas H.G., Schade, A., Schwarz W. Pilot studies on photogrammetric bridge deformation measurement. *IAG Berlin, Proceeding of the 2nd Symposium on Geodesy for Geotechnical and Structural Engineering*, Berlin, Germany, May 21-24, 2002.

[5] Gordon, S., et. al. Measurement of structural deformation using terrestrial laser scanners. *1st FIG International Symposium on Engineering Surveys for Construction Works and Structural Engineering*, Nothingham, UK, 28. junij - 1. julij, 2004.

[6] Vodopivec, F. *Trigonometric heights*. Department of civil engineering and Department of geodesy FAGG. University of Ljubljana, 1985. (In Slovenian)

[7] Moseru, A., *Ingeneering geodesy, Basics.* 3rd Ed. Heidelberg: Wichmann, Germany, 2000. (In German)

[8] Wunderlich, T. A. Geodetic monitoring with prismless polar methods. *INGEO 2004 and FIG Regional Central and Eastern European Conference on Engineering Surveying*, Bratislava, Slovakia, November 11-13, 2004.

[9] Gorjup, Z. *Photogrammetric basis.* University of Ljubljana, FGG, Ljubljana, 2001. (In Slovenian)

[10] Maas, H.G., Hampel, U. Photogrammetric tehniques in civil engineering material testing and structure monitoring. *Photogrammetric Sensing & Remote Sensing*, vol. 72, no. 1, 2006.

[11] *CEN, Eurocode 2: Design of concrete structures – Part 1: General rules and rules for buildings*, 2002.

Strojniški vestnik - Journal of Mechanical Engineering 54(2008)5, 372-378
UDC 531.1
Paper received: 17.5.2007
Paper accepted: 19.12.2007

Hyper-Chaotic Mapping Newton Iterative Method to Mechanism Synthesis

Youxin Luo[1] - Xianfeng Fan[2] - Dazhi Li[1] - Xiao Wu[1]
[1]Hunan University of Arts & Science, Department of Mechanical Engineering, P.R.China
[2]University of Ottawa, Department of Mechanical Engineering, Canada

*The synthesis and approximate synthesis problems for planar mechanism can be transformed into a system of multivariable polynomial equations or general nonlinear equations. Newton iterative method is an important technique to one dimensional and multidimensional variables and iterative process exhibits sensitive dependence on initial guess point. Based on utilizing multi-start point technique and hyper-chaotic mapping (*Hénon *hyper-chaotic system) as initial points of Newton iterative method, an innovative new method to find all solutions of general nonlinear equations in kinematics quickly and effectively was proposed. The computing step and method was given. The numerical examples in linkage synthesis and approximate synthesis show that the method is correct and effective.*

Keywords: hyper-chaotic systems, linkage mechanism, mechanism synthesis, nonlinear equations

0 INTRODUCTION

Kinematic motion analysis and design of mechanical systems lead naturally to system of nonlinear algebraic and/or transcendental equations. One of the most frequently occurring problems in kinematics is to find solutions to this system of equations [1] and [2]. The research of analysis and synthesis for planar mechanisms refers the solution of nonlinear equations and this has not commendably resolved [3]. How to find out all solutions of nonlinear equations quickly and effectively is important to mechanisms analysis & synthesis and engineering fields, so mathematics worker and engineering expert have paid attention to it. The solution approaches for such equations can be broadly divided into two classes: closed-form (analytical) techniques and numerical (iterative) methods.

Analytical or closed-form solutions to kinematics equations can be obtained by using elimination theories based on resultants [4], Gröbner-Sylvester hybrid method [1] and [5] to [7] or Wu elimination [6] and [7] and so on. The analytical solution approaches entail successive elimination of problem unknowns to reduce a multivariable system into a single variable equation or triangular equations. These can find all solutions. In elimination process with resultant, it may be possible to express the resultant as a quotient of one determinant divided by another. The divisor is the extraneous factor. Since it is difficult to identify whether or not extraneous factors exist, it is impossible to insure that a resultant is devoid of extraneous solutions. For homogeneous systems, extraneous factors can be identified and eliminated as demonstrated by Macaulay [8]. However, problems arising in synthesis and analysis of mechanism often result in a system of non-homogeneous polynomials. Hence, Macaulay's approach is not suitable for such problems because the system of equations has extraneous solutions including solutions at infinity, and thus the eliminant matrix is degenerate [1]. For kinematics problems of "reasonable" complexity [1], Wu elimination method, Gröbner base method are quite inefficient because of their excessive computation times and exploding intermediate results [1] and [8]. For a comprehensive contents of Gröbner base method and Wu elimination method see [6] to [8]. Specially, in general, analytical or closed-form solutions are effective to polynomial equations.

The numerical (iterative) methods mainly include Newton method and its improved methods [9] and [10], continuation iteration method [9] to [11], interval analysis method [12], universal gray

*Corr. Author's Address: Hunan University of Arts & Science, Department of Mechanical Engineering, Changde, Hunan, 415000, P.R.China, LLyx123@126.com

analysis method [13] to [15], optimum method [10] and [16] and so on. These numerical methods are adaptive to polynomials equations as well as non-polynomials equations in kinematics. Using numerical methods, a kinematics problem is considered solved if a tight upper bound on the number of solutions can be established, and an efficient algorithm for computing all solutions can be implemented. The commonly used iterative methods are variants of the Newton, conjugate gradient methods or optimum methods. These methods require an initial guess to the solution. If the initial guess is not close enough to a solution, the iterations may converge slowly, converge to an unacceptable solution or may diverge altogether, and, in general, these methods can only find a solution. However, Newton's method is a valuable tool and is used as the building block for numerical continuous methods, interval iterative method or universal gray method. Interval method can find all solutions, but some algebraic nature of interval mathematics cannot be extended and compiling program is very complicated [14] and [17], so that this limits its application. The universal gray analysis method also can find all solutions of kinematics problem [14] in which, algebraic nature of universal mathematics can be extended like general algebra and overcome the disadvantages of interval analysis, but the universal number operator is also complicated [13], so the efficiency of solution-finding is not very high. Numerical continuation (homotopy) methods have been used in solving kinematics equations of motion for planar as well as spatial mechanisms. If the system of equations to be solved can be cast in a polynomial form, numerical continuous methods are capable of finding all possible solutions and eliminating the need for a good initial estimate to the solution. But computing efficiency is not high, and it is difficult to deal with non-polynomial equations in kinematics [10].

To overcome the difficulties of the above approaches, it is necessary to explore innovate approaches to find out all solutions quickly and effectively. The Newton iteration technique possesses two-order convergence speed, its computing speed is fast, its iteration function is clearly understood, and its dynamics specific property is relatively easy to be hold, so that it is widely used in engineering and science research. But it is comparatively sensitive to initial value, its calculation capacity is great, and it can only get one solution. All the improved work on Newton methods put the emphases on computing arithmetic and the researchers do not notice that these numerical iteration system are discrete dynamical system resulted from numerical iteration process. Recently, the finding-solution methods based on chaos have made some progress. Xie and Chen [18] had proposed an innovative chaos method for the all solutions of nonlinear equations and Luo [19] had proposed an improved method for enhancing its efficiency by rough and accurate iteration. However, the chaos method related in [18] and [19] assumed the lumped Julia points of Newton iteration method to appear in the neighborhood where the Jacobian matrix of resolved equation set is zero. Nevertheless, it has not been tested and its resolving procedure is complex. Recently, Jovanonic et al. [20] proposed an innovative Newton chaos iteration method to obtain all resolutions of nonlinear equation set to mechanism synthesis. The method assumes Newton iteration method be a nonlinear discrete dynamic system to obtain the chaos fractal sensitive region of the Newton iteration method with the exclusive two-cycle point to make inverse image iteration to find Julia points and then take initial points in the neighborhood of Julia points. But Luo [21] found that its efficiency is to be further enhanced when the Julia points are researched by using the exclusive two-cycle point to operate inverse image iteration. And thus, Luo [22] proposed an innovative three-cycle chaos orbit method to find the Julia points of non-linear equations in kinematics, but its validity and adaptability to find Julia points with three-cycle inverse image iteration method are valuable to be researched ulteriorly. On the other hand, multi-start technique is a sort of technique in global optimization. The biggest difficulty of Newton iterative method is how to define initial value. To take chaos sequences as initial points of Newton iterative method, it can find all solutions of nonlinear equations. Liao et al. [23] proposed two dimension chaos mapping Newton iterative method which is applied to found all solutions of linkage accurate points movement synthesis.

To overcome the difficulties of approaches, this paper presents a new method for solving algebraic system of equations in kinematics, which utilizes Hénon hyper-chaotic mapping system to

produce sensitive initial points of Newton iterative method and find all solutions of nonlinear equations. After analyzing hyper-chaotic the characteristic of Hénon hyper-chaotic mapping system, the simulation is done with MATLAB software, and the step and methods of finding equations in kinematics are also given. Numerical examples for linkage synthesis & approximate synthesis are presented. At last, the comparison with other methods to find all solutions of non-linear equations in kinematics is given. The examples show the new method is verified to be correct and effective.

1 HÉNON HYPER-CHAOTIC SYSTEM

Lyapunov exponent is one of effective method depicting the Chaos specific property of nonlinear system, and the number of Lyapunov exponents is identical with the dimension ***n*** of system state space. If one of the Lyapunov exponents is positive, system is chaotic. If system has two or more positive Lyapunov exponents, system is hyper-chaotic. The more positive number of Lyapunov exponents, the higher in-stability has the system [24]. In general, if the systematic state variable number is more (for high dimension system, e.g. the discrete system, ***n*** > 2), it probably appeares the unsteady level is higher.

The Ref. [25] designed a general Hénon mapping:

$$\begin{Bmatrix} x_{1,k+1} \\ x_{i,k+1} \end{Bmatrix} = \begin{Bmatrix} a - x_{n-1,k}^2 - bx_{n,k} \\ x_{i-1,k} \end{Bmatrix} \qquad (1),$$

where, $i = 2,3,\cdots,n$ express the dimension of system; k is discrete time; a and b are adjustable parameters. When i = 2, the above mapping is called as famous Hénon mapping. When fixed parameters $a = 1.76, b = 0.1$ and the dimensions vary from 2 to 10, after computing, the ref. [25] found that with increasing ***n***, the simple relation of the number N of positive Lyapunov exponents with the system dimension n is $N = n - 1$, namely, when the system dimension is larger of two, system is hyper-chaotic. For $n > 10$ situation, we also have done simulating study and we also obtained the same results $N = n - 1$.

For example, n = 5, we compiled program MATLAB with time series method [24] and we obtain four positive Lyapunov exponents, shown in Figure 1. When n = 13, the simulating result is that the system has twelve positive Lyapunov exponents with lesser values, shown in Figure 2.

2 NEWTON ITERATION FUNCTION

To find solution of nonlinear equations:

$$f(\mathbf{x}) = 0 \qquad (2).$$

Newton iterative method can be described as follows roughly:

(1) To select initial value $\mathbf{x}_0$

(2) To take iteration by formation

$$\mathbf{x}_{k+1} = \mathbf{x}_k - \frac{f(\mathbf{x}_k)}{f'(\mathbf{x}_k)} \qquad k = 0,1,2,\cdots \qquad (3),$$

where $\boldsymbol{f}(\mathbf{x}_k)$ is the function value of $\boldsymbol{f}(\mathbf{x})$ at the point $\mathbf{x}_k$, $\boldsymbol{f}'(\mathbf{x}_k)$, is one-order derivative of $\boldsymbol{f}(\mathbf{x})$ at the point $\mathbf{x}_k$, also called as Jacobian matrix of $\boldsymbol{f}(\mathbf{x}_k)$

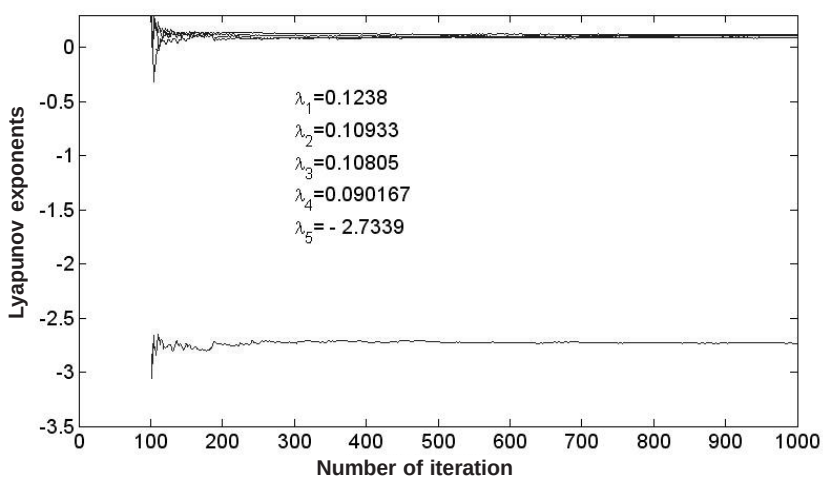

Fig.1. *Lyapunov exponent of Hénon maps with n=5*

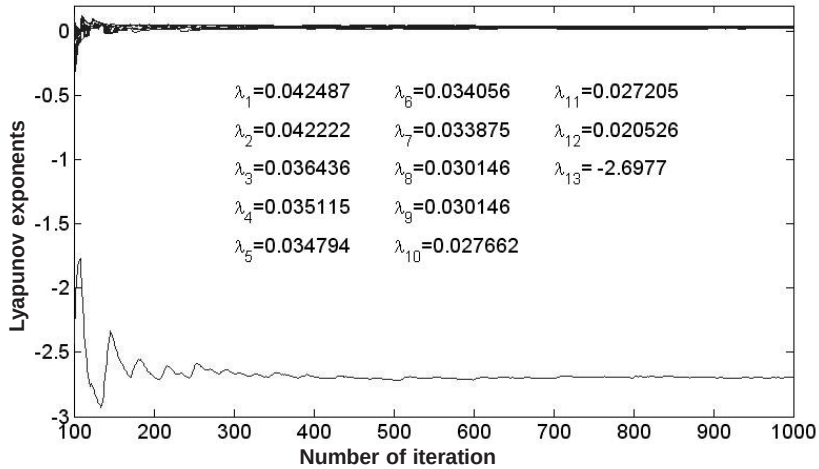

Fig.2. *Lyapunov exponent of Hénon maps with n = 13*

and it is denoted by $\boldsymbol{J}$. $\boldsymbol{f}(\mathbf{x})$ is Newton iteration function value. When some conditions are satisfied, Newton iterative method is two-order convergent [9]. We must note that when using Newton iterative method, we want to avoid $\boldsymbol{f}'(\mathbf{x}_k) = 0$, otherwise singularity will be produced. To improve the performance of Newton iterative method, there have some improved methods, but the improved methods pay attention to arithmetic study and not mechanism study. In other words, these methods avoid singularity and do not make use of singularity.

3 NEWTON ITERATIVE METHOD BASED ON HÉNON HYPER-CHAOTIC MAPPING

Based on hyper-chaotic mapping, the process of the finding all solutions of nonlinear equations is as follows:

(1) By formulation (1), to construct hyper-chaotic set $\boldsymbol{x}0(\boldsymbol{i}+1, \boldsymbol{j})$ ($\boldsymbol{i} = 1, 2, ..., \boldsymbol{n}, \boldsymbol{n}+1$ is the variable number of hyper-chaotic system, $\boldsymbol{n}$ is the positive number of Lyapunov exponents, n is also the number of variables, $\boldsymbol{j} = 1, 2, ..., \boldsymbol{N}$, $\boldsymbol{N}$ is the length of hyper-chaotic sequences) and obtain $\boldsymbol{x}0(\boldsymbol{i}, \boldsymbol{j})$;

(2) Suppose the interval of $\boldsymbol{x}(\boldsymbol{i})$ is $[a(i), b(i)]$, to map hyper-chaotic sequences to variable interval with $x(i, j) = (b(i) - a(i))/2 + x0(i, j)(b(i) + a(i))/2$ and produce jth $\boldsymbol{x}(\boldsymbol{i}, \boldsymbol{j})$ of $\boldsymbol{x}(\boldsymbol{i})$.

(3) To take jth $\boldsymbol{x}(\boldsymbol{i}, \boldsymbol{j})$ of $\boldsymbol{x}(\boldsymbol{i})$ as initial value of Newton iterative method, and implement j time operations of Newton iterative method with formulation (3) to find all solutions $\mathbf{x}^*$. Note that: in computing process, $\mathbf{X}$ is used to save all solutions, when some solution $\mathbf{x}^*$ is in $\mathbf{X}$, $\mathbf{x}^*$ is abandoned, otherwise, $\mathbf{x}^*$ is saved in $\mathbf{X}$.

4 APPLICATION TO MECHANISM SYNTHESIS

For four-linkage function mechanism synthesis, in general, it's input angles θ_{1j} and the output angles φ_{1j} satisfy some function relation, we construct orthogonal system (shown in Fig. 3) and take the coordinate of C point is (1,0). Suppose the coordinates A_x, A_y, B_x, B_y of pin-joined points A and B are design variables, denoted by x_1, x_2, x_3, x_4 respectively.

According to constrained condition of the invariable length of linkage and displacement matrix, we can deduce the synthesis equation as follows:

$$f_j(\mathbf{x}) = P_{1j}x_1x_3 + P_{2j}x_1x_4 + P_{3j}x_2x_3 + P_{4j}x_2x_4 + P_{5j}x_1 + P_{6j}x_2 + P_{7j}x_3P_{8j}x_4 + P_{9j} \quad (4),$$

where $j = 2, 3, \ldots m$, m is point number of synthesis.

$$P_{1j} = 1 - \cos(\theta_{1j} - \phi_{1j}); P_{2j} = -\sin(\theta_{1j} - \phi_{1j})$$

$$P_{3j} = \sin(\theta_{1j} - \phi_{1j}); P_{4j} = 1 - \cos(\theta_{1j} - \phi_{1j})$$

$$P_{5j} = \cos(\theta_{1j} - \phi_{1j}) - \cos(\theta_{1j})$$

$$P_{6j} = \sin(\theta_{1j} - \phi_{1j}) + \sin(\theta_{1j})$$

$$P_{7j} = \cos(\phi_{1j}) - 1; P_{8j} = -\sin(\phi_{1j})$$

$$P_{9j} = 1 - \cos(\phi_{1j})$$

There have four design variables m-1 and design equations in formulation (4), the most accurate point synthesis number is five points.

In most situations, the problem of mechanism synthesis and approximate synthesis can be transformed into an unconstrained optimum problem, namely:

$$\min F(\mathbf{x}) = \sum_{j=1}^{m} (f_j(\mathbf{x}))^2 \qquad (5).$$

And the essential condition of min objective function is the grads $\partial F(\mathbf{x})/\partial \mathbf{x} = 0$, namely:

$$\begin{cases} \sum_{j=2}^{m-1} f_{j-1}(P_{1j}x_3 + P_{2j}x_4 + P_{5j}) = 0 \\ \sum_{j=2}^{m-1} f_{j-1}(P_{3j}x_3 + P_{4j}x_4 + P_{6j}) = 0 \\ \sum_{j=2}^{m-1} f_{j-1}(P_{1j}x_1 + P_{3j}x_2 + P_{7j}) = 0 \\ \sum_{j=2}^{m} f_{j-1}(P_{2j}x_1 + P_{4j}x_2 + P_{8j}) = 0 \end{cases} \qquad (6),$$

where m is synthesis point number.

For example, given plane four-linkage mechanism synthesis problem, the data of input θ_{1j} and output φ_{1j} are shown in Table 1. Using Newton iteration method based on Hénon hyper-chaotic sequences, we transform nonlinear equations (4) into iterative form of formulation (3), take variable intervals all $[-20, 20]^T$, and produce initial point of hyper-chaotic sequences with random number method and for example, x_0 = $[0.37948, 0.8318, 0.50281, 0.70947, 0.42889]^T$. To take $\boldsymbol{n} = 5$ for general Hénon hyper-chaos system expressed by formulation (1), and, with initial value x_0 of hyper-chaotic sequences, produce hyper-chaotic sequences with four positive Lyapunov exponents (to take the length $\boldsymbol{N} = 20$), then map variable intervals and obtain initial values of Newton iterative method and obtain all solutions, the first to fourth solution (Table 2). The solutions are accordant with methods in [10], but it dissipative time is 0.16 second less that time 0.4 second with Logistic chaos mapping Newton iterative method (only initial points of Newton iterative method produced by Logistic chaos mapping). If we produce initial point x_0 of hyper-chaotic sequences with random number method and for example, x_0 = $[0.28973, 0.34119, 0.53408, 0.72711, 0.30929]^T$, the length of hyper-chaotic sequences is $\boldsymbol{N} = 200$, the accurate synthesis problem is dealt with approximate synthesis method in formulation (6), and results are shown in Table 2, besides the first to fourth solution, there have other approximate solutions. Notes that with different initial point of hyper-chaotic sequences and the length of hyper-chaotic sequences, approximate solutions may be different.

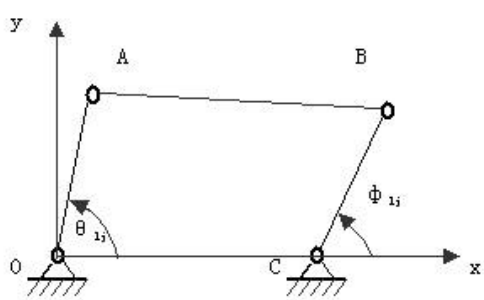

Fig.3. *The diagram of linkage mechanism*

Table 1. *Five group data of input and output*

$\boldsymbol{j}$	1	2	3	4	5
$\theta_{1\boldsymbol{j}}(^0)$	0	60	130	200	280
$\varphi_{1\boldsymbol{j}}(^0)$	0	17	44	61	50

5 CONCLUSIONS

In this paper, using Hénon hyper-chaos sequences and mapping sequences into variable intervals as initial values of Newton iterative method, an innovative new method to find all solutions of nonlinear equations in kinematics is proposed. The computing steps are presented. Numerical examples of mechanism synthesis and approximate synthesis are given. It shows that this method is effective and correct. This method overcomes the shortcomings of the existing methods, namely, extraneous solutions of resultant method, low computing efficiency of existing analytical solutions, and, low computing efficiency to find all solutions with existing numerical methods or only finding a solution with Newton method & optimum method. Newton method is adaptive to polynomials nonlinear equations as well as the general non-polynomial non-linear equations, so, the proposed method is also adaptive to the general non-polynomial non-linear equations. The hyper-chaos iterative method effectively resolves the dependent on initial guess of Newton

Table 2. *The results of synthesis*

Variables / Serial number	x_1	x_2	x_3	x_4	Notes
1	0.34688351864093	0.15532289223008	2.37621431901423	1.07108276520215	Satisfy request
2	0.33802375122182	0.35284403147775	1.52301342502732	1.46008672456456	Satisfy request
3	0.00876050327329	0.19878954898663	0.24358820102367	0.42972805218513	Satisfy request
4	0.00000000000000	0.00000000000000	1.00000000000000	0.00000000000000	Degenerate solution
5	0.24810590331448	0.09742519788478	0.62411520956186	0.49721188127604	Approximate solution
6	0.35261614308389	0.17452815063814	2.35195172736808	1.14692673024341	Approximate solution
7	0.36183730535318	0.25046832860287	2.06025448656341	1.35405078472152	Approximate solution
8	0.35262221231194	0.17455139128299	2.35192171459211	1.14701706830115	Approximate solution
9	-0.05656808459818	0.10789498343339	0.45524276496406	0.22173945773667	Approximate solution
10	0.26879875742049	0.34866142549433	0.37945885805080	0.74548350193159	Approximate solution
11	0.33698078149853	0.35516826106660	1.51946559173426	1.46634536242020	Approximate solution
12	0.36143253460429	0.26070352447913	2.00210092194291	1.36915944896681	Approximate solution

iterative method based on multi-start point technique and hyper-chaos sequences. This method also overcomes the deficiency of existing chaos iterative method. Besides, compared with chaos Newton iterative method, hyper-chaos Newton iterative method has high computing speed and can obtain all solutions of nonlinear equations. It can quickly and effectively find out all solutions of nonlinear equations in kinematics, set up basis for other engineering application and optimization, and provide beneficial idea for chaos characteristic study of other iterative method.

Acknowledgement

This research is supported by the grant of the 11th Five-Year Plan for the construct program of the key discipline (Mechanical Design and Theory) in Hunan province (XJT2006180), Hunan Provincial Natural Science Foundation of China (07JJ3093), Hunan Province Foundation Research Program (2007FJ3030,2007GK3058) and Scientific Research Fund of Ministry of Education of China (02108).

6 REFERENCES

[1] Dhingra, A.K., Almadi , A.N., et al. A Gröbner-Sylvester hybrid method for closed-form displacement analysis of mechanisms. *ASME J. Mech. Des.*, 122(4), 2000, p. 431-438.

[2] Norton, L.R. *An introduction to the synthesis and analysis of mechanisms and machines*. McGraw-Hill Companies, Inc., Asia, 2001.

[3] Waldron, K.J., Sreenivasan, S.V. A study of the solvability of the position problem for multi-circuit mechanisms by way of example of the double butterfly linkage. *ASME J. Mech. Des.*, 118(3), 2996, p. 390-395.

[4] Dhingra, A.K., Almadi, A.N., et al. A closed-form approach to coupler-curves of multi-loop mechanisms. *ASME J. Mech. Des.*, 122(4), 2000, p.464-471.

[5] Bhubaneswar M. *Algorithmic algebra*. New York: Springer-Verlag Inc., 1993.

[6] Wang D.M. *Elimination method and its application*. Beijing: Chinese Science Press, 2002. (in Chinese).

[7] Wu, W. T. *Mathematics mechanization*. London: Kluwer Academic Publishers, 2000.

[8] Macaulay, F.S. *The algebraic theory of modular systems*. New York: Cambridge University Press, 1994.

[9] Burden, L.R., Faires D.J. *Numerical analysis*, 8th Ed. Brooks-Cole Publishing, USA, 2004.

[10] Yang, T.L. *The basic theory of mechanical system*. Beijing: Chinese Machine Press, 1996.

[11] Liu A.X., Yang T.L. Finding all solutions to unconstrained nonlinear optimization for approximate synthesis of planar linkages using continuation method. *ASME J. Mech. Des*., 121(3), 1999, p. 368-374.

[12] Moore, R.E. *Interval analysis*. Englewood Cliffs: Prentice-Hall, 1966.

[13] Luo, Y.X. Universal grey mathematics and its application to interval analysis of uncertain structural systems. *Advances in Systems Science and Applications*, 3(4), 2003, p. 522-530.

[14] Luo, Y.X., Guo, H.X., Zhang, L.T. The application of universal grey mathematics to the analysis of mechanism errors. *Journal of Machine Design*, 19(2), 2002, p. 11-14. (in Chinese).

[15] Luo, Y.X., Huang, H.Z., Fan, X.F. Universal grey transfer matrix method and its application to natural frequencies calculation of systems. *ASME J. Mech. Eng*., 52(9), 2006, p. 592-598.

[16] Nokleby, B.S., Podhorodeski, R.P. Optimization-based synthesis of Grashof geared five-bar mechanisms. *ASME J. Mech. Des.*, 123(4), 2001, p. 529-534.

[17] Eldonhansen, G., Walster, W. *Global optimization using interval analysis*, 2nd Ed. Monticello, NewYork: Marcel Dekker, Inc., 2004.

[18] Xie, J., Chen, Y. Application of chaos theory to synthesis of plane rigid guidance. *Mechanical science and technology*, 19(4), 2002, p. 524-526. (in Chinese).

[19] Luo, Y.X. Chaos method for function synthesis of planar crank—slider mechanism. *Journal of machine design*, 20(7), 2003, p. 27-30. (in Chinese).

[20] Jovanonic, V. T., Kazerounian, K. Using chaos to obtain global solutions in computational kinematics. *ASME J. Mech. Des.*, 120(7), 1998, p. 299-304.

[21] Luo, Y.X. The research of Newton chaos iteration solution method and its application to mechanism synthesis. *Machine design and research*, 21(5), 2005, p. 19-22.

[22] Luo, Y.X. A new 3-cycle Newton chaos iteration solution method and its application to mechanism synthesis. T*he International Conference on Mechanical Transmissions*, Chongqing, China, 2006, p. 102-105.

[23] Liao, D.G., Luo, Y.X. Two dimension chaos mapping Newton iterative method and its application to function analysis of planar linkage mechanism. *Journal of Mechanical Transmission*, 30(3), 2006, p. 21-23. (in Chinese).

[24] Wolf, A., Swift, J.B., Swinney, H.L., et al. Determining Lyapunov exponents from a time series. *Physica D: Nonlinear Phenomena*, 16(3), 1985, p. 285-317.

[25] Richter H. The generalized Hénon maps: examples for higher-dimensional chaos. *International Journal of Bifurcation and Chaos*, 12, 2002, p. 1371-1381.

Instructions for Authors

From 2008 the Journal of Mechanical Engineering is to be published in English only, but with separate Slovene abstracts. The authors are entirely responsible for the correctness of the language. If a reviewer indicates that the language in the paper is poor, the editor will require the author to correct the text with the help of a native English speaker before the paper is reviewed again.

Papers can be submitted electronically to the journal's e-mail address (info@sv-jme.eu) or by post.

Papers submitted for publication should comprise the following:

- Title, Abstract, Keywords,
- Main body of text,
- Tables and Figures (graphs, drawings or photographs) with captions,
- List of References,
- Information about the authors, the corresponding author and a full set of addresses.

For papers from abroad (in the case that none of the authors is a Slovene) the editor will obtain a Slovenian translation of the Abstract.

Papers should be short, about 8 to 12 pages of A4 format, or at most, 7000 words. Longer papers will be accepted if there is a special reason, which should be stated by the author in the accompanying letter. Short papers should be limited to less than 3000 words.

THE FORMAT OF THE PAPER

The paper should be written in the following format:

- A Title, which adequately describes the content of the paper.
- An Abstract, which should not exceed 250 words. The Abstract should state the principal objectives and the scope of the investigation, the methodology employed, summarize the results and state the principal conclusions.
- An Introduction, which should provide a review of recent literature and sufficient background information to allow the results of the paper to be understood and evaluated.
- A Theory and the experimental methods used.
- An Experimental section, which should provide details of the experimental set-up and the methods used for obtaining the results.
- A Results section, which should clearly and concisely present the data using figures and tables where appropriate.
- A Discussion section, which should describe the relationships and generalisations shown by the results and discuss the significance of the results, making comparisons with previously published work.
- Because of the nature of some studies it may be appropriate to combine the Results and Discussion sections into a single section to improve the clarity and make it easier for the reader.
- Conclusions, which should present one or more conclusions that have been drawn from the results and subsequent discussion and do not duplicate the Abstract.
- References, which must be numbered consecutively in the text using square brackets [1] and collected together in a reference list at the end of the paper.

THE LAYOUT OF THE TEXT

Texts should be written in Microsoft Word format. The paper must be submitted in an electronic version, by e-mail or by post on a CD.

Do not use a LaTeX text editor, since this is not compatible with the publishing procedure of the Journal of Mechanical Engineering.

Equations should be on a separate line in the main body of the text and marked on the right-hand side of the page with numbers in round brackets.

Units and abbreviations

Only standard SI symbols and abbreviations should be used in the text, tables and figures. Symbols for physical quantities in the text should be written in italics (e.g., *v, T, n,* etc.). Symbols for units that consist of letters should be in plain text (e.g. m/s, K, min, mm, etc.).

All abbreviations should be spelt out in full on first appearance, e.g., variable time geometry (VTG).

The meaning of symbols and units belonging to symbols should be explained in each

case or quoted in special table at the end of the paper before the References.

Figures

Figures must be cited in consecutive numerical order in the text and referred to in both the text and the caption as Fig. 1, Fig. 2, etc. Pictures should be saved in a resolution good enough for printing, and in any common format, e.g., BMP, GIF or JPG. However, graphs and line drawings should be prepared as vector images, e.g., CDR, AI.

All Figures should be prepared in black and white, without borders and on a white background. All the figures should be sent separately in their original formats.

When labeling axes, physical quantities, e.g., *t, v, m,* etc., should be used whenever possible. Multi-curve graphs should have the individual curves marked with a symbol. The meaning of the symbol should be explained in the figure caption.

In the case that the author wishes, for whatever reason, to publish Figures in colour, the author must pay the resulting costs.

Tables

Tables must be cited in consecutive numerical order in the text and referred to in both the text and the caption as Table 1, Table 2, etc. In addition to the physical quantity, e.g., *t* (in italics), units (normal text), should be added in square brackets. Each column should have the title line. Tables should not duplicate information that is already noted anywhere in the paper.

Acknowledgement

An acknowledgement for cooperation or help can be included before the References. The author should state the name of the research (co)financer.

The list of references

All references should be collected at the end of the paper in the following styles for journals, proceedings and books, respectively:

[1] Wagner, A., Bajsić, I., Fajdiga, M. Measurement of the surface-temperature field in a fog lamp using resistance-based temperature detectors. *Strojniški vestnik – Journal of Mechanical Engineering*, February 2004, vol. 50, no. 2, p. 72-79.

[2] Boguslawski L. Influence of pressure fluctuations distribution on local heat transfer on flat surface impinged by turbulent free jet. *Proceedings of International Thermal Science Seminar II*, Bled, June 13.-16., 2004.

[3] Muhs, D., et al. *Roloff/Matek mechanical parts*, 16th ed. Wiesbaden: Vieweg Verlag, 2003. 791 p. (In German). ISBN 3-528-07028-5

ACCEPTANCE OF PAPERS AND COPYRIGHT

The Editorial Board reserves the right to decide whether a paper is acceptable for publication, obtain professional reviews for submitted papers, and if necessary, require changes to the content, length or language.

The corresponding author must, in the name of all authors, also enclose a written statement that the paper is original unpublished work, and not under consideration for publication elsewhere.

On publication, copyright of the paper shall pass to the Journal of Mechanical Engineering. The JME must be stated as a source in all later publications.

Submitted materials will not be returned to the author. Unpublished materials are not preserved and will not be sent anywhere without the author's consent.

The paper, prepared for publication, will be sent to the author in PDF format. The author should check for any necessary corrections, which should be the minimum required. With this the author confirms that the paper is ready for publication.

PUBLICATION FEE

For all papers the authors will be asked to pay a publication fee prior to the paper appearing in the journal. However, this fee only needs to be paid after the paper is accepted for publication by the Editorial Board. The fee is €180.00 (for all papers with a maximum of 6 pages), €220.00 (for all papers with a maximum of 10 pages) and €20.00 for each additional page. The publication fee includes 25 off-prints of each paper, which will be sent to the corresponding author.

Vsebina

Strojniški vestnik - Journal of Mechanical Engineering
letnik 54, (2008), številka 5
Ljubljana, maj 2008
ISSN 0039-2480

Izhaja mesečno

Povzetki razprav

Osebne vesti

Strojniški vestnik - Journal of Mechanical Engineering 54(2008)5, SI 53
UDK 621.914
Prejeto: 7.4.2008
Sprejeto: 15.5.2008

Določanje značilnosti CAD modela izdelka za izbiro frezalnih strategij

Jože Balič* - Simon Klančnik - Simon Brezovnik
Univerza v Mariboru, Fakulteta za strojništvo

V članku je opisan postopek določevanja značilk iz CAD modela. Iz modela izluščimo informacije, ki imajo največji vpliv na tehnološke parametre obdelave in jih nato preoblikujemo v obliko, ki je primerna kot vhodni podatek v različne inteligentne sisteme za napovedovanje strategije obdelave (na primer z umetno nevronsko mrežo ali z genetskimi algoritmi). Pri oblikovno zahtevnih CAD modelih so na enem obdelovancu potrebne različne obdelovalne strategije, zato s pomočjo opisane delitve, površino CAD modela razdelimo na regije tako, da vsako regijo obravnavamo kot samostojen model in za njo določimo značilke. Te so nato vhodni podatek v sistem inteligentne izbire frezalnih strategij.

Ključne besede: CAD-CAM sistemi, strategije frezanja, izločanje značilk, CAD modeli, segmentacija

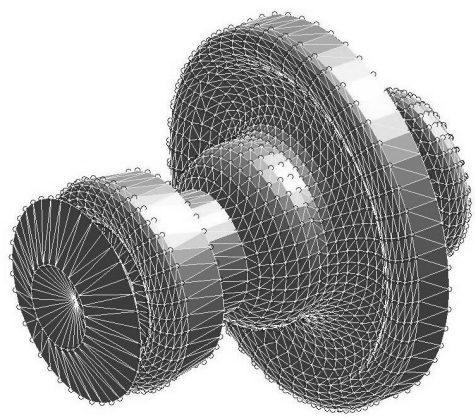

Sl. 1. *CAD model primera, sestavljenega iz površinskih trikotnikov*

*Naslov odgovornega avtorja: Univerza v Mariboru, Fakulteta za strojništvo, Smetanova 17, 2000 Maribor, joze.balic@uni-mb.si

Strojniški vestnik - Journal of Mechanical Engineering 54(2008)5, SI 54
UDK 658.5
Prejeto: 13.9.2007
Sprejeto: 19.12.2007

Napovedovanje pretočnih časov

Tomaž Berlec* - Edvard Govekar - Janez Grum - Primož Potočnik - Marko Starbek
Univerza v Ljubljani, Fakulteta za strojništvo

Pri vstopu na trg se podjetja srečujejo z različnimi problemi. Največji problemi današnjega časa so predolgi pretočni časi naročil. Naročnik določenega naročila se odloči za tistega ponudnika, ki posreduje najboljšo ponudbo glede na čas dobave naročila.

Izdelati ponudbo zgolj na osnovi izkušenj zaposlenih je dandanes zelo tvegano. Iz tega razloga predlagamo postopek, s katerim lahko na osnovi zbranih podatkov o doseženih pretočnih časih opravilnih naročil, izvedenih v preteklem časovnem obdobju na delovnih mestih podjetja, napovemo pričakovane pretočne čase načrtovanih opravil in posredno tudi naročil. Rezultat predlaganega postopka je izkustvena porazdelitev možnih pretočnih časov za novo naročilo in na osnovi te porazdelitve napoved najverjetnejšega pretočnega časa novega naročila. S pomočjo predlaganega postopka lahko prodaja napove kupcu oziroma naročniku, v kolikšnem času bo mogoče dobaviti načrtovano naročilo.

Postopek napovedovanja pretočnih časov naročil je predstavljen na primeru napovedovanja pretočnega časa naročila "orodje za izdelavo okrova filtra", ki se izdeluje v orodjarni Slovenskega podjetja ETI d.d.

Ključne besede: pretočni časi, napovedovanje, opravilna naročila, izkustvene porazdelitve

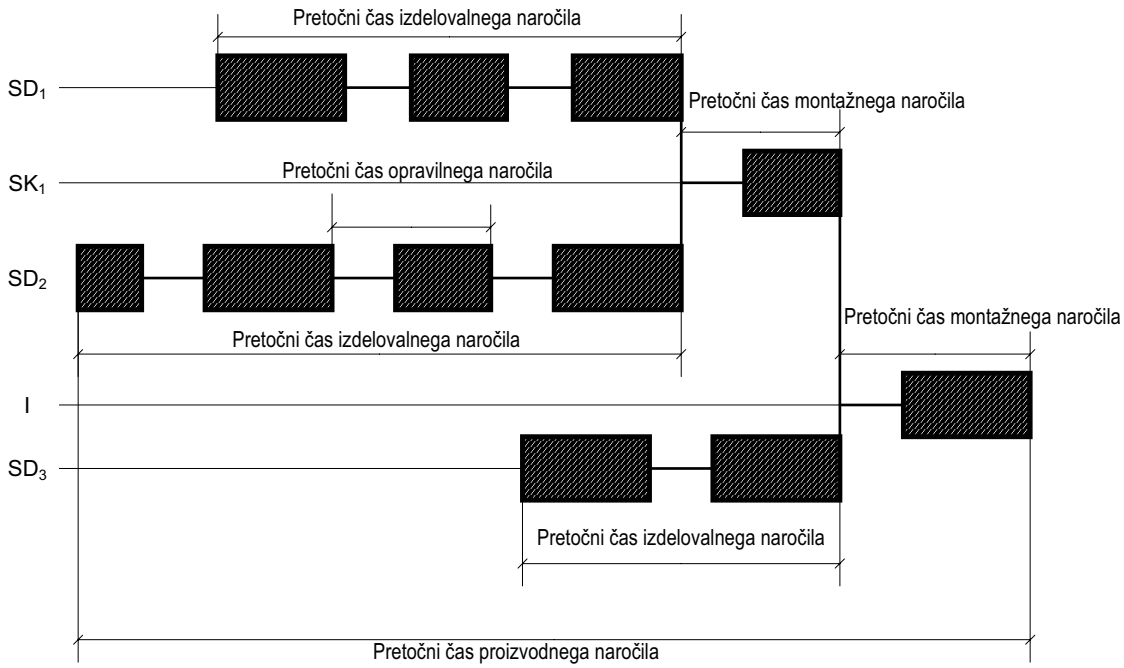

Sl. 1. *Pretočni časi naročil*

*Naslov odgovornega avtorja: Univerza v Ljubljani, Fakulteta za strojništvo, Aškerčeva 6, 1000 Ljubljana, tomaz.berlec@fs.uni-lj.si

Strojniški vestnik - Journal of Mechanical Engineering 54(2008)5, SI 55
UDK 621.941
Prejeto: 16.7.2007
Sprejeto: 28.9.2007

Raziskava in modeliranje vpliva rezalnih parametrov na rezalno silo in hrapavost površine pri vzdolžnem struženju

Dražen Bajić[1] - Branimir Lela[1] - Goran Cukor[2]
[1]Univerza v Splitu, Fakulteta za elektrotehniko, strojništvo in ladjedelništvo, Hrvaška
[2]Univerza v Rijeki, Fakulteta za inženirstvo, Hrvaška

V prispevku raziskujemo vpliv treh rezalnih parametrov na hrapavost površine in komponente rezalne sile pri vzdolžnem struženju. Kot faktorje vpliva smo upoštevali rezalno hitrost, podajalno razmerje in globino reza. Na podatkih, dobljenih s preizkusi, smo uporabili modelirni metodi, regresijsko analizo in nevronalne mreže. Za obe metodi smo tudi preizkusili zmožnost interpolacije in ekstrapolacije. Rezultate, pridobljene z modelom nevronalnih mrež smo primerjali s tistimi, pridobljenimi z regresijskim modelom. Z obema metodama dobimo, v primeru interpolacije, podobne rezultate. V primeru ekstrapolacije, pa dobimo z modelom nevronalnih mrež boljše rezultate. Da bi dobili optimalne vrednosti rezalnih parametrov, smo izvedli optimizacijo.

Ključne besede: vzdolžno struženje, rezalne sile, hrapavost površin, nevronalne mreže

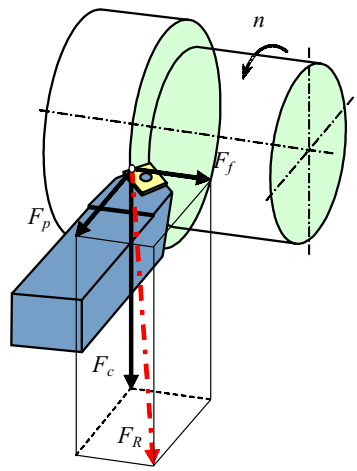

Sl. 1. *Komponente rezalne sile pri vzdolžnem struženju*

*Naslov odgovornega avtorja: Univerza v Splitu, Fakulteta za elektrotehniko, strojništvo in ladjedelništvo, Ruđera Boškovića bb, HR-21000 Split, Hrvaška, dbajic@fesb.hr

Strojniški vestnik - Journal of Mechanical Engineering 54(2008)5, SI 56
UDK 625.739
UDK 656.142

Prejeto: 19.7.2007
Sprejeto: 19.12.2007

Uporaba mikro-simulacije pri določanju zmogljivosti krožišča z upoštevanjem večkanalnega prehoda za pešce

Tomaž Tollazzi[1] - Tone Lerher[2] - Matjaž Šraml[1,*]
[1]Univerza v Mariboru, Fakulteta za gradbeništvo
[2]Univerza v Mariboru, Fakulteta za strojništvo

Glavni namen prispevka je analiza vpliva večkanalnega sistema toka pešcev na zmogljivost enopasovnega krožišča z uporabo diskretne simulacijske metode. Predlagani model temelji na teoriji pričakovane časovne praznine med enotami prometnega toka pešcev, ki imajo pri prečkanju kraka krožišča prednost pred motornimi vozili. Predlagani model predstavlja nadgradnjo predhodnih raziskav na področju modeliranja prometnih tokov v enopasovnem krožišču. Medtem ko je v predhodnem modelu prehod za pešce obravnavan kot enokanalni sistem v katerega prihajajo pešci naključno samo iz ene strani prehoda za pešce, je v tem modelu prehod za pešce obravnavan kot večkanalni sistem, v katerega prihajajo pešci naključno iz obeh strani prehoda za pešce. S tem je doseženo, da matematični model še bolje ponazarja dejansko dogajanje. Predhodni model je upošteval le motnje, ki na uvoznem prometnem toku motornih vozil povzroča tok pešcev, ki prečka krak krožišča, nadgrajeni model pa upošteva tudi motnje zaradi krožečega toka motornih vozil. Simulacijska analiza je bila izvedena na krožišču, ki se nahaja na Koroški ulici v Mariboru, kjer so bile v jutranji konični uri izvedene meritve prometnega toka motornih vozil in pešcev. Rezultati analize so pokazali sorazmerno veliko teoretično rezervo zmogljivosti za pešce, ki prihajajo iz leve in desne strani krožišča glede na dejansko stanje prihoda motornih vozil v analiziranem kraku krožišča. Dejanska rezerva zmogljivosti bo sicer manjša v odvisnosti od povečanja toka motornih vozil v prihodnosti, vendar pa bo še vedno dovolj velika, da bo omogočen nemoten prometni tok motornih vozil skozi krožišče.

Predstavljena metodologija predstavlja uporabno in prilagodljivo orodje za načrtovanje zmogljivosti krožišč v praksi in analizo vpliva posameznih spremenljivk na propustno sposobnost krožišča.

Ključne besede: krožišča, prehodi za pešce, modeliranje prometnih tokov, simulacijski modeli

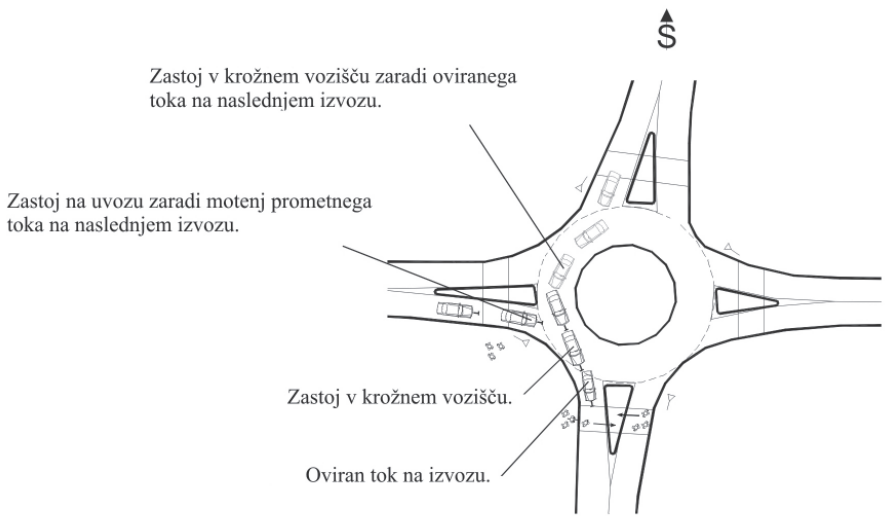

Sl. 1. *Zastoji v krožišču [3]*

*Naslov odgovornega avtorja: Univerza v Mariboru, Fakulteta za gradbeništvo, Smetanova 17, 2000 Maribor, sraml.matjaz@uni-mb.si

Strojniški vestnik - Journal of Mechanical Engineering 54(2008)5, SI 57
UDK 007.52
Prejeto: 6.6.2007
Sprejeto: 28.9.2007

PI+PD mehkologično krmiljenje dvoročnega robota za premike bremena

Yuksel Hacioglu - Yunus Ziya Arslan - Nurkan Yagiz*
Univerza v Istanbulu, Tehnična fakulteta, Turčija

V prispevku je predstavljena PI+PD mehkologična krmilna metoda za sočasno usklajeno gibanje dvoročnega robota za premike bremena. Najprej smo predstavili fizični model dvoročnega robota z bremenom ter izpeljali dinamične enačbe sistema ob upoštevanju omejitev. Ker lahko mehkologična krmilja uspešno načrtujemo, tudi če ne poznamo natančnega matematičnega modela sistema, ima ta krmilna metoda prednost v različnih primerih uporabe. PI+PD mehkologični krmilnik smo tako uvedli, da bi dosegli usklajenost dvojnih rok. Da bi preverili varnost delovanja predlaganega krmilnika, smo v sistem uvedli nepričakovane motnje. To so komponente hrupa, ki predstavljajo moteči vrtilni moment, in elastični element, ki nenamerno ovira prvo roko robota. Na koncu smo predstavili numerične rezultate in obravnavali predlagano regulacijsko metodo.

Ključne besede: mehka logika, robotske roke, kontrola gibanja, premik bremena

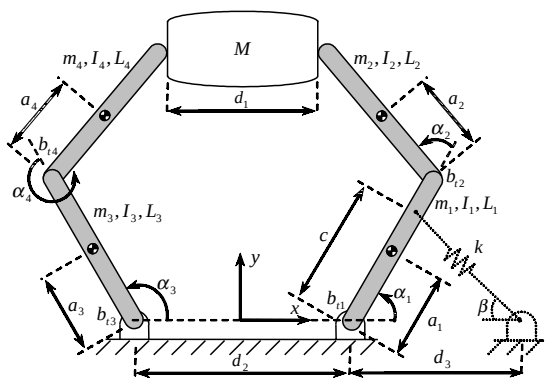

Sl. 1. *Rokovanje dvoročnega robota z bremenom*

*Naslov odgovornega avtorja: Univerza v Istanbulu, Tehnična fakulteta, Oddelek za strojništvo, 34320 Avcilar, Istanbul, Turčija, nurkany@istanbul.edu.tr

Strojniški vestnik - Journal of Mechanical Engineering 54(2008)5, SI 58
UDK 620.92
UDK 629.3.021.2
Prejeto: 20.7.2007
Sprejeto: 19.12.2007

Gorivo avtomobilov prihodnosti

Paul McGuiness
Institut "Jožef Stefan", Ljubljana

Ne glede na to, ali nas skrbi globalno segrevanje, ki ga povzročamo z uporabo fosilnih goriv, se moramo soočiti z dejstvom, da so zaloge surove nafte, iz katere pridobivamo bencin in dizelsko gorivo omejene ter se približuje čas, ko oskrba ne bo več sledila našim potrebam po gorivu. Napovedi se razlikujejo, a tudi po nabolj optimističnih pričakovanjih nam do tedaj ne preostane več kot 20 let. Zato moramo resno začeti iskati načine pridobivanja goriv za vozila v času, ki bo sledil izrabi surove nafte. Izraba vodika se zdi obetavna, pa je tudi zares realna? Ali Brazilci za pogon svojih avtomobilov ne uporabljajo alkohola? Je mar to rešitev, ki jo lahko uporabimo v svetovnem merilu? In kaj lahko rečemo o akumulatorskih vozilih? So mar ta uporabna le za prevažanje igralcev golfa? Odgovor ni le en, saj se bomo morali za rešitev problema poslužiti več različnih tehnologij.

Ključne besede: avtomobili, motorji z notranjim zgorevanjem, hibridna električna vozila, goriva, obnovljivi viri energije

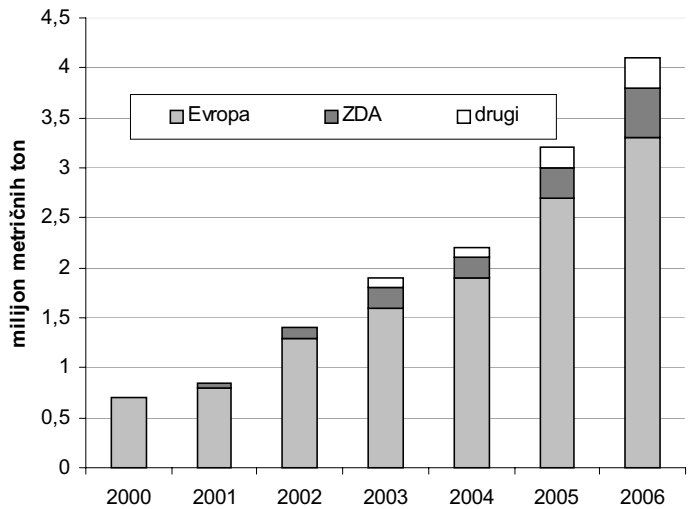

Sl. 2. *Svetovna proizvodnja biodizla od 2000 do 2006*

*Naslov odgovornega avtorja: Institut "Jožef Stefan", Odsek za nanostrukturne materiale, Jamova 39, 1000 Ljubljana, paul.mcguiness@ijs.si

Strojniški vestnik - Journal of Mechanical Engineering 54(2008)5, SI 59
UDK 528.02
Prejeto: 20.6.2007
Sprejeto: 28.9.2007

Najsodobnejše metode merjenja deformacij in njihova primerjava

Boštjan Kovačič[1,*] - Rok Kamnik[1] - Miroslav Premrov[1] - Nenad Gubeljak[2] - Jožef Predan[2] - Zdravko Tišma[2]
[1]Univerza v Mariboru, Fakulteta za gradbeništvo
[2]Univerza v Mariboru, Fakulteta za strojništvo

Izveden je bil deformacijski obremenilni preizkus betonske plošče. Betonska plošča je bila obremenjevana z računalniško vodenim hidravličnim valjem PZ 100 do sile 42 kN. Uporabljen je bil elektronski tahimeter znamke Nikon 800 in fotoaparat Fuji Pro S3. Izmerila se je vsaka dodatna obremenitev po 3 kN. Uporaba elektronskih tahimetrov za takšne namene je kar pogosta, vendar se v kombinaciji z digitalno fotogrametrijo le redko pojavlja. Kombinacija je zelo obetavna, saj je bil standardni odstopek fotogrametričnih meritev 0,16 mm, geodetskih meritev pa 0,7 mm, opazovanja pa so lahko bila izvedena tako za signalizirane in nesignalizirane točke hkrati. Betonska plošča je bila dodatno tudi analitično zmodelirana, model pa se je primerjal s fotogrametrično, geodetsko in hidravlično metodo.

Ključne besede: meritve deformacij, geodezija, digitalna fotogrametrija

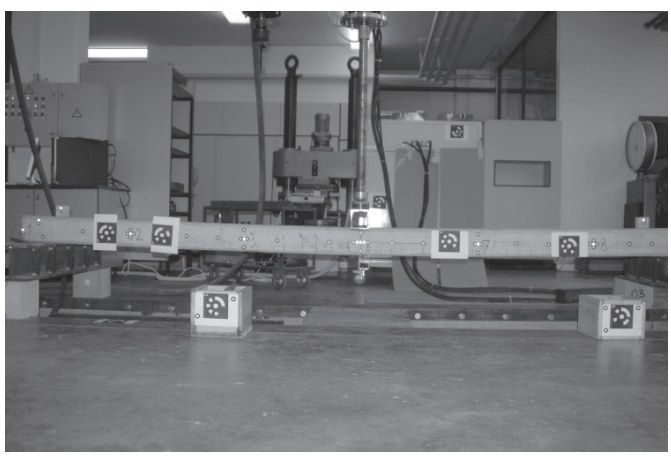

Sl. 3. *Tipska prednapeta armirano-betonska plošča z merskimi mesti*

*Naslov odgovornega avtorja: Univerza v Mariboru, Fakulteta za gradbeništvo, Smetanova 17, 2000 Maribor, bostjan.kovacic@uni-mb.si

Strojniški vestnik - Journal of Mechanical Engineering 54(2008)5, SI 60
UDK 531.1
Prejeto: 17.5.2007
Sprejeto: 19.12.2007

Hiper-kaotično načrtovanje Newtonove ponavljanje metode do sinteze mehanizma

Youxin Luo[1] - Xianfeng Fan[2] - Dazhi Li[1] - Xiao Wu[1]
[1]Univerza umetnosti in znanosti Hunan, Oddelek za strojništvo, L.R. Kitajska
[2]Univerza Ottawa, Oddelek za strojništvo, Kanada

Sintezo in približno sintezo problemov ravninskega mehanizma lahko spremenimo v sistem polinomov z več spremenljivkami ali splošne nelinearne enačbe. Newtonova ponavljana metoda, pomembna tehnika eno in večrazsežnih spremenljivk ter ponavljalnih postopkov, kaže občutljivo odvisnost od začetne točke. Na osnovi uporabe tehnike z več začetnimi točkami in hiper-kaotičnega načrtovanja (hiper-kaotični sistem Hénon*) kot začetnih točk Newtonove ponavljalne metode smo predlagali inovativno novo metodo hitrega in učinkovitega iskanja vseh rešitev splošnih nelinearnih enačb v kinematiki. Podali smo računski korak in metodo. Numerični primeri v spojitveni sintezi in približni sintezi kažejo, da je metoda pravilna in učinkovita.*

Ključne besede: hiper-kaotični sistemi, mehanizmi spajanja, sinteza mehanizmov, nelinearne enačbe

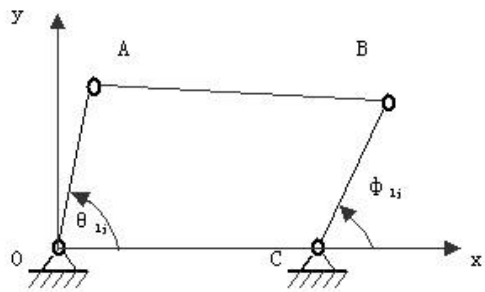

Sl.3. *Ravninski mehanizem*

*Naslov odgovornega avtorja: Univerza umetnosti in znanosti Hunan, Oddelek za strojništvo, Changde, Hunan, 415000, L.R. Kitajska, LLyx123@126.com

Osebne vesti

Doktorat in diplome

DOKTORAT

Na Fakulteti za strojništvo Univerze v Ljubljani je z uspehom zagovarjal svojo doktorsko disertacijo:

dne *18. aprila 2008*: **Boštjan Berginc**, z naslovom: "Vplivni dejavniki tehnologije visokotlačnega brizganja kovinskih prašna tih materialov" (mentorja: izr. prof. dr. Zlatko Kampuš in doc. dr. Borivoj Šuštaršič);

Za eksperimentalno določitev vplivnih dejavnikov procesov brizganja in sintranja je bila uporabljena Taguchijeva metoda z analizo variance. Pri sintranju se je poleg parametrov sintranja, opazoval tudi vpliv podtlaka na gostoto, poroznost, kemijsko sestavo in oksidacijo. Na podlagi eksperimentalnih rezultatov je bilo v nadaljevanju, z genetskim programiranjem izdelanih več empiričnih modelov za napovedovanje skrčkov pri procesu brizganja in izračun gostote po sintranja. Z genetskimi algoritmi so bili optimizirani koeficienti matematičnih modelov, ki popisujejo obnašanje materiala med brizganjem. Narejena je bila tudi nadgradnja analitičnega modela za sintranje v trdnem stanju, ki je služil kot osnova za numerične simulacije sintranja.

S tem je navedeni kandidat dosegel akademsko stopnjo doktorja znanosti.

DIPLOMIRALI SO

Na Fakulteti za strojništvo Univerze v Ljubljani so pridobili naziv univerzitetni diplomirani inženir strojništva:

dne *28. aprila 2008*: Peter APAT, Tomaž ILOVAR, Marko LAMOVŠEK, Samo RESNIK.

Na Fakulteti za strojništvo Univerze v Mariboru so pridobili naziv univerzitetni diplomirani inženir strojništva:

dne *10. aprila 2008*: Mitja GOLENKO;

dne *24. aprila 2008*: Dejan GLAVAČ, Marjan MARKOČIČ, Boštjan OGRIZEK, Damjan ŽERDIN.

*

Na Fakulteti za strojništvo Univerze v Ljubljani so pridobili naziv diplomirani inženir strojništva:

dne *10. aprila 2008*: Boris KRALJIČ, Milorad NIKOLIĆ, Aleš SAJE, Miran SLEVEC, Sašo ŠOŠKO;

dne *11. aprila 2008*: Marko OBID, Mitja VARL, Matjaž VIDMAR;

dne *14. aprila 2008*: Klemen BURGAR, Jure GOLOB, Maja MENART, Janez VRHKAR.

Na Fakulteti za strojništvo Univerze v Mariboru so pridobili naziv diplomirani inženir strojništva:

dne *17. aprila 2008*: Aleš TRUDEN;

dne *24. aprila2008*: Simon-Jernej ČANŽEK, Slavko JURIČ, Iztok MLAKAR, Leon PROSENC, Aleš TRUDEN.

http://www.sv-jme.eu